Spin-polarized atomic hydrogen : devices and phenomena

Please check the document version of this publication:

• A submitted manuscript is the version of the article upon submission and before peer-review. There can be important differences between the submitted version and the official published version of record. People interested in the research are advised to contact the author for the final version of the publication, or visit the DOI to the publisher's website.
• The final author version and the galley proof are versions of the publication after peer review.
• The final published version features the final layout of the paper including the volume, issue and page numbers.

Link to publication

Download date: 04. Oct. 2023

Spin-Polarized Atomic Hydrogen:
Devices and Phenomena

A. C. Maan

Spin-Polarized Atomic Hydrogen:
Devices and Phenomena

PROEFSCHRIFT

ter verkrijging van de graad van doctor aan de Technische Universiteit Eindhoven, op gezag van de Rector Magnificus, prof. dr. J. H. van Lint, voor een commissie aangewezen door het College van Dekanen in het openbaar te verdedigen op dinsdag 15 juni 1993 om 16.00 uur

door

ANTHONIUS CORNELIS MAAN

Geboren te Schiedam

Dit proefschrift is goedgekeurd
door de promotoren
prof. dr. B. J. Verhaar
en
prof. dr. H. C. W. Beijerinck

aan mijn ouders

Contents

Chapter 1

Introduction

In this thesis we deal with several questions in which the spin-polarization of atomic hydrogen is involved:

- Can we improve (our insight into) the operation of one of the most important devices based on the properties of spin-polarized atomic hydrogen: the hydrogen maser?

- What is the mechanism of one of the main processes by which the spin-polarization in a gas of atomic hydrogen disappears: the recombination reaction $H + H + H \rightarrow H_2 + H$ in three-body collisions?

In this introductory chapter we will sketch briefly the physical background of these questions to help the reader in understanding the broader context of this thesis work.

1.1 The hydrogen maser

The origin of the maser dates back to the year 1954. In a series of publications [1]-[3] Townes *et al.* announced the development of a new apparatus, called a maser, which is an acronym of "microwave amplification by stimulated emission of radiation". Based on
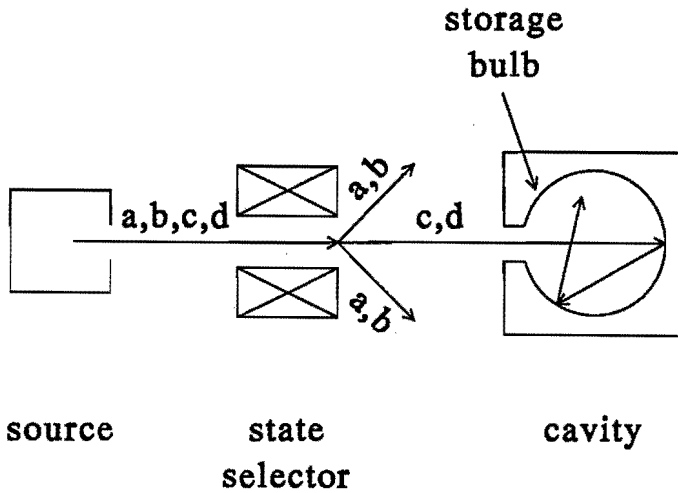
Figure 1.1: Schematic drawing of the experimental setup of the hydrogen maser.

one of these papers [3], Ramsey *et al.* [4],[5] gave, in 1962, a description of a so-called hydrogen maser. One of the changes is the replacement of the electric dipole transition involved in the ammonia maser of Townes *et al.* by a magnetic dipole transition. The weakness of this transition is compensated by the much longer interaction time of the atoms with the maser field, which is realized by storing the atoms in a certain volume, instead of using an atomic beam.

The experimental setup of the hydrogen maser is schematically shown in Fig. 1.1 [5]. Molecular hydrogen is dissociated in an atomic hydrogen source. In the beam of hydrogen atoms leaving the source the atoms are distributed between all four hyperfine levels of the $1s$-groundstate (see Fig. 1.2). The hydrogen maser is based on the c to a transition for $B \simeq 0$, i.e., $f = 1$, $m_f = 0 \rightarrow f = 0$, $m_f = 0$, where the lower-case symbols denote single-atom spins. In order to create the overpopulation of c-state atoms with respect to a-state atoms necessary for maser oscillation to take place the beam is passed through a state selector. This state selector consists of a magnet producing a magnetic field, e.g., a sextupole field, which is zero at the axis and increases away from it. The a and b atoms, the so-called high-field seeking atoms, are removed from the

$|d\rangle = |\uparrow \uparrow\rangle$

$|c\rangle = \cos\theta \, |\uparrow \downarrow\rangle + \sin\theta \, |\downarrow \uparrow\rangle$

$|b\rangle = |\downarrow \downarrow\rangle$

$|a\rangle = \cos\theta \, |\downarrow \uparrow\rangle - \sin\theta \, |\uparrow \downarrow\rangle$

E

a_{hf}

B
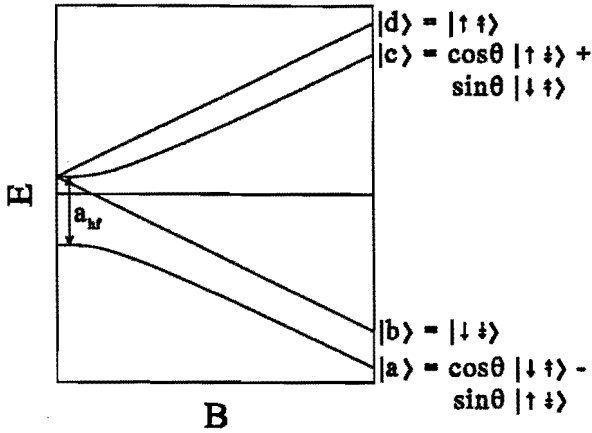
Figure 1.2: *The four hyperfine levels of the hydrogen 1s-groundstate as function of the magnetic field. The* $\uparrow$ *denotes the electron spin projection whereas* $\updownarrow$ *denotes the proton spin projection. Furthermore,* a_{hf} *is the hyperfine splitting at zero magnetic field and the mixing angle* θ *is given by* $\tan 2\theta = \frac{1}{2}a_{hf}/[(\mu_e + \mu_p)B]$, *with* μ_e (μ_p) *the electron (proton) magnetic moment.*

beam, whereas the c and d atoms, the low-field seeking atoms, are bent towards the axis and are focussed into a storage bulb which is placed in a microwave cavity. In this cavity the maser oscillation takes place. The atoms reside in the storage bulb for times between one and ten seconds before leaving through the same opening they originally entered. This whole system is operated at room temperature.

To this date the room temperature hydrogen maser is the most stable frequency standard for measuring times between one second and several days with a relative frequency instability observed to be below one part in 10^{15} for measuring times of one hour [6]. As such the hydrogen maser is being used in tests of general relativity, very long baseline interferometry (VLBI) and interplanetary navigation such as the Voyager 2 mission [6]-[8]. In order to keep track of the position of the Voyager on its way to Neptune three earth-based radio telescopes emitted signals to the Voyager which returned them to these telescopes. By measuring the time elapsed between sending and receiving

the signals the radial and angular positions of the Voyager could be determined. At each telescope two hydrogen masers were used to achieve the required accuracy in the time measurement.

The optimization of the frequency stability, which is necessary to perform even more accurate measurements, requires a detailed theoretical knowledge of the processes which influence this stability. This is the subject of Chapter 2 of this thesis. For an evaluation of the frequency stability it is essential to realize oneself that the atomic transition is not the only oscillator in the hydrogen maser: The cavity also is an oscillator in its own right. The maser frequency is thus the resonance frequency of a system of two nonlinearly coupled oscillators, each with its own frequency. It is determined by the cavity-pulling relation [5],[9],[10]

$$\frac{\omega_m - \omega_{at}}{\Gamma_{at}} = \frac{\omega_c - \omega_m}{\Gamma_c} , \qquad (1.1)$$

where ω_m is the maser frequency, ω_{at} the atomic transition frequency, ω_c the cavity frequency, and Γ_{at} and Γ_c the width of the frequency profiles of the atomic transition and the cavity mode, respectively. This relation indicates which parameters determine the frequency of the maser. A time dependence of these parameters, e.g., a systematic drift or fluctuations, will lead to a time dependence and thus an instability of the maser frequency.

Processes which influence the stability can, according to Eq. (1.1), be separated in two different groups, namely those which affect the cavity frequency and width and those which affect the atomic transition frequency and width. In order to reduce the influence of the former, the ratio Γ_{at}/Γ_c is made as small as possible. This is achieved in two different ways. By storing the atoms as long as possible in the storage bulb without a significant loss of coherence the interaction time with the field is increased and thus, by Heisenbergs uncertainty principle, the atomic linewidth is reduced. The loss rate of the cavity is subsequently increased up to the point were Γ_c is as large as possible while still maintaining maser oscillation. Due to the small ratio of Γ_{at} to Γ_c the influence of the cavity on the stability of the maser is negligible [11].

The atomic transition frequency and linewidth entering Eq. (1.1) differ from the values for a hydrogen atom in free space. For example, during their stay in the storage

bulb, the hydrogen atoms will collide many times with the walls of this bulb and with a certain probability will stick to it. Only in the case of sticking, due to the long interaction time, the perturbation of the energy levels of the hydrogen atoms has to be taken into account. This causes a shift in the atomic transition frequency. A statistical distribution of the sticking times, furthermore, causes a broadening of the atomic line. This effect, however, is reproducible and time-independent which means that it does not affect the stability of the maser. Other effects that influence the atomic transition are the finite storage time, inhomogeneities in the static magnetic field and the second order Doppler effect. The effect, however, which is of most concern to the stability of the maser and which is treated in Chapter 2 of this thesis are collisions between hydrogen atoms.

Qualitatively, the influence of collisions on ω_{at} and Γ_{at} may be understood as follows. The wave function of a hydrogen atom participating in the maser oscillation can be written as a superposition of the c and the a state

$$C_c e^{-i\epsilon_c t/\hbar}|c\rangle + C_a e^{-i\epsilon_a t/\hbar}|a\rangle , \tag{1.2}$$

with ϵ_c and ϵ_a the energies of the c and a level, respectively, $(\epsilon_c - \epsilon_a)/\hbar$ the transition frequency in the absence of collisions, and C_c and C_a amplitudes. After an elastic collision of such an atom with another atom both parts of Eq. (1.2) are multiplied by a different diagonal element of the scattering matrix. This causes a phase shift $\Delta\phi$ and with N collisions per second this leads to a frequency shift $\Delta\omega_{at} = d\phi/dt = N\Delta\phi$. The number of collisions per atom will not be equal but will be statistically distributed as will the velocities of the two colliding atoms. Apart from the shift of the atomic transition this also causes a broadening. It is clear that this effect depends on the density of hydrogen atoms in the storage bulb. In practice, a fluctuation in the density has a large effect on the stability of the maser.

The broadening and shift of the atomic transition were calculated in 1963 by Bender [12], based on earlier work of Wittke and Dicke [13] and Dalgarno [14]. Semiclassical methods were used, neglecting the hyperfine splitting in the collision. A year later Balling *et al.* [15] made a full quantum mechanical calculation, still neglecting, however, the hyperfine interaction. Both theories led essentially to the same result and gave rise to a procedure called spin-exchange cavity tuning [16],[17]. This method uses two effects

which influence the maser frequency, cavity pulling and collisions between atoms. The above calculations showed that the frequency shift due to collisions is proportional to the atomic linewidth. In that case the cavity pulling relation (1.1) can be written as

$$\omega_m - \omega_{at}^0 = \{\frac{1}{\Gamma_c}(\omega_c - \omega_{at}^0) + \alpha\}\Gamma_{at}, \qquad (1.3)$$

where ω_{at}^0 is the transition frequency in the absence of collisions and α is a proportionality constant. In Eq. (1.3) the difference between ω_{at}^0 and ω_m has been neglected in the righthand side. By choosing $\omega_c = \omega_{at}^0 - \Gamma_c\alpha$ the maser frequency can be made stable against fluctuations in Γ_{at} and thus fluctuations in the density. The stability of the maser is then determined by thermal noise and receiver noise.

In 1975 Crampton and Wang [18] performed a semiclassical calculation of the collision process in which they included the hyperfine splitting. This introduced an extra contribution to the frequency shift which is not proportional to the total atomic linewidth but only to the collisional part Γ_{at}^{coll}:

$$\omega_m - \omega_{at}^0 = \{\frac{1}{\Gamma_c}(\omega_c - \omega_{at}^0) + \alpha\}\Gamma_{at} + \beta\Gamma_{at}^{coll}, \qquad (1.4)$$

$$= \{\frac{1}{\Gamma_c}(\omega_c - \omega_{at}^0) + \alpha + \beta\}\Gamma_{at} - \beta\Gamma_{at}^0,$$

with Γ_{at}^0 the single-atom contribution to the atomic linewidth and β a proportionality constant. The main contribution to Γ_{at}^0 is due to the storage time of the atoms in the storage bulb. Equation (1.4) shows that the extra contribution to the frequency shift remains density independent after cavity tuning, but leads to a dependence of the maser stability on fluctuations in Γ_{at}^0. It turns out that this source of frequency instability is negligible for a hydrogen maser operating at room temperature.

In 1978 two groups, Crampton *et al.* [19] and Vessot *et al.* [20], proposed to construct a hydrogen maser operating at sub-Kelvin temperatures, the cryogenic hydrogen maser (CHM). The main advantages would be much smaller collisional cross sections, allowing for much larger densities and thus a larger output power, less thermal noise and a better control over the cavity. In 1982 Berlinsky and Hardy [21] predicted that with the cryogenic hydrogen maser an increase in frequency stability can be achieved with respect to the room temperature maser of three orders of magnitude. Essential in this approach is again the possibility of spin-exchange cavity tuning. Three groups [22]-[24]

succeeded in building such a cryogenic hydrogen maser almost simultaneously in 1986. Stabilization of the hydrogen gas at these low temperatures is possible by covering the walls of the storage bulb with superfluid helium [25]. Due to the virtual absence of a spin-dependent interaction between hydrogen and helium atoms and the low binding energy of hydrogen to a helium film the atoms can hit the walls of the storage bulb many times without a significant loss of coherence.

In our group at Eindhoven University of Technology calculations on volume and surface collisions of hydrogen atoms had been going on since 1982. This knowledge, however, was applied to the hydrogen maser only after 1985, as stimulated by a request from Crampton. For the first time the expressions for the frequency shift and line broadening were based on a systematic derivation from the BBGKY hierachy [26],[27]. A fundamentally new aspect discovered in this work was the insight that the hyperfine splitting of the internal states of the colliding atoms contributes to the line shift in a way which precludes its compensation by spin-exchange cavity tuning. Not only does the maser stability become dependent on the storage time of the atoms as in the semiclassical calculations of Crampton and Wang, but the frequency shift depends on the density even after cavity tuning. Specifically, it means that the proportionality parameter β in Eq. (1.4) becomes density dependent. Although this contribution is rather small, it turns out to be so important in the sub-Kelvin hydrogen maser [26]-[28] that most of the improvement of the frequency stability is lost: The maximum improvement in frequency stability realizable with respect to the room temperature hydrogen maser was shown to be a factor of 10, two orders of magnitude less than originally predicted.

This fact is the main motivation for Chapter 2 of this thesis. The hydrogen maser is normally operated at very low magnetic field strengths of less than 10^{-6} T. Both the hyperfine energies and the spin structure of the states involved in the maser transition show a dependence on the magnetic field (see Fig. 1.2). This means that by varying the magnetic field collisions between hydrogen atoms will evolve in a totally different way since the interaction between these atoms will change considerably. This could have a pronounced effect on the frequency shift, in particular its dependence on the partial densities, which might be used to improve the frequency stability. In this connection it should be noted that the hyperfine-induced changes of collisional T-matrix elements

are in general a very small part of the total T-matrix elements, so that already a rather small new effect could introduce a considerable influence. In Chapter 2 the effect of an introduction of a magnetic field is treated and it is shown that the hoped for improvement in frequency stability can not be realized [29].

Recently, two experiments, one at room temperature [30],[31] and one at sub-Kelvin temperatures [32],[33], as well as a reanalysis [11] of the earliest room temperature experiment [18] to measure the hyperfine-induced collisional shifts have shown a discrepancy with the quantum mechanical calculations of our group. Specifically, one of the collisional shift terms which is the direct consequence of the inclusion of the hyperfine interaction has a different sign, although its order of magnitude is correct. Two possible causes for this sign difference have been proposed. The original papers in which our group presented the calculations [26],[27] could contain a sign error in the hyperfine-induced shifts. In this connection it is of importance to notice that in Eq. (13) of Ref. [26] and Eqs. (56), (57) and (58) of Ref. [27] a sign convention for Δ^f is used which is different from that in the final results. A rigorous check on the calculations, however, has ruled out the possibility of a sign change in the final results. A second possible cause was given by Silvera *et al.* [30],[31], in which they cast doubt on the hydrogen potentials used in the numerical calculations. A recalculation with the most up-to-date data on these potentials shows virtually no differences with previous calculations. As yet, there is no solution for this problem which will be the subject of further study. Measurements of the magnetic field dependence of the collisional frequency shifts and a comparison with the predictions of Chapter 2 of this thesis may shed further light on this problem.

Both experimental and theoretical work on the hydrogen maser have during the last three decades been concentrated on its use as a primary frequency standard. Interest in phenomena taking place inside the maser itself has arisen only in the last 5 years [10],[34]-[37]. Some of these phenomena are treated in Chapters 3, 4 and 5.

A process which does not contribute to the frequency instability in the hydrogen maser but is nevertheless important for its operation is the above-mentioned wall shift resulting from the fact that the atomic transition frequency at the surface is different from the frequency in the volume. The size of this effect depends on the construction and on the specific operating conditions of the maser, such as the area to volume ratio of the

storage bulb and the exact temperature [38]-[41]. For the room temperature hydrogen maser it depends in addition on the purity of the material which is used for the wall of the storage bulb, i.e., teflon. As a consequence the atomic transition frequency but also the maser frequency is determined by device parameters and by the specific operating conditions. This inhibits the use of the hydrogen maser as a primary time standard. If, however, the fraction of time that the atoms spend at the surface would be much smaller than in the present sub-Kelvin maser this device dependent shift would disappear and the possibility arises that the hydrogen maser could indeed be used as a primary time standard. This, however, is not possible in the sub-Kelvin hydrogen maser. The so-called wall shift can only be reduced by increasing the temperature of the maser given a fixed size of the storage bulb. Not only do the collisional cross sections increase in this case but due to the evaporation of the superfluid helium film the rate at which hydrogen atoms collide with helium atoms in the volume increases as well which introduces an additional frequency shift [21],[42],[43]. In fact, the sum of the latter shift and the wall shift is only stationary with respect to temperature changes at 0.5 K.

This is the motivation to investigate the possibility to operate a maser in which most of the atoms are adsorbed on the superfluid helium surface. By decreasing the temperature it is possible to interchange the roles of surface and volume and it is even possible to reduce any shifts occurring due to the presence of the volume which is desirable from the point of view of a primary time standard, but now based on the transition frequency of hydrogen atoms adsorbed on a superfluid helium surface. This is the subject of Chapter 3. A new method is developed to describe the interaction of the maser field with both the atoms residing in the volume and at the surface. Starting from this description the realizability of a so-called surface cryogenic hydrogen maser (SCHM) is investigated. It turns out that it is indeed possible to operate such a surface cryogenic hydrogen maser but that such a device does not have the prospects to serve as a primary time standard. It does have the potential, however, to be an accurate source of new information on the hydrogen-liquid helium surface system [37].

Chapters 4 and 5, finally, emphasize the dynamics of the hydrogen maser. Instead of focussing on collisions between hydrogen atoms these chapters deal with the interaction between the atomic magnetization, the population inversion and the oscillating electro-magnetic field in the cavity. In analogy to Haken in 1975 [44] the equivalence between

the Maxwell-Bloch equations which govern the hydrogen maser and the Lorenz equations is demonstrated. These equations appeared in 1963 in a study by the meteorologist Lorenz [45] as a strongly simplified model of the Navier-Stokes equations. Although it soon became clear that they were not an accurate approximation in this specific situation these equations have been the subject of many investigations and are one of the primary examples of equations known to exhibit so-called chaotic behavior [46]. In Chapter 4 we show that the hydrogen maser is indeed a very clear example of a system governed by these equations and that it is possible to reach a regime of time-dependent chaotic, but also periodic, pulsed behavior in the sub-Kelvin maser in contrast to the room temperature maser [10]. In Chapter 5 the Lorenz equations are further examined for the parameter regime of the sub-Kelvin hydrogen maser and by a systematic search a detailed picture of the expected behavior is given. Apart from being an interesting subject of study of nonlinear dynamics, the time-dependent regime promises to give more detailed information on the hydrogen maser itself, including collisional phenomena, than the time-independent regime does [36].

1.2   Mechanisms for three-body recombination

The storage of hydrogen atoms by covering the walls of the storage bulb with a film of superfluid helium as applied in the sub-Kelvin hydrogen maser is one of the experimental techniques which during the past one and a half decade have been developed to produce gaseous samples of atomic hydrogen at such low temperatures and high densities that the conditions for Bose-Einstein condensation (BEC) are fulfilled [25],[47]-[50]. A more recent line of research is based on (evaporative) cooling of samples of atomic hydrogen in a magnetic trap [51]-[55]. The contrast between these two approaches is visible in Fig. 1.3, taken from Refs. [56],[57]. In this figure the condition for Bose-Einstein condensation is given along with the densities and temperatures achieved in various experiments. Whereas the storage of hydrogen in a gas cell covered with superfluid helium is used in attempts to achieve Bose-Einstein condensation by increasing the density the cooling of atoms in a magnetic trap is intended to produce a relatively low density sample of hydrogen atoms with a temperature low enough to observe Bose-Einstein condensation. This last approach is outside the scope of this thesis.

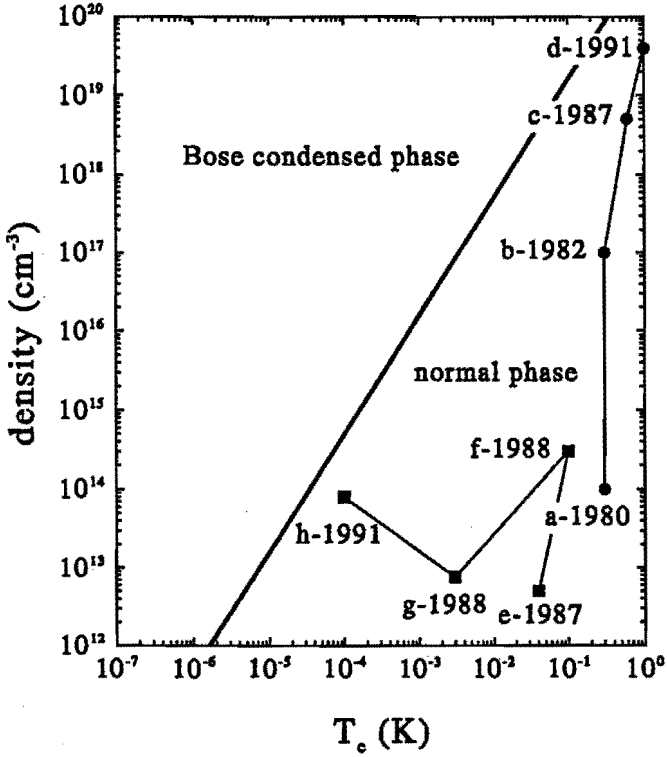*Figure 1.3: Phase diagram for BEC in spin-polarized atomic hydrogen, with T_c the critical temperature at a given density: a Ref. [25], b Ref. [47], c Refs. [48],[49], d Ref. [50], e Ref. [51], f Ref. [52], g Ref. [53] and h Ref. [54]. The progress towards BEC is indicated for experiments with superfluid helium covered walls by the line connecting a, b, c and d and for trap experiments by the line connecting e, f, g and h.*

initial   dipole   final
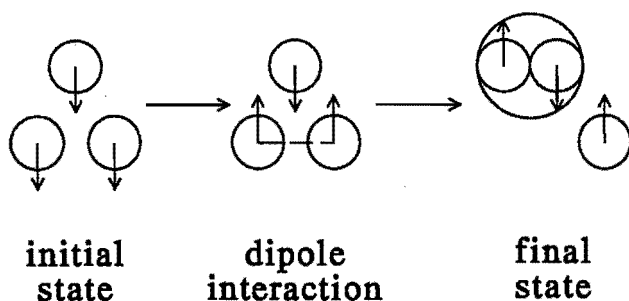state   interaction   state

Figure 1.4: Schematic picture of the Kagan dipole mechanism. Only the double spin-flip contribution arising from the dipole interaction is presented.

In experiments devised to observe Bose-Einstein condensation in the high-density scheme a gas cell is loaded with a and b atoms at high magnetic field strengths. In the b state both the electron and proton spins are down (see Fig. 1.2), whereas in the a state the electron spin is down and the proton spin is up but there is a small admixture of electron spin up and proton spin down. At low temperatures a large fraction of the gas is adsorbed at the wall of the gas cell. Due to the small admixture of electron spin up in the a state a collision of two a atoms and a collision of an a and b atom evolve partially via the singlet interaction which means that the two atoms can recombine to form a molecule if the collision takes place at the surface. Two b atoms, however, can not recombine. This process, which is called preferential recombination of the a atoms, produces a sample of hydrogen gas in which almost all atoms are in the b state.

The only way in which a gas of purely b atoms can decay is by the magnetic dipole interaction between the spins of the atoms. In a collision of two b atoms the dipole interaction can induce an electron-spin flip by the transfer of atomic orbital momentum to intrinsic angular momentum. An atom which has undergone such a spin flip can subsequently recombine with a b atom at the surface. Another possible decay mechanism, which is the subject of Chapter 6, is the three-body recombination of atomic hydrogen.

Up to now all experiments which have tried to reach Bose-Einstein condensation in the high-density scheme have failed due to the large three-body decay rates of the

initial   dipole   final
state   interaction   state

exchange
interaction
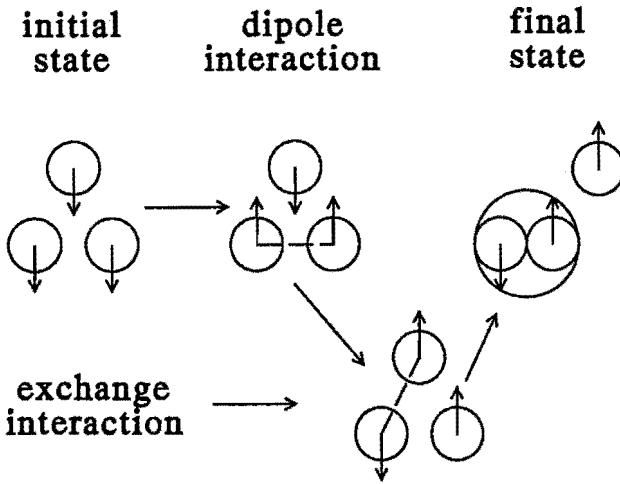
*Figure 1.5: Schematic picture of the dipole-exchange mechanism. The essential differ-
ence with Fig. 1.4 is that the dipole-interacting pair of atoms eventually recombines.*

gas. This has given rise to a considerable effort, both experimentally [58],[59] and
theoretically [60]-[68], in the study of this process. Specific attention has been paid
to the possibility that by varying the applied magnetic field the decay constants can be
manipulated in such a way that Bose-Einstein condensation is possible.

One of the earliest descriptions of the three-body recombination process has been
given by Kagan *et al.* [60]. In this description one starts with three atoms all with
their electron spin down, i.e., three *b* atoms. Two of these atoms interact via the dipole
interaction. Although the total spin state of these two atoms remains triplet the precession
of both electron spins in their mutual dipole fields introduces a singlet component with
respect to the third atom. It is then possible for one of the atoms to recombine with this
third atom. This process is schematically depicted in Fig. 1.4.

Although these calculations have given a good insight in the properties of atomic
hydrogen gas at low temperatures the discrepancies with experimental data showed that
this mechanism is not sufficient to describe the observed decay rates. As a solution our

Figure 1.6: The two momenta involved in a three-body problem: the relative momentum $\vec{p}$ between two atoms and the relative momentum $\vec{q}$ of the third atom relative to the center of mass of the pair. A numerical solution of the Faddeev equations by discretization of these two momenta is not possible at present for the final state.

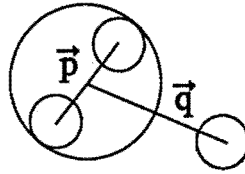group in Eindhoven proposed a different mechanism which has turned out to be the most important contribution to the decay process, the dipole-exchange mechanism which is schematically drawn in Fig. 1.5 [62],[65]. Again the dipole interaction introduces a precession of the spins of two of the atoms while preserving their triplet spin state. Instead of a recombination of one of these atoms with the remaining third atom the strong central interaction causes a spin-exchange between this latter pair of atoms. The spin state of the two atoms which originally interacted via the dipole interaction has thus acquired a singlet component and it is possible for these two atoms to recombine. It should be noted that, contrary to the Kagan dipole process, it is the dipole-interacting pair of atoms that eventually recombines. Using various approximations our group has calculated the three-body recombination rate including this dipole-exchange mechanism [62],[63],[65]-[68].

The approach which is taken treats the magnetic dipole interaction between the electron spins in first order. This has turned out to be a very well satisfied approximation. The calculation of the decay rate thus involves the evaluation of a matrix element of the interatomic magnetic dipole interaction between an initial and a final state. In both these states the central singlet/triplet interaction is included in an exact way. Already in the first approach the initial state has been calculated rigorously by solving the Faddeev equations. It turned out that an approach in which this initial state was replaced by a

Jastrow approximation introduced only slight deviations in the decay rates of less than 15 % [62],[65]. The final state can, in principle, be calculated in the same way. Due to the large number of channels in the final state, i.e., the large number of bound states, however, the "conventional" method of solving the Faddeev equations, i.e., a discretization of the two momenta involved in this problem (see Fig. 1.6), makes the problem too cumbersome for present-day supercomputers. Therefore our group has so far tried to calculate the final state in an approximate way. In a first approach [63],[65] the calculation of the final state involved the collision of an atom with a molecule. This molecule underwent all possible changes in its internal states except a change of identity of the atoms it consists of. This means that rearrangement and thus the dipole-exchange mechanism was not included in this approach. The large discrepancies with experiment [58],[59],[66],[68] were another indication that this mechanism is essential in the description of the three-body recombination. In a subsequent calculation also rearrangement was included [67],[68]. The results of this approach, the resonating group theory, showed that a resonance effect caused by quasi-bound $S = 1/2$ states of the H_3 molecule contributes significantly to the recombination process. In this state the dominant configuration of the hydrogen atoms is an equilateral triangle with an interatomic distance of about 7 a_0. The largest bound state of the hydrogen molecule H_2, however, extends to approximately 5 a_0. This means that a description of three-body recombination in which only bound states of the hydrogen molecule are included is not sufficient. The continuum should also be taken into account.

Although an inclusion of the continuum is necessary to describe the recombination process the asymptotic form of the wave function still consists of a molecule and a freely moving atom. The continuum is thus only important in a part of space in which the three atoms are closely together, i.e., there is only "virtual break-up". This fact forms the basis for the present approach. Stimulated by a suggestion of Glöckle a set of functions is created which are orthogonal to the bound state wave functions and which are eigenfunctions of the central two-body singlet/triplet interaction problem within the subspace spanned by this selected set [67]-[70]. This set represents the continuum in our calculations. If it would contain an infinite number of functions the representation would be exact. However, we restrict ourselves to a finite number of functions which are localized in space at a position where the relevant H_3 resonances are expected to

be located. With these functions the Faddeev equations are solved. The expectation is that only a few cleverly chosen functions are sufficient to obtain convergence in the calculations. This method thus enables us to solve the Faddeev equations.

The validity of the method has been tested on an important three-body process in nuclear physics: neutron-deuteron scattering. In this case a neutron collides with a deuteron which is a bound state of a proton and a neutron, treated as two identical particles in different isospin states [70]-[73]. The analysis of this problem with the above mentioned method is presented in Chapter 6.

Bibliography

[1] J. P. Gordon, H. J. Zeiger, and C. H. Townes, Phys. Rev. **95**, 282 (1954).

[2] J. P. Gordon, H. J. Zeiger, and C. H. Townes, Phys. Rev. **99**, 1264 (1955).

[3] K. Shimoda, T. C. Wang, and C. H. Townes, Phys. Rev. **102**, 1308 (1956).

[4] H. M. Goldenberg, D. Kleppner, and N. F. Ramsey, Phys. Rev. Lett. **5**, 361 (1960).

[5] D. Kleppner, H. M. Goldenberg, and N. F. Ramsey, Phys. Rev. **126**, 603 (1962).

[6] R. F. C. Vessot, Proc. IEEE **79**, 1040 (1991).

[7] R. F. C. Vessot, Contemp. Phys. **25**, 355 (1984).

[8] N. F. Ramsey, Rev. Mod. Phys. **62**, 541 (1990).

[9] S. B. Crampton, Phys. Rev. **158**, 57 (1967).

[10] A. C. Maan, H. T. C. Stoof, B. J. Verhaar, and P. Mandel, Phys. Rev. Lett. **64**, 2630 (1990); **65**, 2319 (1990).

[11] S. B. Crampton (private communication).

[12] P. L. Bender, Phys. Rev. **132**, 2154 (1963).

[13] J. P. Wittke and R. H. Dicke, Phys. Rev. **103**, 620 (1956).

[14] A. Dalgarno, Proc. Roy. Soc. A **262**, 132 (1961).

[15] L. C. Balling, R. J. Hanson, and F. M. Pipkin, Phys. Rev. **133**, A607 (1964); **135**, AB1 (1964).

[16] S. B. Crampton, D. Kleppner, and N. F. Ramsey, Phys. Rev. Lett. **11**, 338 (1963).

[17] J. Vanier and R. F. C. Vessot, Appl. Phys. Lett. **4**, 122 (1964).

[18] S. B. Crampton and H. T. M. Wang, Phys. Rev. A **12**, 1305 (1975).

[19] S. B. Crampton, W. D. Phillips, and D. Kleppner, Bull. Am. Phys. Soc. **23**, 86 (1978).

[20] R. F. C. Vessot, M. W. Levine, and E. M. Mattison, NASA Technical Memorandum No. 78104, 1978 (unpublished), p. 549.

[21] A. J. Berlinsky and W. N. Hardy, NASA Conference Publication No. 2220, 1982 (unpublished), p. 547.

[22] H. F. Hess, G. P. Kochanski, J. M. Doyle, T. J. Greytak, and D. Kleppner, Phys. Rev. A **34**, 1602 (1986).

[23] M. D. Hürlimann, W. N. Hardy, A. J. Berlinsky, and R. W. Cline, Phys. Rev. A **34**, 1605 (1986).

[24] R. L. Walsworth, I. F. Silvera, H. P. Godfried, C. C. Agosta, R. F. C. Vessot, and E. M. Mattison, Phys. Rev. A **34**, 2550 (1986).

[25] I. F. Silvera and J. T. M. Walraven, Phys. Rev. Lett. **44**, 164 (1980).

[26] B. J. Verhaar, J. M. V. A. Koelman, H. T. C. Stoof, O. J. Luiten, and S. B. Crampton, Phys. Rev. A **35**, 3825 (1987).

[27] J. M. V. A. Koelman, S. B. Crampton, H. T. C. Stoof, O. J. Luiten, and B. J. Verhaar, Phys. Rev. A **38**, 3535 (1988).

[28] W. N. Hardy, M. D. Hürlimann, and R. W. Cline, Jpn. J. Appl. Phys. **26**, 2065 (1987).

[29] A. C. Maan, H. T. C. Stoof, and B. J. Verhaar, Phys. Rev. A **41**, 2614 (1990).

[30] R. L. Walsworth, Ph.D. thesis, Harvard University, USA, 1991.

[31] R. L. Walsworth, I. F. Silvera, E. M. Mattison, and R. F. C. Vessot, Phys. Rev. A **46**, 2495 (1992).

[32] M. E. Hayden, Ph.D. thesis, University of British Columbia, Canada, 1991.

[33] M. E. Hayden, M. D. Hürlimann, and W. N. Hardy, IEEE Trans. Instrum. Meas. (accepted for publication).

[34] R. L. Walsworth, I. F. Silvera, E. M. Mattison, and R. F. C. Vessot, Phys. Rev. Lett. **64**, 2599 (1990).

[35] R. L. Walsworth and I. F. Silvera, Phys. Rev. A **42**, 63 (1990).

[36] P. Mandel, A. C. Maan, B. J. Verhaar, and H. T. C. Stoof, Phys. Rev. A **44**, 608 (1991).

[37] A. C. Maan, B. J. Verhaar, H. T. C. Stoof, and I. F. Silvera, Phys. Rev. A (submitted for publication).

[38] P. W. Anderson and P. R. Weiss, Rev. Mod. Phys. **25**, 269 (1953).

[39] P. W. Anderson, J. Phys. Soc. Jpn. **9**, 316 (1954).

[40] A. Abragam, *The Principles of Nuclear Magnetism* (Clarendon Press, Oxford, 1961).

[41] M. Morrow and W. N. Hardy, Can. J. Phys. **61**, 956 (1983).

[42] M. Morrow, R. Jochemsen, A. J. Berlinsky, and W. N. Hardy, Phys. Rev. Lett. **46**, 195 (1981); **47**, 455 (1981).

[43] M. D. Hürlimann, Ph.D. thesis, University of British Columbia, Canada, 1989.

[44] H. Haken, Phys. Lett. **53A**, 77 (1975).

[45] E. N. Lorenz, J. Atmos. Sci. **20**, 130 (1963).

[46] C. Sparrow, *The Lorenz Equations: Bifurcations, Chaos, and Strange Attractors* (Springer-Verlag, New York, 1982).

[47] R. Sprik, J. T. M. Walraven, G. H. van Yperen, and I. F. Silvera, Phys. Rev. Lett. **49**, 153 (1982).

[48] R. Sprik, J. T. M. Walraven, and I. F. Silvera, Phys. Rev. Lett. **51**, 479 (1983).

[49] T. Tommila, E. Tjukanov, M. Krusius, and S. Jaakkola, Phys. Rev. B **36**, 6837 (1987).

[50] E. Tjukanov, A. Y. Katunin, A. I. Safonov, P. Arvela, M. Karhunen, B. G. Lazarev, G. V. Shlyapnikov, I. I. Lukashevich, and S. Jaakkola, Physica B **178**, 129 (1992).

[51] H. F. Hess, G. P. Kochanski, J. M. Doyle, N. Masuhara, D. Kleppner, and T. J. Greytak, Phys. Rev. Lett. **59**, 672 (1987).

[52] R. van Roijen, J. J. Berkhout, S. Jaakkola, and J. T. M. Walraven, Phys. Rev. Lett. **61**, 931 (1988).

[53] N. Masuhara, J. M. Doyle, J. C. Sandberg, D. Kleppner, T. J. Greytak, H. F. Hess, and G. P. Kochanski, Phys. Rev. Lett. **61**, 935 (1988).

[54] J. M. Doyle, J. C. Sandberg, I. A. Yu, C. L. Cesar, D. Kleppner, and T. J. Greytak, Phys. Rev. Lett. **67**, 603 (1991).

[55] O. J. Luiten, H. G. C. Werij, I. D. Setija, M. W. Reynolds, T. W. Hijmans, and J. T. M. Walraven, Phys. Rev. Lett. **70**, 544 (1993).

[56] I. F. Silvera and M. Reynolds, J. Low Temp. Phys. **87**, 343 (1992).

[57] I. F. Silvera, J. Low Temp. Phys. **89**, 287 (1992).

[58] J. D. Gillaspy, I. F. Silvera, and J. S. Brooks, Phys. Rev. B **38**, 9231 (1988).

[59] J. D. Gillaspy, I. F. Silvera, and J. S. Brooks, Phys. Rev. B **40**, 210 (1989).

[60] Y. Kagan, I. A. Vartanyants, and G. V. Shlyapnikov, Zh. Eksp. Teor. Fiz. **81**, 1113 (1981) [Sov. Phys. JETP **54**, 590 (1981)].

[61] L. P. H. de Goey, J. P. J. Driessen, B. J. Verhaar, and J. T. M. Walraven, Phys. Rev. Lett. **53**, 1919 (1984).

[62] L. P. H. de Goey, T. H. M. v. d. Berg, N. Mulders, H. T. C. Stoof, B. J. Verhaar, and W. Glöckle, Phys. Rev. B **34**, 6183 (1986).

[63] L. P. H. de Goey, H. T. C. Stoof, B. J. Verhaar, and W. Glöckle, Phys. Rev. B **38**, 646 (1988).

[64] L. P. H. de Goey, H. T. C. Stoof, J. M. V. A. Koelman, B. J. Verhaar, and J. T. M. Walraven, Phys. Rev. B **38**, 11500 (1988).

[65] L. P. H. de Goey, Ph.D. thesis, Eindhoven University of Technology, The Netherlands, 1988.

[66] H. T. C. Stoof, L. P. H. de Goey, B. J. Verhaar, and W. Glöckle, Phys. Rev. B **38**, 11221 (1988).

[67] H. T. C. Stoof, B. J. Verhaar, L. P. H. de Goey, and W. Glöckle, Phys. Rev. B **40**, 9176 (1989).

[68] H. T. C. Stoof, Ph.D. thesis, Eindhoven University of Technology, The Netherlands, 1989.

[69] W. Glöckle and R. Offermann, Phys. Rev. C **16**, 2039 (1977).

[70] A. C. Maan, B. J. Verhaar, H. T. C. Stoof, and W. Glöckle, Phys. Rev. C (to be published).

[71] W. M. Kloet and J. A. Tjon, Ann. Phys. (N.Y.) **79**, 407 (1973).

[72] G. L. Payne, J. L. Friar, and B. F. Gibson, Phys. Rev. C **26**, 1385 (1982).

[73] G. L. Payne, W. H. Klink, W. N. Polyzou, J. L. Friar, and B. F. Gibson, Phys. Rev. C **30**, 1132 (1984).

Chapter 2

Cryogenic H maser in a strong B field

Abstract

We study the spin-exchange frequency shift of the cryogenic hydrogen maser for $B \neq 0$. A general expression is derived in terms of populations of ground-state hyperfine levels. The coefficients in this expression are calculated in the degenerate-internal-states approximation, as well as to first order in the hyperfine plus Zeeman splitting. Numerical results are compared with rigorous coupled-channel calculations. Some implications are pointed out for the frequency stability of the H maser in a magnetic field.

2.1 Introduction

Almost thirty years after its first realization by Goldenberg, Kleppner, and Ramsey [1], the hydrogen maser continues to be the most stable of all frequency standards. For measuring times of about 1 h the relative frequency instability is observed to be below one part in 10^{15}. This extreme stability makes the hydrogen maser a very valuable research tool in fields as diverse as physics, astronomy, geodesy, and metrology.

As pointed out a decade ago [2],[3], a hydrogen maser operating at liquid-helium temperature would have an even better frequency stability. This is mainly due to the much smaller collisional line broadening at lower temperatures, allowing for a larger

radiating atom density, and hence for a larger radiated power without increasing the atomic linewidth above the room-temperature value. Furthermore, lower temperatures also increase the signal-to-noise ratio by decreasing thermal noise, and help to get a better control of the cavity resonance frequency. A third advantage is the possibility at sub-Kelvin temperatures to use a very reproducible wall coating of superfluid helium, with an associated wall frequency shift going through a minimum at $T = 0.52$ K [4], which produces a very high thermal stability. Berlinsky and Hardy [5] predicted that with such types of cryogenic hydrogen masers an improvement in frequency stability of more than two orders of magnitude over that of a room-temperature hydrogen maser should be realizable.

Up until now we did not mention the frequency shifts due to collisions between hydrogen atoms. Analysis of the effect of spin-exchange collisions [6] showed that they shift the maser frequency in the same way as cavity pulling does: via a proportionality to the atomic linewidth. This opens the possibility to tune the cavity such that cavity pulling and spin-exchange frequency shifts compensate one another. The above-mentioned papers, however, all ignored the effect of the hyperfine energy-level separation during the collisions, which is an essential omission in the case of cryogenic H masers as was shown in two more recent papers [7],[8]. The effect of the hyperfine interaction during collisions introduces large frequency shifts which cannot be eliminated by the above spin-exchange cavity tuning method and strongly limit the achievable stability. For a survey of the present experimental and theoretical situation we refer to Ref. [9].

In this paper we investigate the magnetic field dependence of the spin-exchange frequency shift in the H maser. This may be of interest for experiments in which the H maser is operated in a much stronger field than usual. In this context one could think in the first place of attempts to improve the frequency stability by eliminating the hyperfine-induced shift. For this application it would be essential that persistent-current solenoids and superconducting magnetic shields make it possible to operate at a much stronger constant field than usual, outside the extreme low-B regime where the first-order fluctuations of transition frequency with B vanish. It is outside the scope of the present paper to discuss the technical possibilities to keep a magnetic field of, for instance, 0.05 T stable to within a required relative variation of 10^{-18}. We confine ourselves to the question whether a magnetic field might eliminate the "dangerous" terms in the

hyperfine-induced spin-exchange frequency shift. To that end it is necessary to derive the dependence of this shift on the partial densities of the four $1s$ hyperfine levels. At first sight it does not look improbable that such an elimination might succeed. Introducing a magnetic field of the order of 0.05 T changes the hyperfine spin wave functions and thus the collision amplitudes significantly. In addition, we will see that the symmetry lost in a collision by $B \neq 0$ introduces contributions from inelastic elements to the frequency shift besides the elastic S-matrix elements, which already play a role for $B = 0$.

A second application is the present experimental activity in measuring the various contributions to the spin-exchange frequency shift. Experimental groups are interested in measuring them as a function of various experimental parameters, in particular, the atomic density in the storage bulb, to compare them with theoretical predictions but also to provide information on the population dynamics in the H maser, which is of interest for the sight into its operation. Extension of such measurements and analyses to $B \neq 0$ would enlarge the scope of present experiments. The introduction of a stronger magnetic field not only influences the collisional frequency shift, but has also a more direct influence on the maser operation, for instance, on the maser oscillation condition.

A third type of application is associated with the use of the H maser as a precision instrument enabling one to measure very sensitively certain phenomena in atomic hydrogen gas. For some of these phenomena it may be desirable or even essential to operate the maser at stronger B fields. In this context one could think of the possibility to detect bulk or surface spin waves [10], as well as possibilities for measuring magnon effects [11] by means of the cryogenic H maser.

This paper is organized as follows. In Sec. 2.2 we derive the general expression for the $B \neq 0$ spin-exchange frequency shift starting from the quantum Boltzmann equation. In Sec. 2.3 we evaluate the various terms of zeroth and first order in the hyperfine level splitting by an extension of the existing method for $B = 0$. In Sec. 2.4 we present numerical results of this approach and of the rigorous coupled-channel method and discuss their application to the H maser. Some conclusions will be given in Sec. 2.5.

2.2   Spin-exchange frequency shift for $B \neq 0$

We start from the evolution equation [7],[8] for the one-atom spin-density matrix

$$\frac{d}{dt}\rho_{\kappa\kappa'} + \frac{i}{\hbar}(\epsilon_\kappa - \epsilon_{\kappa'})\rho_{\kappa\kappa'} \;=\; \dot{\rho}_{\kappa\kappa'}|_{\text{rad}} + \dot{\rho}_{\kappa\kappa'}|_0 + \dot{\rho}_{\kappa\kappa'}|_c \,. \tag{2.1}$$

The Greek subscripts take values a, b, c, and d, the ground-state hyperfine levels in order of increasing energy ϵ_α. The first term on the right-hand side is the radiation term resulting from the interaction of the atomic magnetic moments with the rf cavity magnetic field. The second term represents all one-atom terms such as wall collisions, finite cavity residence time, and interactions with magnetic field inhomogeneities. The third term, the collision term, is the primary point of interest in this paper. We are interested in a situation where the cavity mode is almost resonant with a particular transition $\kappa \rightarrow \kappa'$. For the corresponding density-matrix element the one-atom and collision terms then have the form

$$\dot{\rho}_{\kappa\kappa'}|_0 \;=\; -[(1/T_2)_0 - i\delta\omega_0]\rho_{\kappa\kappa'} \,, \tag{2.2}$$

$$\dot{\rho}_{\kappa\kappa'}|_c \;=\; n_H \rho_{\kappa\kappa'} \sum_\nu \rho_{\nu\nu} \sum_\lambda [(1+\delta_{\kappa\lambda})(1+\delta_{\kappa'\lambda})(1+\delta_{\kappa\nu})(1+\delta_{\kappa'\nu})]^{1/2}$$
$$\times \langle v\sigma_{\kappa\kappa',\nu\rightarrow\lambda}\rangle_{\text{th}} \,, \tag{2.3}$$

in which off-resonant terms have been omitted. The complex coefficient $(1/T_2)_0 - i\delta\omega_0$ generally depends in a complicated way on the values of the diagonal density-matrix elements $\rho_{\nu\nu}$, but is independent of $\rho_{\kappa\kappa'}$. The complex "cross sections" $\sigma_{\kappa\kappa',\nu\rightarrow\lambda}$ describe the contribution of collisions in which a ν-state atom makes a transition to the λ state in colliding with an atom which is in a coherent superposition of the κ and κ' states:

$$\sigma_{\kappa\kappa',\nu\rightarrow\lambda} \;=\; \frac{\pi}{k^2}\sum_l (2l+1)[S^l_{\{\kappa\lambda\},\{\kappa\nu\}}S^{l*}_{\{\kappa'\lambda\},\{\kappa'\nu\}} - \delta_{\lambda\nu}] \,. \tag{2.4}$$

In this equation Greek subscripts between brackets are a shorthand notation for normalized symmetric (antisymmetric) two-body spin states for even (odd) partial wave l. The S-matrix elements are to be calculated for a common relative kinetic energy $E_k = \hbar^2 k^2/m_H$ in the entrance channels $\{\kappa\nu\}$ and $\{\kappa'\nu\}$. The brackets $\langle\,\rangle_{\text{th}}$ in Eq. (2.3) denote thermal averaging.

The calculation of the collision term is based on a two-atom Hamiltonian containing, in addition to the central interaction and hyperfine interactions already included [7],[8]

for $B = 0$, the Zeeman term

$$V^Z = [\mu_e(\sigma_{e1} + \sigma_{e2}) - \mu_p(\sigma_{p1} + \sigma_{p2})] \cdot \mathbf{B}, \qquad (2.5)$$

with μ_e (μ_p) the electron (proton) magnetic moment and σ the Pauli spin vector. Magnetic dipolar interactions are again negligible. The collision problem has SO(3)$_{\text{orbit}}$×SO(2)$_{\text{spin}}$ as a symmetry group, i.e., the direct product of the three-dimensional orbital rotation group and the two-dimensional spin rotation group about the z axis ($\|\mathbf{B}$). Due to SO(3) orbital symmetry the S matrix is diagonal in the relative orbital angular momentum quantum numbers l and m_l, and independent of m_l. This is taken into account in the notation of Eq. (2.4). Due to SO(2)$_{\text{spin}}$ symmetry the total spin magnetic quantum number is conserved. Consequently, for odd l only elastic S-matrix elements play a role in Eq. (2.4), i.e., $ab \rightarrow ab$, $cb \rightarrow cb$, $ad \rightarrow ad$, and $cd \rightarrow cd$, the same combinations as for $B = 0$ but with $B \neq 0$ values. For even l we have the elastic elements for $aa \rightarrow aa$, $ac \rightarrow ac$, and $cc \rightarrow cc$, and the inelastic elements for $aa \leftrightarrow ac$ and $ac \leftrightarrow cc$. The latter were absent for $B = 0$ for reasons of symmetry: under a combined 180° rotation of the electron and proton spins of a single atom about an axis in the xy plane $|a\rangle \rightarrow |a\rangle$ and $|c\rangle \rightarrow -|c\rangle$, so that $|aa\rangle$ and $|cc\rangle$ are invariant and $|\{ac\}\rangle \rightarrow -|\{ac\}\rangle$. Note that by the same argument the equality of the $B = 0$ elastic S-matrix elements for ab and ad and for cb and cd is lost for $B \neq 0$.

We now concentrate on the experimental situation in which $\kappa\kappa' = ac$. Substituting

$$\rho_{ac}(t) = \rho_{ac}(0)\exp[i(\epsilon_c - \epsilon_a)/\hbar + i\delta\omega - 1/T_2]t \qquad (2.6)$$

in Eq. (2.1), we find without radiation term the total frequency shift and total atomic linewidth

$$\delta\omega = \delta\omega_0 + \delta\omega_c, \qquad (2.7)$$

$$1/T_2 = (1/T_2)_0 + (1/T_2)_c. \qquad (2.8)$$

Here the collisional contributions are related to the cross sections by

$$\delta\omega_c = n_H\langle v\rangle[(\rho_{cc} - \rho_{aa})\bar\lambda_0 + (\rho_{cc} + \rho_{aa})\bar\lambda_1 + \bar\lambda_2 + (\rho_{dd} - \rho_{bb})\bar\lambda_3], \quad (2.9)$$

$$(1/T_2)_c = n_H\langle v\rangle[(\rho_{cc} - \rho_{aa})\bar\sigma_0 + (\rho_{cc} + \rho_{aa})\bar\sigma_1 + \bar\sigma_2 + (\rho_{dd} - \rho_{bb})\bar\sigma_3], \quad (2.10)$$

with

$$i\lambda_0 - \sigma_0 = \sigma_{ac,c\to c} - \sigma_{ac,a\to a} - \sigma_{ac,a\to c} + \sigma_{ac,c\to a} ,$$

$$i\lambda_1 - \sigma_1 = \sigma_{ac,c\to c} + \sigma_{ac,a\to a} + \sigma_{ac,a\to c} + \sigma_{ac,c\to a}$$

$$\qquad\qquad -\tfrac{1}{2}\sigma_{ac,b\to b} - \tfrac{1}{2}\sigma_{ac,d\to d} , \qquad\qquad (2.11)$$

$$i\lambda_2 - \sigma_2 = \tfrac{1}{2}\sigma_{ac,d\to d} + \tfrac{1}{2}\sigma_{ac,b\to b} ,$$

$$i\lambda_3 - \sigma_3 = \tfrac{1}{2}\sigma_{ac,d\to d} - \tfrac{1}{2}\sigma_{ac,b\to b} .$$

Note that the new $\rho_{dd} - \rho_{bb}$ terms arise because of the above-mentioned loss of symmetry.

2.3 Collisional shift and broadening

Apparently, the collisional frequency shift and line broadening can be determined once the S matrix has been calculated. As for $B = 0$, this has been done both by the coupled-channel method and by approximate methods. We refer to Refs. [7] and [8] for a description of the coupled-channel method as applied to the H maser.

2.3.1 Degenerate internal states

The calculation is much easier when energy differences of internal states are neglected. The advantage of this approximation is that the internal atomic Hamiltonian reduces effectively to a constant times the unit operator. Using this, one can turn to a new basis of internal states to simplify the collision problem, i.e., the internal basis with total electron and proton spin quantum numbers $S M_S I M_I$, which diagonalizes the interatomic interaction. With respect to this basis the coupled-channel problem reduces to a simple potential-scattering problem for singlet and triplet scattering separately.

For $B = 0$ this approximation was relatively straightforward to apply. In Refs. [7] and [8] we obtained results in agreement with expressions obtained previously [6]. It is less trivial how the approximation is to be applied most effectively to the inelastic processes for $B \neq 0$. We have shown previously [12],[13] that spin-exchange and dipolar transitions in H + H scattering in the sub-Kelvin regime can be described very successfully if one does not replace an S-matrix element as a whole by its value for degenerate internal states (DIS), but rather a related quantity: one first splits off

two factors depending on initial and final channel wave numbers and subsequently approximates the remaining quantity by its value for degenerate internal states, i.e., equal wave numbers in all channels. Simple expressions in terms of scattering lengths, but still rather accurate for low energies, are obtained by calculating the remaining quantity in the zero-energy limit (vanishing wave numbers). For somewhat higher energies accurate agreement with coupled-channel values is obtained by taking the collision energy equal to the average of initial and final relative kinetic energies. Recently we applied the same so-called DIS method to the scattering of dressed H atoms in a microwave trap [14] and to the reflection of H atoms from a superfluid ^{4}He surface [15].

As an example we give the S-matrix element for the $ac \rightarrow aa$ transition (even l),

$$S^l_{aa,\{ac\}} = (k_{aa}k_{ac}/\bar{k}^2)^{l+1/2}\tfrac{1}{8}\sqrt{2}\sin4\theta(\exp2i\delta^l_T - \exp2i\delta^l_S). \tag{2.12}$$

In this expression k_{ac} (k_{aa}) is the initial (final) wave number, $\bar{k}$ is their "average," δ_T (δ_S) is the triplet (singlet) scattering phase, and θ is the usual B-dependent angle characterizing the hyperfine states

$$\theta = \tfrac{1}{2}\arctan B_0/B, \quad B_0 = \tfrac{1}{2}a/(\mu_e + \mu_p), \quad 0 < \theta \le \frac{\pi}{4}. \tag{2.13}$$

Making use of such expressions the λ_i and σ_i cross sections are easily obtained,

$$\lambda_0^{(\mathrm{DIS})} = \frac{\pi}{2k^2}(1 - 3\cos^2 2\theta) \sum_{l\,\mathrm{even}} (2l + 1)\sin2\Delta\delta^l,$$

$$\lambda_1^{(\mathrm{DIS})} = \lambda_2^{(\mathrm{DIS})} = 0,$$

$$\lambda_3^{(\mathrm{DIS})} = -\frac{\pi}{k^2}\cos2\theta \sum_{l\,\mathrm{odd}} (2l + 1)\sin2\Delta\delta^l,$$

$$\sigma_0^{(\mathrm{DIS})} = \frac{\pi}{8k^2}\sin^2 4\theta \sum_{l\,\mathrm{even}} (2l + 1)\chi^l_-, \tag{2.14}$$

$$\sigma_1^{(\mathrm{DIS})} = \frac{\pi}{k^2} \sum_{l\,\mathrm{even}} (2l + 1)[(1 + \cos^2 2\theta)\sin^2\Delta\delta^l + \tfrac{1}{8}\sin^2 4\theta\chi^l_+]$$
$$\qquad\qquad - \frac{\pi}{k^2}\sum_{l\,\mathrm{odd}}(2l + 1)(1 + \cos^2 2\theta)\sin^2\Delta\delta^l,$$

$$\sigma_2^{(\mathrm{DIS})} = \frac{\pi}{k^2}\sum_{l\,\mathrm{odd}}(2l + 1)(1 + \cos^2 2\theta)\sin^2\Delta\delta^l,$$

$$\sigma_3^{(\mathrm{DIS})} = 0,$$

in which $\Delta\delta^l$ stands for $\delta^l_T - \delta^l_S$ and the χ coefficients for

$$\chi_+^l(k) = (kk_>/\bar{k}_>^2)^{2l+1}\sin^2\Delta\delta_>^l + (kk_</\bar{k}_<^2)^{2l+1}\sin^2\Delta\delta_<^l$$
$$- 2\sin^2\Delta\delta^l, \tag{2.15}$$
$$\chi_-^l(k) = (kk_>/\bar{k}_>^2)^{2l+1}\sin^2\Delta\delta_>^l - (kk_</\bar{k}_<^2)^{2l+1}\sin^2\Delta\delta_<^l.$$

In these expressions k is the wave number in the entrance channel, $k_>$ is a larger wave number obtained by adding the a-c level splitting at the magnetic field strength considered to the initial relative kinetic energy, and $k_<$ is a similar wave number found by subtracting the same splitting. Furthermore, $\bar{k}_>$ and $\bar{k}_<$ are wave numbers corresponding to averaged initial and final kinetic energies. Finally, $\Delta\delta_>^l$ and $\Delta\delta_<^l$ are the $\Delta\delta^l$ phase differences at the average wave numbers $\bar{k}_>$ and $\bar{k}_<$.

Apparently, $\lambda_1^{(\text{DIS})}$ and $\lambda_2^{(\text{DIS})}$ vanish as for $B = 0$. This is a central conclusion of the present paper. For $B = 0$ we obtained dangerous λ_1 and λ_2 terms only as a correction of first order in the hyperfine level splitting. Nonvanishing values of $\lambda_1^{(\text{DIS})}$ and $\lambda_2^{(\text{DIS})}$ for $B \neq 0$ would have implied the possibility of a drastic change of these parameters already upon application of a weak magnetic field and hence, in principle, the possibility of a vanishing or density independent frequency stability parameter [7] Ω. On the basis of the above-mentioned result we can only expect a nonvanishing value of λ_1 and λ_2 for $B \neq 0$ in first order in the hyperfine level splitting. Intuitively, one thus expects that the purpose of eliminating the effect of the dangerous terms can only be achieved with stronger B fields at least of order $B_0 \simeq 50.7$ mT.

One can understand the vanishing values of $\lambda_1^{(\text{DIS})}$ and $\lambda_2^{(\text{DIS})}$ on the basis of a symmetry argument. Since the DIS two-body Hamiltonian no longer contains the two proton spins, one can carry out the above 180° rotations for electrons and protons about perpendicular axes in the xy plane. This induces the transformations $|a\rangle \to i|c\rangle$, $|c\rangle \to -i|a\rangle$, $|b\rangle \to i|d\rangle$, and $|d\rangle \to -i|b\rangle$, so that $|aa\rangle \to -|cc\rangle$, etc. As a consequence, the cross sections $\sigma_{ac,a\to a}$ and $\sigma_{ac,c\to c}$ are complex conjugated, as are $\sigma_{ac,b\to b}$ and $\sigma_{ac,d\to d}$, while $\sigma_{ac,a\to c}$ and $\sigma_{ac,c\to a}$ are real. By the same symmetry argument $\sigma_3^{(\text{DIS})} = 0$.

2.3.2 First-order correction

The vanishing values of λ_1 and λ_2 for degenerate internal states prompt us to resort to a more rigorous approach for gaining insight into the $B \neq 0$ frequency stability. This leads

us to calculate first-order corrections in the hyperfine level splittings. As pointed out in Refs. [7] and [8], these cannot be calculated by straightforward first-order perturbation theory, i.e., the Born approximation: The perturbation $V^{hf} + V^Z - \bar{\epsilon}$, in which $\bar{\epsilon}$ is the average internal energy, does not fall off with interatomic distance, so that distorted-wave Born integrals do not converge. We have shown that a first-order method previously devised for nuclear reactions [16] can also be applied successfully to individual partial waves in sub-Kelvin H + H elastic scattering. In this paper we have to deal also with inelastic S-matrix elements, i.e., we would like to dispose of a first-order correction to the above-mentioned DIS approximation. The following elegant expression can be derived [17]:

$$
\begin{aligned}
\Delta S^l_{\{\alpha'\beta'\},\{\alpha\beta\}} &= (k_{\alpha'\beta'}k_{\alpha\beta}/\bar{k}^2)^{l+1/2} \\
&\times \langle\{\alpha'\beta'\}|(P_T - P_S)(V^{hf} + V^Z - \bar{\epsilon})(P_T - P_S)|\{\alpha\beta\}\rangle \\
&\times \Delta^l(\bar{k}),
\end{aligned}
\tag{2.16}
$$

where

$$
\begin{aligned}
\Delta^l(\bar{k}) &= \frac{i}{4}\frac{m_H}{\hbar}\left[\int_0^{r_0}(u_T^{l(0)} - u_S^{l(0)})^2 dr\right. \\
&\left. + \frac{1}{2\bar{k}}(S_T^{l(0)} - S_S^{l(0)})^2 W_r\left[O_l(\bar{k},r), \frac{\partial}{\partial\bar{k}}O_l(\bar{k},r)\right]\right].
\end{aligned}
\tag{2.17}
$$

For the notation we refer to Refs. [7] and [8]. The integral term in Eq. (2.17) is the Born-type integral that would have been obtained with a perturbation $V^{hf} + V^Z - \bar{\epsilon}$ confined to a sphere with radius r_0 in relative orbital space, enclosing the range of the central interaction $V^c(r)$. The Wronskian surface term takes into account the effect of the perturbation outside this sphere.

As an example we give the expression for one of the inelastic S-matrix elements, corresponding to the zeroth-order equation (2.12),

$$
\Delta S^l_{aa,\{ac\}} = (k_{aa}k_{ac}/\bar{k}^2)^{l+1/2}\frac{1}{8}\sqrt{2}\sin 4\theta\frac{2\epsilon_a - \epsilon_b - \epsilon_d}{\hbar}\Delta^l(\bar{k}).
\tag{2.18}
$$

Making use of such expressions we find the hyperfine-plus-Zeeman-induced frequency-shift parameters

$$\Delta\lambda_0 \;=\; \frac{\pi a}{\hbar k^2}\sum_{l\;\text{even}}(2l+1)[(\tfrac{1}{2}-\tfrac{3}{2}\cos^2 2\theta)\mathrm{Im}\xi_T^l - \tfrac{1}{4}\sin 2\theta\cos^2 2\theta\mathrm{Im}\eta_-^l]\,,$$

$$\Delta\lambda_1 \;=\; \frac{\pi a}{\hbar k^2}\sum_{l\;\text{odd}}(2l+1)\tfrac{1}{2}\sin 2\theta\mathrm{Im}(\xi_T^l+\xi_S^l)$$

$$\qquad -\frac{\pi a}{\hbar k^2}\sum_{l\;\text{even}}(2l+1)(\sin 2\theta\mathrm{Im}\xi_T^l+\tfrac{1}{4}\sin 2\theta\cos^2 2\theta\mathrm{Im}\eta_+^l)\,,$$

$$\Delta\lambda_2 \;=\; -\frac{\pi a}{\hbar k^2}\sum_{l\;\text{odd}}(2l+1)\tfrac{1}{2}\sin 2\theta\mathrm{Im}(\xi_T^l+\xi_S^l)\,,$$

$$\Delta\lambda_3 \;=\; 0\,, \tag{2.19}$$

$$\Delta\sigma_0 \;=\; \frac{\pi a}{\hbar k^2}\sum_{l\;\text{even}}(2l+1)\sin 2\theta\{\mathrm{Re}\xi_T^l-\tfrac{1}{4}\cos^2 2\theta\mathrm{Re}[2(\xi_T^l-\xi_S^l)+\eta_-^l]\}\,,$$

$$\Delta\sigma_1 \;=\; -\frac{\pi a}{\hbar k^2}\sum_{l\;\text{even}}(2l+1)[(\tfrac{1}{2}+\tfrac{1}{2}\cos^2 2\theta)\mathrm{Re}\xi_T^l+\tfrac{1}{16}\sin^2 4\theta\mathrm{Re}\eta_+^l]\,,$$

$$\Delta\sigma_2 \;=\; 0\,,$$

$$\Delta\sigma_3 \;=\; -\frac{\pi a}{\hbar k^2}\sum_{l\;\text{odd}}(2l+1)\tfrac{1}{4}\sin 4\theta\mathrm{Re}(\xi_T^l-\xi_S^l)\,,$$

in which the shorthand notation

$$\xi_T^l(k) \;=\; \Delta^{l*}(k)e^{2i\delta_T^l(k)} \tag{2.20}$$

has been introduced for triplet scattering and similarly for the singlet case, while

$$\eta_+^l(k) \;=\; (kk_>/\bar{k}_>^2)^{2l+1}[\xi_T^l(\bar{k}_>)-\xi_S^l(\bar{k}_>)]+(kk_</\bar{k}_<^2)^{2l+1}[\xi_T^l(\bar{k}_<)-\xi_S^l(\bar{k}_<)]$$

$$\qquad -2[\xi_T^l(k)-\xi_S^l(k)]\,, \tag{2.21}$$

$$\eta_-^l(k) \;=\; (kk_>/\bar{k}_>^2)^{2l+1}[\xi_T^l(\bar{k}_>)-\xi_S^l(\bar{k}_>)]-(kk_</\bar{k}_<^2)^{2l+1}[\xi_T^l(\bar{k}_<)-\xi_S^l(\bar{k}_<)]\,.$$

2.4   Numerical results and consequences for H maser

The introduction of a strong B field has a number of consequences for the operation of the hydrogen maser which are associated with the dependence of hyperfine spin functions and level splittings on B. In the first place the coupling of the a and c levels due to the interaction with the magnetic field of the radiation mode varies with B. As a consequence, B has a direct influence on the maser operation and in particular on the oscillation condition. This can be derived in complete analogy to the $B=0$ case [18]. The result is

$$\frac{1}{T_1 T_2} \;<\; \frac{n_H V_b Q_c \mu_0 \mu_e^2 \eta(\rho_{cc}-\rho_{aa})_0}{\hbar V_c T_b}\sin^2 2\theta\,, \tag{2.22}$$

where $(\rho_{cc} - \rho_{aa})_0$ characterizes the substate populations for the H atoms entering the cavity. The further notation follows Ref. [18].

A second effect, on which we have concentrated already in the foregoing, is the influence of B on H + H collisions and consequently on hyperfine population dynamics and collisional frequency shift. Elastic S-matrix elements, which already determine this frequency shift for $B = 0$, change considerably by the introduction of a B field of, for instance, 0.05 T. In addition, significant contributions from inelastic transitions are introduced.

We evaluated the above-mentioned DIS frequency parameters corrected to first order for the hyperfine level splitting. The total parameters have also been calculated rigorously using the coupled-channel method. Deviations are expected to occur close to and below inelastic thresholds, for instance, in the aa channel due to the cc channel. As for $B = 0$ [7], discontinuities due to these thresholds are described by the coupled-channel method, but not by the DIS approximation plus first-order correction. Despite these shortcomings, the DIS plus first-order method is very useful because it leads to more explicit expressions, especially with respect to the B dependence, which facilitates qualitative insight. In addition, it serves as an important test case for the coupled-channel calculations.

In Fig. 2.1 we present the λ and σ parameters as a function of B at a fixed collision energy of 0.6 K, as predicted by the coupled-channel calculations. It turns out that the field dependence is remarkably accurately (to the percent level relative to the values at the maxima) described by the simple DIS plus first-order polynomials in $\sin2\theta$ and $\cos2\theta$ of the expressions (2.14) and (2.19). In particular, the $\sin2\theta$ proportionality of λ_1 and λ_2 is fully confirmed, as well as the $1 + \cos^2 2\theta$ dependence of σ_1 and σ_2. It is also of interest to point to the change of sign of λ_0 at $B = 35.9$ mT, due to its $1 - 3\cos^2 2\theta$ field dependence. At this field strength the spin-exchange tuned cavity frequency is expected to be equal to the atomic frequency. We note also that λ_0, λ_3, σ_1, and σ_2 are dominated by their DIS contributions and λ_1, λ_2, and σ_3 by their first-order parts. The σ_0 cross section receives significant contributions from both zeroth- and first-order parts.

The same characteristics are found at higher collision energies. As pointed out previously, for lower collision energies pronounced deviations occur due to thresholds in inelastically coupled channels. The Boltzmann averaged frequency shift parameters at the relevant temperatures $T = 0.52$ K and higher are, however, much less sensitive to

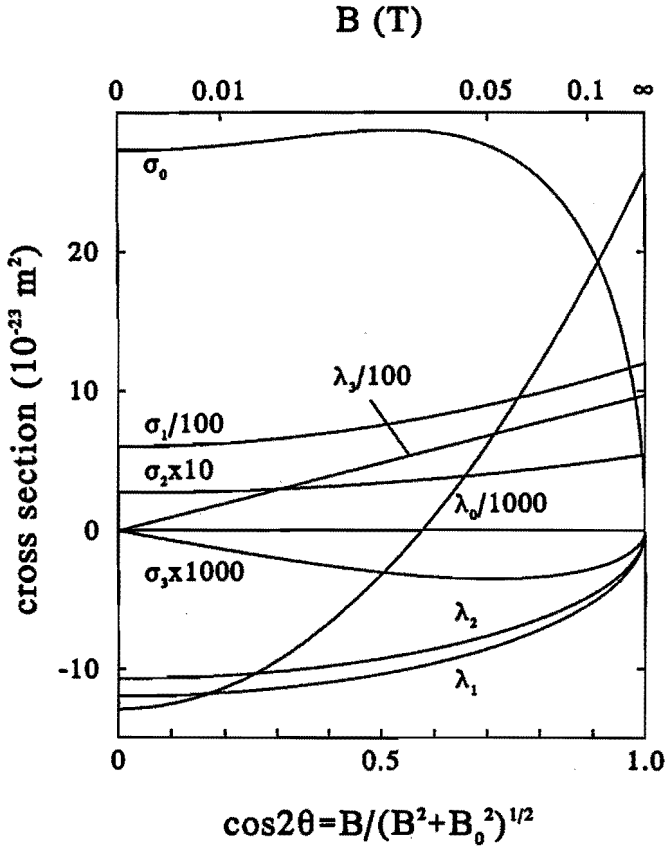Figure 2.1: *Magnetic field dependence of frequency-shift parameters for fixed collision energy 0.6 K.*
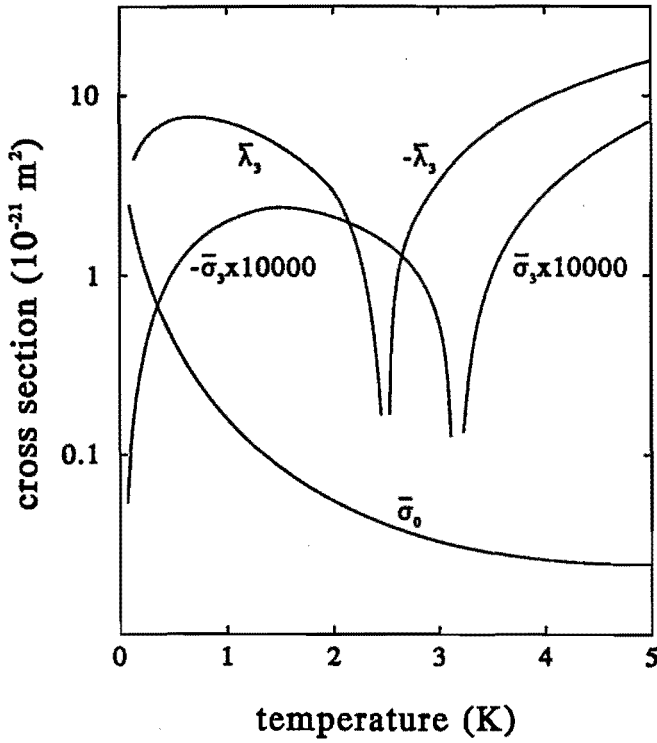
Figure 2.2: Temperature dependence of $\bar{\sigma}_0$, $\bar{\lambda}_3$, and $\bar{\sigma}_3$ for fixed magnetic field $B_0 \simeq 50.7$ mT.

such deviations. Using the simple field dependences, the $\bar{\lambda}_i$ and $\bar{\sigma}_i$ parameters may be expressed simply in their previously given values [7],[8] for $B = 0$, except for $\bar{\sigma}_0$, $\bar{\lambda}_3$, and $\bar{\sigma}_3$. The latter two are "new" parameters, which vanish at $B = 0$. In Fig. 2.2 we give them at $B = B_0 \simeq 50.7$ mT. Values for other fields may be obtained from their field dependences $\cos 2\theta$ and $\sin 4\theta$, respectively. Furthermore, $\bar{\sigma}_0$ can be expressed linearly in terms of its previously given values at $B = 0$ and those at $B = B_0$,

$$\bar{\sigma}_0(B,T) = \bar{\sigma}_0(0,T)\sin 2\theta(1 - 2\cos^2 2\theta) + \bar{\sigma}_0(B_0,T)2\sqrt{2}\sin 2\theta \cos^2 2\theta \,. \quad (2.23)$$

In Fig. 2.2 we also present $\bar{\sigma}_0(B_0,T)$.

We now turn to the implications of a stronger B field for the frequency stability. With present experimental possibilities in connection with hyperfine state selection in H masers it is possible to inject equal populations of the b and d hyperfine levels into the storage bulb. Making use of conservation of the total electronic plus nuclear spin projection along $\mathbf{B}$, one thus expects that the $\rho_{dd} - \rho_{bb}$ term in the frequency shift can be sufficiently eliminated. We are then left with a collisional frequency shift of the form

$$\delta\omega_c = n_H\langle v\rangle[(\rho_{cc} - \rho_{aa})\bar{\lambda}_0 + (\rho_{cc} + \rho_{aa})\bar{\lambda}_1 + \bar{\lambda}_2]\,, \quad (2.24)$$

with coefficients $\bar{\lambda}_i(B,T)$. From a self-consistent calculation of the H-maser oscillation similar to that for $B = 0$, we again find $\rho_{cc} - \rho_{aa}$ to be proportional to the transverse relaxation rate

$$\rho_{cc} - \rho_{aa} = \frac{\hbar V_c(1 + \Delta^2)}{m_H\mu_0(\mu_e + \mu_p)^2\eta Q_c V_b\sin^2 2\theta}T_2^{-1}\,, \quad (2.25)$$

which again contains a B-dependent $\sin^2 2\theta$ factor. For the further notation we refer to Ref. [7]. It follows that the spin-exchange cavity tuning procedure can still be used to eliminate the $\rho_{cc} - \rho_{aa}$ term of the frequency shift. On the basis of the usual very weak magnetic field the remaining frequency shift could not be eliminated by a similar cavity tuning procedure. For the prospects for $B \neq 0$ to be more favorable, it should be possible to write the shift as a linear function of

$$T_2^{-1} = (T_2^{-1})_0 + n_H\langle v\rangle[\bar{\sigma}_1(\rho_{cc} + \rho_{aa}) + \bar{\sigma}_2]\,. \quad (2.26)$$

In this equation we have left out a negligible $\bar{\sigma}_0(\rho_{cc} - \rho_{aa})$ term. Clearly, the remaining collisional frequency shift is insensitive to experimental fluctuations in n_H if the

dimensionless frequency-shift parameter

$$\Omega = -\frac{\bar{\lambda}_1(\rho_{cc} + \rho_{aa}) + \bar{\lambda}_2}{\bar{\sigma}_1(\rho_{cc} + \rho_{aa}) + \bar{\sigma}_2} \tag{2.27}$$

is zero or at least independent of $\rho_{cc} + \rho_{aa}$.

For $B \neq 0$ it follows from Eq. (2.14) that Ω is again a hyperfine splitting induced quantity. From Fig. 2.1 and Refs. [7] and [8] it follows that $\bar{\lambda}_1$ and $\bar{\lambda}_2$ are both negative and $\bar{\sigma}_1$ and $\bar{\sigma}_2$ both positive for all reasonable field strengths, so that a value zero for Ω cannot be expected to be achieved. In fact, because of the similar field dependences of λ_1 and λ_2, and of σ_1 and σ_2, Ω depends on B via a $\sin 2\theta/(1 + \cos^2 2\theta)$ overall factor.

The next-best possibility, an Ω value independent of $\rho_{cc} + \rho_{aa}$, would be possible when for certain B the ratio $\bar{\lambda}_2/\bar{\lambda}_1$ would be equal to $\bar{\sigma}_2/\bar{\sigma}_1$ at $T = 0.52$ K. Since these ratios are in good approximation field independent, this weaker condition is already excluded by our previous $B = 0$ results: $\bar{\sigma}_2/\bar{\sigma}_1$ is at least two orders of magnitude smaller than $\bar{\lambda}_2/\bar{\lambda}_1$. We conclude that a stronger B field does not create new possibilities to eliminate the frequency instability associated with fluctuations in n_H.

2.5 Conclusions

The operation of the (cryogenic) H maser, especially its recent recirculating version, depends on a complicated interplay of hyperfine level occupations and coherences. A valuable source of information on these quantities is the maser oscillation frequency. From its measured value as a function of experimental parameters such as cavity frequency and atomic flux, and using its dependence on level populations it is possible to gain information on the population dynamics. From this point of view it would seem very useful to introduce an external constant magnetic field as an additional experimental parameter to diagnose the population dynamics. In this paper we have predicted the theoretical B dependence of the maser oscillation frequency needed for the above-mentioned analysis. We have derived a $B \neq 0$ expression for the collisional frequency shift in terms of hyperfine level populations. The coefficients $\bar{\lambda}_i$ in this expression, as well as the corresponding quantities $\bar{\sigma}_i$ determining the transverse relaxation rate, have been calculated in zeroth and first order in the hyperfine level splittings, as well as on the basis of the rigorous coupled-channel method.

A second context in which our results might be useful is associated with a possible use of the (cryogenic) hydrogen maser as a precision instrument for measuring specific phenomena in a dilute quantum gas. Insofar as an external magnetic field is essential for such effects, for instance, in the case of nuclear or electronic spin waves in atomic hydrogen, it is essential to understand the influence of a B field on the operation of the H maser.

Finally, we have discussed the implications of our calculated frequency-shift parameters for the frequency stability of the cryogenic H maser. We find that the introduction of a stronger B field does not eliminate the source of frequency instabilities pointed out previously for the conventional setup based on a very weak B field.

Bibliography

[1] H. M. Goldenberg, D. Kleppner, and N. F. Ramsey, Phys. Rev. Lett. **5**, 361 (1960).

[2] S. B. Crampton, W. D. Phillips, and D. Kleppner, Bull. Am. Phys. Soc. **23**, 86 (1978).

[3] R. F. C. Vessot, M. W. Levine, and E. M. Mattison, NASA Technical Memorandum No. 78104, 1978 (unpublished), p. 549.

[4] M. Morrow, R. Jochemsen, A. J. Berlinsky, and W. N. Hardy, Phys. Rev. Lett. **46**, 195 (1981).

[5] A. J. Berlinsky and W. N. Hardy, NASA Conference Publication No. 2220, 1982 (unpublished), p. 547.

[6] L. C. Balling, R. J. Hanson, and F. M. Pipkin, Phys. Rev. **133**, A607 (1964); **135**, AB1 (1964); P. L. Bender, *ibid.* **132**, 2154 (1963); A. C. Allison, Phys. Rev. A **5**, 2695 (1972); A. J. Berlinsky and B. Shizgal, Can. J. Phys. **58**, 881 (1980).

[7] B. J. Verhaar, J. M. V. A. Koelman, H. T. C. Stoof, O. J. Luiten, and S. B. Crampton, Phys. Rev. A **35**, 3825 (1987).

[8] J. M. V. A. Koelman, S. B. Crampton, H. T. C. Stoof, O. J. Luiten, and B. J. Verhaar, Phys. Rev. A **38**, 3535 (1988).

[9] M. D. Hürlimann, W. N. Hardy, M. E. Hayden, and R. W. Cline, in *Proceedings of the Fourth Symposium on Frequency Standards and Metrology, Ancona,* 1988, edited by A. De Marchi (Springer-Verlag, Berlin, 1989), p. 95; W. N. Hardy, M. D. Hürlimann, and R. W. Cline, Jpn. J. Appl. Phys. **26,** 2065 (1987).

[10] I. F. Silvera, R. F. C. Vessot, and R. L. Walsworth (private communication).

[11] E. P. Bashkin, Pis'ma Zh. Eksp. Teor. Fiz. **49,** 320 (1989) [JETP Lett. **49,** 363 (1989)]; (private communication).

[12] H. T. C. Stoof, J. M. V. A. Koelman, and B. J. Verhaar, Phys. Rev. B **38,** 4688 (1988).

[13] J. M. V. A. Koelman, H. T. C. Stoof, B. J. Verhaar, and J. T. M. Walraven, Phys. Rev. Lett. **59,** 676 (1987).

[14] C. C. Agosta, I. F. Silvera, H. T. C. Stoof, and B. J. Verhaar, Phys. Rev. Lett. **62,** 2361 (1989).

[15] E. Tiesinga, H. T. C. Stoof, and B. J. Verhaar, Phys. Rev. B **41,** 8886 (1990).

[16] A. M. Schulte and B. J. Verhaar, Nucl. Phys. A **232,** 215 (1974).

[17] A. C. Maan, H. T. C. Stoof, and B. J. Verhaar (unpublished).

[18] D. Kleppner, H. C. Berg, S. B. Crampton, N. F. Ramsey, R. F. C. Vessot, H. E. Peters, and J. Vanier, Phys. Rev. **138,** A972 (1965); S. B. Crampton, *ibid.* **158,** 57 (1967).

Chapter 3

The surface state hydrogen maser

Abstract

We describe a hydrogen maser operating at very low temperatures in which most of the hydrogen atoms are condensed on a superfluid helium surface in long-lived states. This proposed maser can be used to obtain new information on the properties of the hydrogen-liquid helium surface system. In addition, it promises to be an interesting system from the point of view of nonlinear dynamics. It is found that the surface recombination to molecular hydrogen, which might be considered as undesirable, is actually necessary to achieve the masing conditions. We develop the maser equations and consider a number of realistic conditions for operation.

3.1   Introduction

In this paper we propose a new type of maser, the surface cryogenic hydrogen maser (SCHM), in which the dominant species coupled to the radiation field are the hydrogen atoms condensed on a superfluid helium surface. The SCHM provides a new means of studying hydrogen-surface interactions, as well as an interesting device to study nonlinear dynamic behavior.

Our analysis treats atoms in the volume and surface states on an equal footing, using the Maxwell-Bloch equations coupled with the rate equations for the density of

the hydrogen hyperfine states. We find the unexpected result that recombination of the hydrogen atoms is required to satisfy the masing condition. We analyze a "conventional" mode of operation in which the masing takes place on the a to c transition, shown in the hyperfine diagram, Fig. 3.1. In addition, we consider the unusual operation on the a to b transition in which the population inversion is produced not only by the incoming beam, but also by surface recombination of hydrogen in the cavity. Operating conditions are presented in both cases. Before entering into details of the analysis we present some introductory discussion.

The room temperature atomic hydrogen maser is the most stable time standard currently available for measurement intervals between 1 and 10^4 seconds. More recently a sub-Kelvin version, called a cryogenic hydrogen maser (CHM), has been proposed [1] and constructed [2]. The CHM works in essentially the same manner as the room temperature maser, but has a number of advantages due to the low temperature which promise stability greatly enhanced over that of the room temperature maser. The CHM involves atoms in the cavity volume coupled to the radiation field, but perturbed by the helium surface, resulting in a wall frequency shift which depends on temperature as well as the area to volume ratio. The CHM operates at a temperature of about 500 mK. The SCHM takes advantage of the H-liquid helium adsorption isotherm. By cooling to the 50-100 mK temperature range H atoms populate long-lived surface states. In this regime we find conditions in which the surface plays a more prominent role than that of perturbing the effective volume parameters. In this connection one could think of a situation in which the pulse time in a pulsed oscillation regime [3] is so short that it becomes of the order of the average sticking time of atoms to the surface. In this case surface and volume atoms could have different time-dependent spin behaviors and by enhancing the number of atoms at the surface relative to those in the volume, the surface state atoms dominate the maser behavior. Note that due to the sensitivity to perturbations in between pulses the exact time-dependent spin behavior of surface atoms could already be important for the operation of the CHM in the pulsed regime.

A second motivation for the present research is the possibility to use the dependence of the maser operation on the surface for precision measurements. Partially, this has already been done in CHM experiments in which it has been possible to determine the transition frequency of hydrogen atoms adsorbed at the superfluid helium surface with
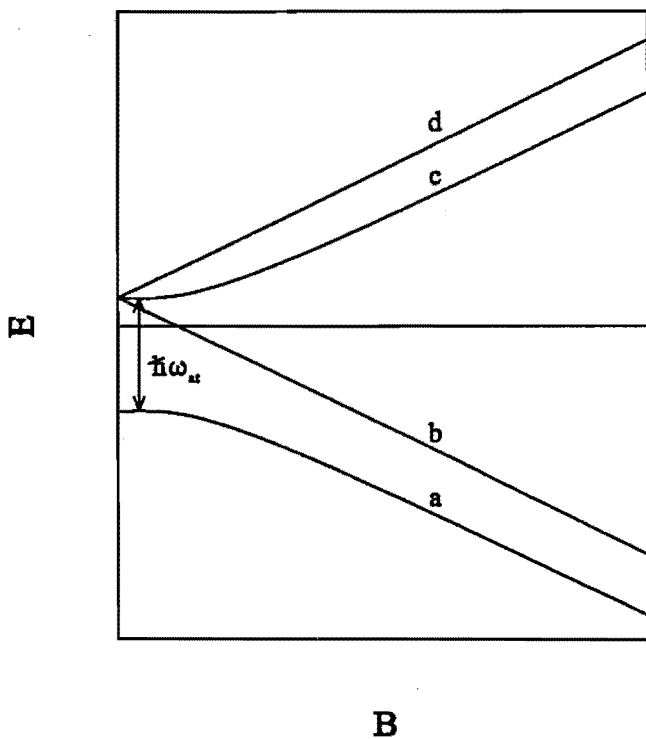
Figure 3.1: Schematic diagram of the energy of the four hyperfine levels of the hydrogen
1s-groundstate as a function of the applied magnetic field. In the "conventional" maser
oscillation takes place between the a and c levels, indicated with an arrow. For the
SCHM the a-b transition is also considered.

great accuracy [4]. One can imagine that in a maser in which the dominant species coupled to the radiation field are hydrogen atoms condensed at the surface, much more information can be obtained about hydrogen-surface interactions, e.g., a new, possibly more accurate, determination of the surface adsorption energy and the influence of dipolar collisions and recombination on the atomic linewidth.

A third motivation for the investigations is the possibility to use the transition frequency of hydrogen atoms adsorbed at the helium surface as the basis for a primary time standard. The wall shift inhibits the use of present hydrogen masers as a primary time standard. In a SCHM one would obviously have to deal with a volume shift. Whereas the wall shift can not be eliminated in the CHM there is every reason to hope that a volume shift can be made arbitrarily small by keeping the atoms at the surface longer, i.e., by lowering the temperature.

In the following, we first generalize the conventional Maxwell-Bloch equations to a combined set of equations for volume and surface in Sec. 3.2. In Sec. 3.3 we show how the usual maser equations and maser parameters follow from the generalized Maxwell-Bloch equations in the limit of small sticking times. In Sec. 3.4 we concentrate on new phenomena both for the traditional scheme in which oscillation takes place between the a and c levels of the hydrogen ground state and for a maser which oscillates between the a and b levels. In Sec. 3.5 we consider some aspects that are related to the experimental realization of the SCHM. Some conclusions are presented in Sec. 3.6.

3.2   Generalized Maxwell-Bloch equations

The usual way to describe the dynamics of the hydrogen maser is by using the Maxwell-Bloch equations

$$\dot{B} = -(\kappa + i\omega_c)B + gM ,$$
$$\dot{M} = -(\gamma_\perp + i\omega_{at})M + gB\Delta ,$$
$$\dot{\Delta} = -\gamma_\parallel(\Delta - \Delta_0) - 2g(BM^* + B^*M) ,$$

(3.1)

for the complex magnetic field B, the complex magnetization M and the population inversion Δ. The field B is normalized so as to equal the square root of the number of photons, whereas $M = N\rho_{ca}$ and $\Delta = N(\rho_{cc} - \rho_{aa})$ in terms of the one-atom spin-density

matrix ρ and the number N of atoms in the storage bulb. The cavity resonance frequency is denoted by ω_c, the atomic transition frequency by ω_{at}, the cavity damping rate by $\kappa = \omega_c/2Q_c = 1/T_c$, with Q_c the quality factor of the cavity, and the damping rates for M and Δ by $\gamma_\perp = 1/T_2$ and $\gamma_\| = 1/T_1$, the transverse and longitudinal relaxation rates. The equilibrium value of Δ in the absence of atom-field interaction is denoted by Δ_0. Finally, the one-photon Rabi frequency g is given by

$$g^2 = \frac{\mu_0(\mu_e + \mu_p)^2 \eta \omega_c}{2\hbar V_c} , \tag{3.2}$$

with V_c the cavity volume, μ_0 the vacuum permeability, μ_e (μ_p) the electron (proton) magnetic moment and η the filling factor.

The atomic transition frequency ω_{at} and the transverse and longitudinal relaxation rates $\gamma_\perp$ and $\gamma_\|$ entering Eqs. (3.1) differ from the values for an unperturbed hydrogen atom due to collisions with other hydrogen atoms and helium atoms and due to the finite residence time in the cavity field. Another effect which influences the frequency and the width of the atomic transition, and which is the primary interest of this paper, is the sticking of atoms to the wall of the storage bulb. The atoms traverse the storage bulb many times before leaving it. Each time an atom hits the wall it has a finite probability to stick. In the case of a sticking event it will desorb after an average time τ_s. The average time τ_s of a sticking event and the average time τ_v between subsequent stickings are given by

$$\frac{1}{\tau_s} = \frac{kT}{2\pi\hbar} s e^{-E_b/kT} , \tag{3.3}$$

$$\frac{1}{\tau_v} = \left(\frac{kT}{2\pi m_H} \right)^{1/2} \frac{A_b}{V_b} s ,$$

where k is Boltzmann's constant, T is the temperature, s ($= 0.33\,\mathrm{K}^{-1}\,T$) is the sticking probability and E_b is the binding energy of hydrogen atoms to the superfluid ^{4}He surface ($E_b = 1.0$ K). The mass of the hydrogen atom is denoted by m_H whereas the surface area of the storage bulb is given by A_b and its volume by V_b. The energy levels of a hydrogen atom bound to the surface will be perturbed due to the interaction with the helium surface which results in a shift of the transition frequency. This means that the transition frequency has two different values, one in the volume and one at the surface.

The net phase effect of two alternating transition frequencies has been discussed by Anderson and Weiss [5] and applied to the hydrogen maser by Morrow and Hardy [6].

The phase shift which the atoms undergo per sticking event due to the difference in atomic transition frequencies is calculated assuming that the sticking time and the time between stickings are distributed according to Poisson statistics. In the usual situation for the cold hydrogen maser the result takes on a particularly simple form. The rapid exchange of atoms among volume and surface states and the very short sticking time compared to the time in the volume result in a shift (wall shift) of the volume frequency due to the influence of the transition frequency at the surface and it is not necessary to deal with the surface atoms explicitly. Consequently, the Maxwell-Bloch equations (3.1) remain valid but with effective values for ω_{at} and $\gamma_\perp$:

$$\omega_{at} = \omega_v + \frac{1}{\tau_v}\frac{\phi_0}{1+\phi_0^2}\,, \tag{3.4}$$

$$\gamma_\perp = \gamma_\perp^v + \frac{1}{\tau_v}\frac{\phi_0^2}{1+\phi_0^2}\,,$$

where ω_v and $\gamma_\perp^v$ are the atomic transition frequency and transverse relaxation rate in the volume and $\phi_0 = \tau_s(\omega_s - \omega_v)$ is the average phase shift per sticking event with ω_s being the atomic transition frequency at the surface.

This approach is valid as long as there is a rapid exchange of atoms between surface and volume and the total time spent at the surface is short compared to the time spent in the volume. This approach also neglects recombination and relaxation effects and any independent interaction with the radiation field during the time that the atoms reside at the surface.

Generalizing the usual derivation [3] of Eqs. (3.1) to the case of a combined system of atoms at the surface and in the volume, we obtain

$$\dot{B} = -(\kappa + i\omega_c)B + g(M^v + M^s)\,,$$

$$\dot{M}^v = -(\gamma_\perp^v + i\omega_v)M^v + gB\Delta^v - \frac{1}{\tau_v}M^v + \frac{1}{\tau_s}M^s\,,$$

$$\dot{M}^s = -(\gamma_\perp^s + i\omega_s)M^s + gB\Delta^s + \frac{1}{\tau_v}M^v - \frac{1}{\tau_s}M^s\,, \tag{3.5}$$

$$\dot{\Delta}^v = -\gamma_\parallel^v(\Delta^v - \Delta_0^v) - 2g(BM^{v*} + B^*M^v) - \frac{1}{\tau_v}\Delta^v + \frac{1}{\tau_s}\Delta^s\,,$$

$$\dot{\Delta}^s = -\gamma_\parallel^s(\Delta^s - \Delta_0^s) - 2g(BM^{s*} + B^*M^s) + \frac{1}{\tau_v}\Delta^v - \frac{1}{\tau_s}\Delta^s\,,$$

with separate quantities M^i and Δ^i ($i = v, s$) for volume and surface. The γ coefficients are the transverse and longitudinal relaxation rates in the volume and at the surface and

the Δ_0 coefficients stand for the equilibrium values of the population inversion in the absence of atom exchange and atom-field interaction.

In order to evaluate possible operating conditions for the SCHM knowledge of the various constants in Eqs. (3.5) is essential. As far as the operation of the hydrogen maser depends on specific device parameters we have assumed values which correspond to the Harvard-Smithsonian CHM [2], except for the area to volume ratio of the storage bulb which we consider to be a free parameter.

The relaxation rates in the volume describe the loss of coherence and population inversion primarily due to atoms leaving the storage bulb and to spin-exchange collisions. We neglect the hyperfine-induced contribution to $\gamma_\perp^v$. Specifically, $\gamma_\parallel^v = \gamma_b + n_v \langle v_v \rangle \bar{\sigma}$ and $\gamma_\perp^v = \gamma_b + \frac{1}{2} n_v \langle v_v \rangle \bar{\sigma}$, where γ_b is the rate at which atoms leave the storage bulb, n_v is the density of atoms in the volume, $\langle v_v \rangle$ is the thermal velocity of atoms in the volume and $\bar{\sigma} \equiv \langle v_v \sigma_c \rangle / \langle v_v \rangle$, with σ_c the spin-exchange cross section. We take γ_b to be proportional to $\sqrt{T}$ with the value 0.2 s^{-1} at $T = 0.5$ K and for $\bar{\sigma}$ we take a constant value of $8 \cdot 10^{-17}$ cm^2 [7] in the temperature range under consideration, using $\rho_{cc} + \rho_{aa} = \rho_{bb} + \rho_{dd} = \frac{1}{2}$. The equilibrium value of the population inversion in the volume is determined by the influx of atoms into the storage bulb and by collisions, $\gamma_\parallel^v \Delta_0^v = I(\rho_{cc} - \rho_{aa})_{\text{entr}} + n_v \langle v_v \rangle \bar{\sigma} \Delta_c^v$, with I the flux of atoms into the storage bulb, $(\rho_{cc} - \rho_{aa})_{\text{entr}} = \frac{1}{2}$ the population inversion of these atoms and Δ_c^v determined by the thermal Boltzmann distribution.

As the direct in- and outflow of atoms is absent at the surface, the relaxation rates and the equilibrium value of the population inversion at the surface are primarily determined by collisions. In analogy with the volume parameters we have $\gamma_\parallel^s = \sigma \langle v_s \rangle \bar{l}$ and $\gamma_\perp^s = \frac{1}{2} \sigma \langle v_s \rangle \bar{l}$, with σ the number of atoms at the surface per cm^2, $\langle v_s \rangle$ the thermal velocity of atoms at the surface and $\bar{l}$ the thermally averaged collisional cross length. We take this cross length as a sum of contributions from recombination and from two-body scattering due to the spin-exchange potential and the dipole-dipole interaction. For the recombination contribution to $\bar{l}$ we take the value $3 \cdot 10^{-9}$ cm [8]. Calculations for the spin-exchange contribution neglecting motion perpendicular to the surface [9] and order of magnitude estimates for the dipolar contribution [8],[10] indicate that these are at most equally important. The product $\gamma_\parallel^s \Delta_0^s$ is a sum of $\gamma \Delta$ products from the above processes. The Δ value associated with recombination vanishes, while the

spin-exchange and dipole-dipole contributions have Boltzmann equilibrium values. It should be noted that the above-mentioned parameter choices are partly based on order of magnitude estimates. The existing theoretical description of two-body exchange and dipolar collisions and two-body recombination at the surface is still rather incomplete. The determination of actual experimental SCHM operating parameters will be a very welcome addition to the available knowledge of the properties of the hydrogen-surface system.

In the a-c maser both Δ_0^v and Δ_0^s decrease due to collisions. In a maser based on the a to b transition, however, one has the interesting situation that preferential relaxation and recombination of the a-state atoms increase the population inversion, which facilitates maser oscillation. This effect will be dealt with in Sec. 3.4. The remaining parameters in Eqs. (3.5) are of the same order of magnitude for the a-b maser as for the a-c maser.

Note that in the derivation of Eqs. (3.5) it was tacitly assumed that the total number of atoms in the volume (N_v) and at the surface (N_s) are constant. If this restriction is relaxed, Eqs. (3.5) have to be supplemented with additional equations for the time dependence of N_v and N_s.

Taking into account the persistent problem from dipolar relaxation in experiments with hydrogen on a helium film, one would expect that the dipolar interaction would also affect the performance of a surface maser drastically. One should, however, keep in mind some differences with the more usual situation of gas samples which are almost completely doubly polarized (H↓⇂ or (H↑↾). Whereas for the latter dipolar relaxation dominates over the direct surface recombination, the situation is different in both the a-c and a-b surface maser because of the large fraction of a-state atoms. Two different processes have to be distinguished, i.e., the loss of coherence and population inversion due to hyperfine state changing collisions and the loss of coherence due to the phase which the oscillating magnetic dipole moment acquires during an elastic dipolar collision. Since we are considering zero magnetic field the dipolar interactions are dominated by the electron spins. This might suggest a large contribution to $\gamma_\parallel^s$ and $\gamma_\perp^s$. However, at zero magnetic field also the recombination rate is large. The magnitude of the dipolar T_1^{-1} and T_2^{-1} due to hyperfine state changing collisions turns out to be negligible compared to the recombination contribution [8] under the conditions considered (ρ_{cc} (ρ_{bb}) $\simeq \rho_{aa}$). This is not necessarily true for the second process mentioned above, i.e., the change of

phase of the oscillating magnetic dipole moment in the magnetic field of a neighboring atom. However, in the case of the a-b maser one can choose a setup based on including in the storage volume a configuration of very smooth plates analogous to that used in Ref. [11], so that variations in the orientation of the surface normal would be negligible producing a single atomic transition frequency at the surface. The dipolar width of the order of 10^5-10^6 Hz, observed in Ref. [10], would be reduced by the 10^5 times lower surface densities (see later) to a value of at most the same order as the recombination T_2^{-1}, given above. In the case of the a-c maser an average dipolar field would be absent if $\rho_{bb} = \rho_{dd}$.

3.3 The influence of the surface for short sticking times

Under the usual operating conditions of the sub-Kelvin hydrogen maser the atoms spend most of their time in the volume and τ_s is by far the shortest time constant in Eqs. (3.5). A treatment in which τ_s is considered as a small parameter therefore seems to be appropriate. However, even for short sticking times the dephasing at the surface can be considerable due to the large difference between ω_v and ω_s. In view of this we eliminate a rapid time dependence $\exp - i\omega_v t$, introduce the reduced time $\bar{t} = t/\tau_s$ and transform to quantities $\bar{M}$ and $\bar{\Delta}$, which can take on the maximum value 1,

$$\bar{B} = Be^{i\omega_v t}, \quad \bar{M}^i = M^i e^{i\omega_v t}/N_i, \quad \bar{\Delta}^i = \Delta^i/N_i, \quad (i = v, s), \quad (3.6)$$

with $N_s/N_v = \tau_s/\tau_v$. By a standard two-times approach [12] we find the rapid changes by leaving out all terms containing τ_s, except ϕ_0. On the time scale τ_s we thus find that $\bar{B}$, $\bar{M}^v$ and $\bar{\Delta}^v$ are constant, while $\bar{M}^s$ and $\bar{\Delta}^s$ decay rapidly to the values

$$\bar{M}^s = \frac{1}{1 + i\phi_0}\bar{M}^v, \quad \bar{\Delta}^s = \bar{\Delta}^v. \quad (3.7)$$

Substituting these values in the terms of order τ_s we find on a longer time scale the usual maser equations (3.1) with precisely the effective atomic frequency and transverse relaxation rates (3.4), found usually by the more complicated derivation in Refs. [5],[6].

3.4   Prospects for constructing a surface maser

The description in which the surface magnetization and population inversion adiabatically follow their volume counterparts requires sticking times that are short compared to other characteristic times appearing in Eqs. (3.5), such as $1/\kappa$, $1/\gamma_\parallel^v$, $1/\gamma_\parallel^s$, $1/\gamma_\perp^v$, $1/\gamma_\perp^s$, $1/gB$ and τ_v. If, however, the temperature of the maser is lowered considerably below present values, τ_s becomes of the order of or even larger than a number of these time constants. The approach of the previous section is then not justified and the dynamics of the surface has to be included in the description of the hydrogen maser.

As τ_s increases, the number of atoms which reside at the surface increases as well. A situation might occur in which the surface atoms determine the behavior of the maser and in which the volume can be treated as a perturbation in much the same way as the surface is treated as a perturbation to the volume frequency. Given the before-mentioned various possible applications for such a surface cryogenic hydrogen maser, it is interesting to investigate under what conditions it might operate.

Based on the knowledge of the last section it seems logical to follow a similar approach but now for small τ_v. Eliminating in this case the rapid time dependence $\exp - i\omega_s t$, introducing the reduced time $\bar{t} = t/\tau_v$ and transforming to normalized magnetizations and population inversions as previously, leads to a system of coupled equations for the time derivatives of $\bar{B}$, $\bar{M}^i$ and $\bar{\Delta}^i$. Note that due to the increased recombination at the surface the ratio of the number of atoms at the surface to the number of atoms in the volume is no longer given by the relation $N_s/N_v = \tau_s/\tau_v$. Instead, the two are related via

$$\frac{n_v}{\tau_v} = \frac{n_s}{\tau_s} + \gamma_{rec}^s n_s^2 , \tag{3.8}$$

where n_s is the density of atoms per unit volume at the surface (defined as $n_s = \sigma A_b/V_b$) and $\gamma_{rec}^s n_s$ is the recombination rate. Consistent with Sec. 3.2 we have assumed $\dot{n}_v = \dot{n}_s = 0$, which implies a restriction to steady oscillation taking into account that γ_{rec}^s depends on the populations of the a and c levels, i.e., on the population inversion, which may be time-dependent. An example of the behavior of n_s and n_v as a function of temperature is displayed in Fig. 3.2, for a flux of $2 \cdot 10^{13}$ atoms per second and an area to volume ratio of 300 cm^{-1}. At temperatures below 500 mK the temperature dependence of the densities starts to deviate from the curves obtained by neglecting

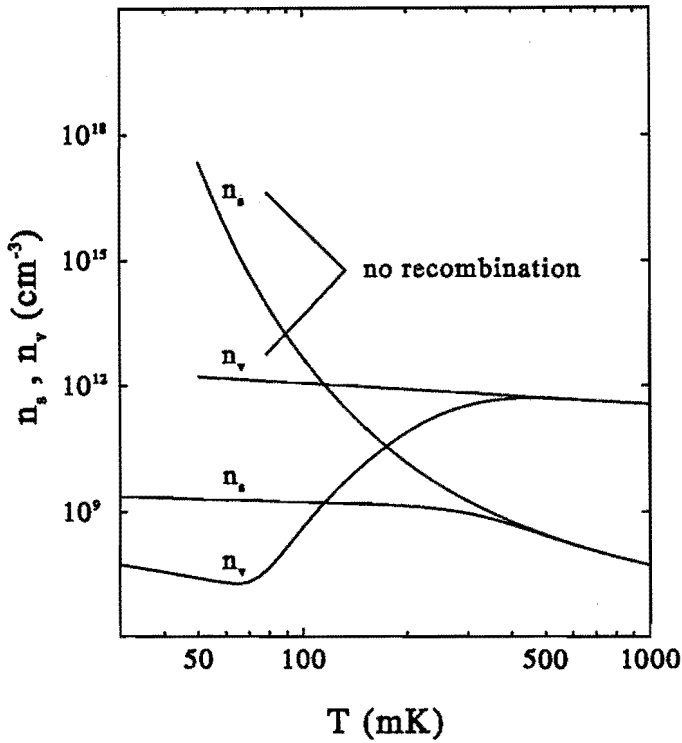Figure 3.2: *Surface density per unit volume n_s and volume density n_v as a function of temperature for a flux of $2 \cdot 10^{13}$ atoms per second and an area to volume ratio of 300 cm^{-1}. For comparison the curves corresponding to $n_s/n_v = \tau_s/\tau_v$, i.e., neglecting recombination, are given. The low temperature part of these curves, where the surface density saturates, is omitted.*

the recombination. This is due to the fact that a significant part of the incoming flux is needed to compensate for recombination at the surface, instead of building up the density. As, however, the recombination time is still large compared to the residence time at the surface the equality $n_s/n_v = \tau_s/\tau_v$ is still valid. Only for temperatures below 80 mK, when the volume density starts to increase again, is the recombination time equal to or smaller than the residence time and is Eq. (3.8) needed to describe the relation between n_s and n_v.

In the spirit of the last section, we now try to express $\bar{M}^v$ and $\bar{\Delta}^v$ in the corresponding surface quantities. This is possible by neglecting all terms containing τ_v in the dynamical equations for $\bar{M}^v$ and $\bar{\Delta}^v$. It is essential, however, to keep the τ_v terms containing $\bar{M}^s$, $\phi_1 = \tau_v(\omega_v - \omega_s)$, Δ_0^v and $\bar{\Delta}^s$. Here we take into account that ϕ_1 is large compared to 1, that $\bar{M}^s$ and $\bar{\Delta}^s$ have to be included to retain the coupling between surface and volume and that the Δ_0^v term is essential for maintaining the population inversion. The result is

$$\bar{M}^v = \frac{1}{1 + i\phi_1}\frac{\tau_v N_s}{\tau_s N_v}\bar{M}^s, \quad \bar{\Delta}^v = \frac{\tau_v N_s}{\tau_s N_v}\bar{\Delta}^s + \tau_v\gamma_{\parallel}^v\frac{\Delta_0^v}{N_v}. \tag{3.9}$$

Note that M^v is 90° out of phase with M^s. Substituting these expressions in the remaining equations and including $O(\tau_v)$ terms again leads to the usual maser equations (3.1) with the effective parameters

$$\begin{aligned}
\omega_{\mathrm{at}} &= \omega_s + \frac{1}{\tau_s}\frac{\phi_1}{1 + \phi_1^2}, \\
\gamma_\perp &= \gamma_\perp^s + \frac{1}{\tau_s}\frac{\phi_1^2}{1 + \phi_1^2}, \\
\Delta_0 &= \Delta_0^s + \frac{\gamma_{\parallel}^v}{\gamma_{\parallel}^s}\Delta_0^v.
\end{aligned} \tag{3.10}$$

It is interesting to point out that the maser will oscillate at a frequency determined by the hyperfine frequency at the surface, i.e., ω_{at} is very close to ω_s as indicated in Fig. 3.3, which should be a characteristic feature of a surface maser. This follows also from our simulations. It is thus indeed possible to make the volume shift small by decreasing the temperature. This means that one of the device dependent processes that affect the transition frequency can possibly be eliminated. In order to assess the feasibility of the SCHM as a primary time standard, however, other processes which influence the transition frequency, such as collisions, have also to be examined. Another important fact is that $\gamma_\perp$ $(\simeq \gamma_\perp^s + 1/\tau_s)$ turns out to have approximately equal contributions from
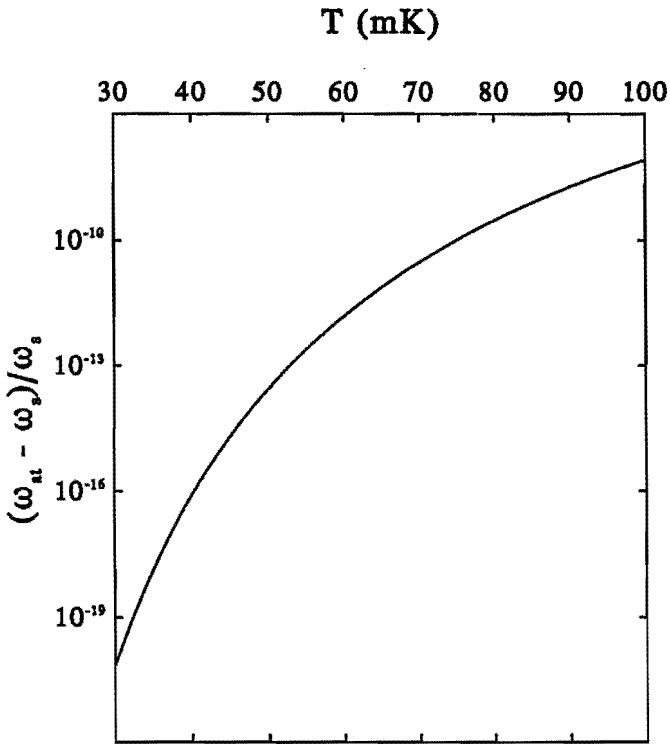
T (mK)

Figure 3.3: Ratio of the volume shift as given by Eqs. (3.10) to the transition frequency as a function of temperature for an area to volume ratio of 300 cm^{-1}.

$\gamma_{\perp}^s$ and dephasing in the volume under the specific conditions of the SCHM that we will examine. Note, furthermore, that the effective value of Δ_0, which deviates significantly from the pure surface value Δ_0^s, is a result of the present treatment and does not follow from the method of Anderson and Weiss. An analogous significant surface correction to Δ_0^v did not occur in the previous case of the CHM.

In order to assess the realizability of a surface maser these parameters have to be substituted in the oscillation condition, which on resonance is given by

$$g^2 \Delta_0 \; > \; \kappa \gamma_{\perp} . \tag{3.11}$$

For usual values of the incident flux the minimum required cavity Q value is determined by $\gamma_{\perp}$, i.e., by the surface density and the temperature via $\gamma_{\perp}^s$ and τ_s. For typical device parameters we have taken the values common to the current hydrogen maser, as mentioned in Sec. 3.2, with the exception of the area to volume ratio of the storage bulb where we used the value given in a recent paper of Pollack *et al.* [11]. For the temperature-density combination 70 mK/10^9 cm^{-3} we then find the oscillation condition to be satisfied with $Q_c = 3 \cdot 10^6$. This result is confirmed by a numerical simulation of the unapproximated set of Eqs. (3.5), leading to Figs. 3.4-3.9. For higher temperatures oscillation can be achieved for higher Q_c values. In Figs. 3.4-3.6 the output power of the maser is shown as a function of density, temperature and cavity quality factor. Figure 3.4 shows the importance of recombination to obtain maser oscillation: instead of the usual characteristic quadratic dependence of the power on the density with a decrease at higher densities, the power now continues to increase. In the CHM the influx of atoms is proportional to the density. At low densities Δ_0 is determined by this influx whose increase is sufficient to compensate for the accompanying increase of $\gamma_{\perp}$. At high densities, however, the increase of Δ_0 with density is less than linear due to longitudinal relaxation, eventually making oscillation impossible. Due to recombination the influx is a quadratic function of the density in the SCHM. In this case the oscillation condition will always be fulfilled above a certain minimum density. The sharp decrease of the power for higher temperatures displayed in Fig. 3.5 indicates the importance of the dephasing in the volume on the effective atomic linewidth. At the low temperature side $\gamma_{\perp}$ is determined by $\gamma_{\perp}^s$. At the high temperature side the dephasing term becomes more important. This results in a rapid increase of the transverse relaxation rate which inhibits

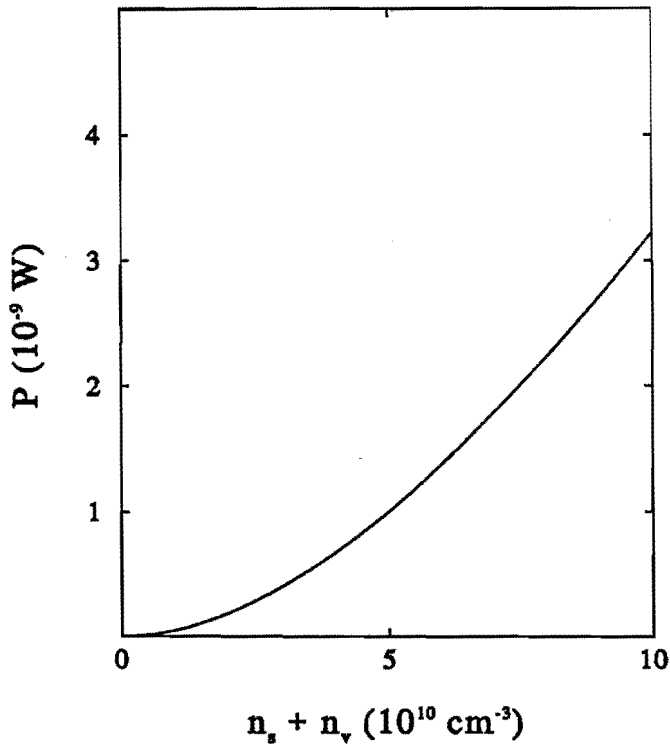Figure 3.4: *The output power of the a-c maser as a function of the total density in the storage bulb for* $A_b/V_b = 300$ *cm*$^{-1}$, $T = 70$ *mK,* $Q_c = 3 \cdot 10^6$ *and* $\omega_c = \omega_s$.

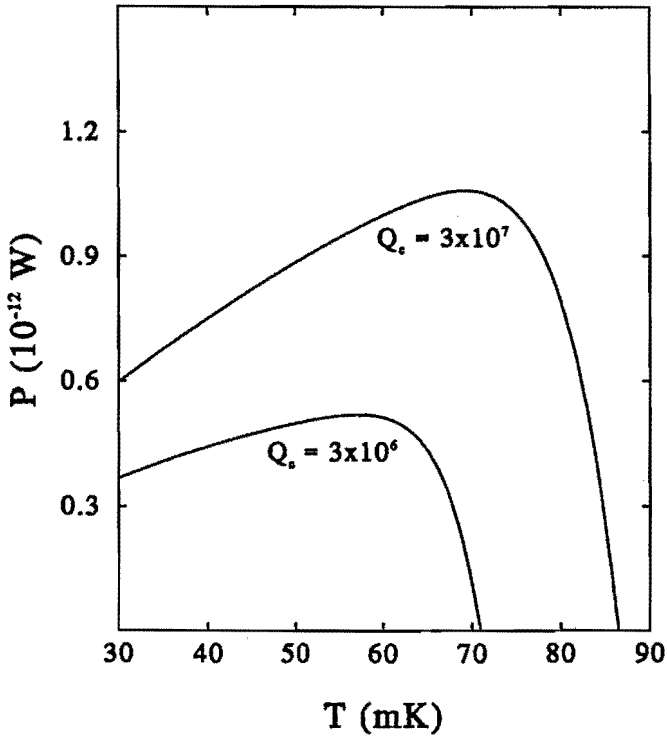Figure 3.5: *The output power of the a-c maser as a function of temperature for* $A_b/V_b = 300$ *cm*$^{-1}$, $n_s + n_v = 10^9$ *cm*$^{-3}$, $Q_c = 3 \cdot 10^6$ *and* $3 \cdot 10^7$ *and* $\omega_c = \omega_s$.
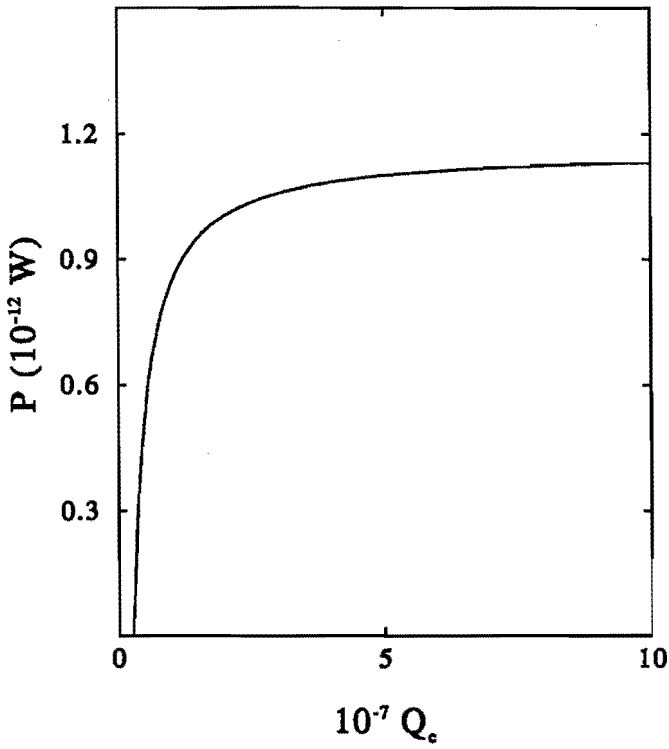
Figure 3.6: *The output power of the a-c maser as a function of the cavity quality factor for $A_b/V_b = 300$ cm^{-1}, $n_s + n_v = 10^9$ cm^{-3}, $T = 70$ mK and $\omega_c = \omega_s$.*

maser oscillation. The relationship between the power and the cavity quality factor in Fig. 3.6, finally, implies the expected linear relationship between the number of photons in the cavity and the quality factor ($|B|^2 \sim PQ_c$).

To shed further light on the interesting role of recombination it is instructive to see what happens if surface recombination would be absent. Without recombination the transverse relaxation rate as given by Eqs. (3.10) will be greatly reduced, which might suggest a favorable condition for operation of a surface maser. An evaluation of the oscillation condition (3.11), however, shows that in this case no oscillation can exist for reasonable maser parameters. The main cause is the importance of Δ_0^v in sustaining maser oscillation. In order for the maser to operate enough population-inverted influx should be supplied to the storage bulb per unit time. In the absence of recombination, however, the flux of new atoms into the storage bulb equals the flux out. This flux is determined by the number of atoms in the volume, which is only a small fraction of the total number of atoms in the storage bulb under the surface-maser conditions examined above (see Fig. 3.2). The flux of new population inversion $\gamma_\parallel^v \Delta_0^v$ is then too small to support maser oscillation. With recombination the incoming flux not only compensates the outgoing flux, but in order to maintain a constant density the atoms which disappear due to recombination must also be replaced. This implies a larger influx of new population inversion for the same value of the surface density and thus a more favorable condition for maser oscillation.

In the previous considerations we needed Δ_0^v for oscillation. A fascinating alternative would be a surface maser based on the a-b transition. In this case, due to preferential recombination and relaxation of the a atoms, Δ_0^s is positive, i.e., oscillation can in principle be realized even without population inversion in the incoming beam. However, it is possible to feed the storage bulb with an incoming beam of b atoms (this will be discussed in the next section). The same analysis which has been applied to the a-c maser can now be used for the a-b maser. For the same operating conditions as above both the oscillation condition and the numerical simulations show that oscillation is already possible for $Q_c = 4 \cdot 10^5$, which is almost 10 times lower than for the a-c maser. More advantages are clearly shown in Figs. 3.7-3.9. Not only does the a-b maser operate at much lower Q_c values, for equal Q_c values it also operates at lower densities and, even more important, at higher temperatures. These higher temperatures could possibly make
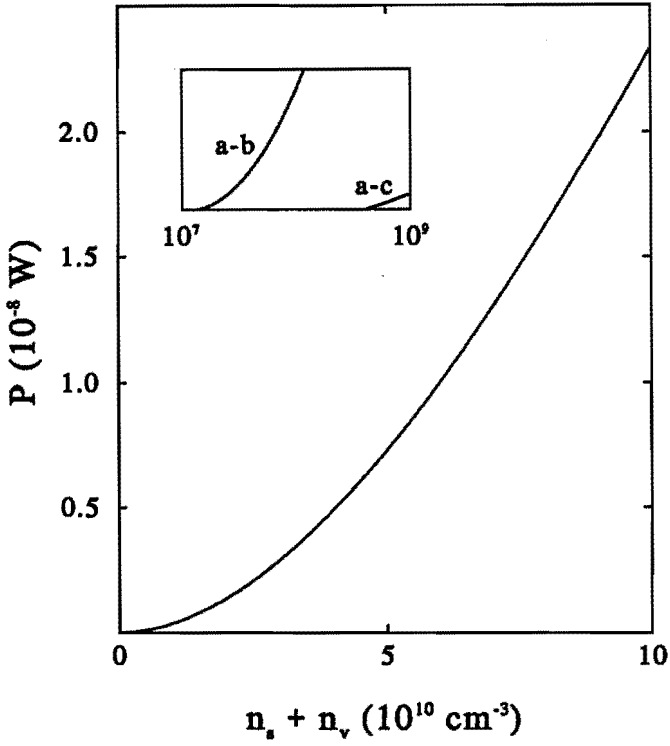
Figure 3.7: Same as Fig. 3.4 for the a-b maser. The inset shows the minimum required densities for maser oscillation for both the a-b and a-c maser obtained by magnifying the left-hand sides of Fig. 3.4 and this figure.
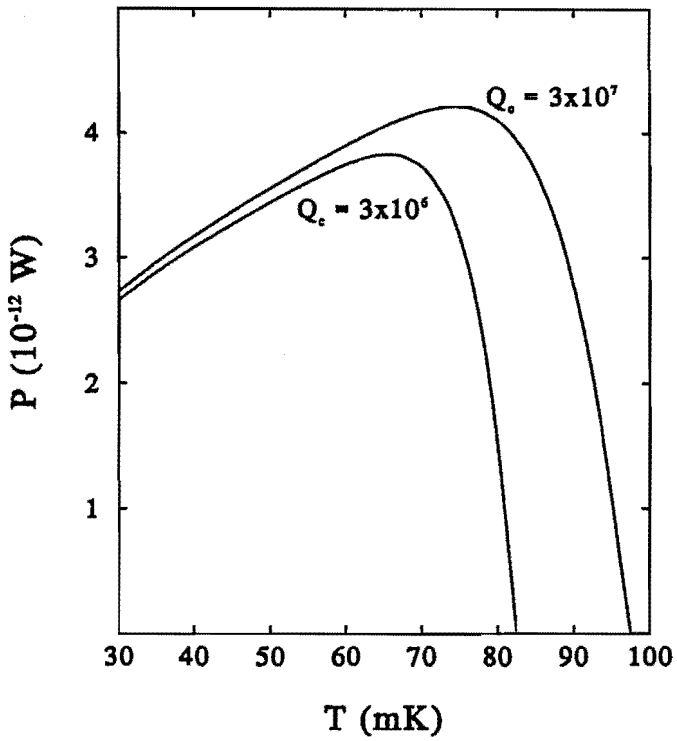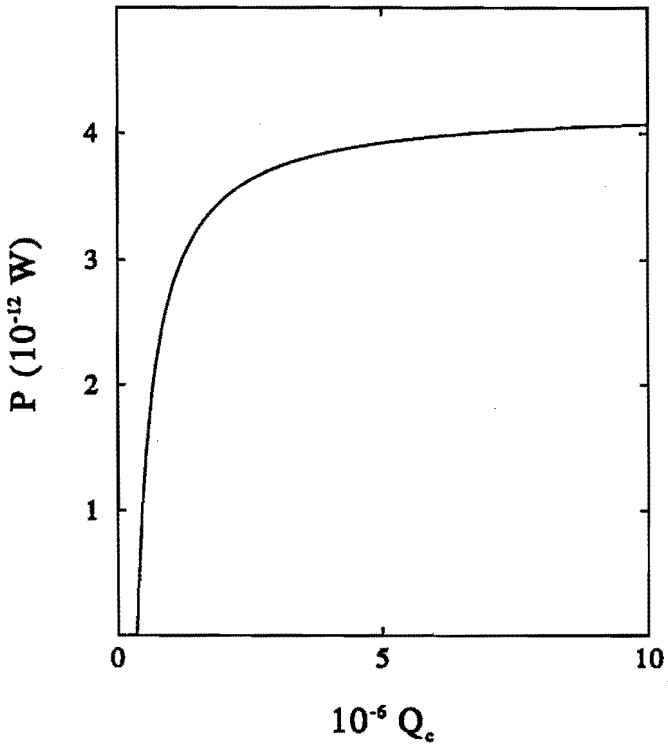
Figure 3.8: Same as Fig. 3.5 for the a-b maser.

Figure 3.9: Same as Fig. 3.6 for the a-b maser.

the a-b maser easier to operate.

Comparing the conditions under which the SCHM operates with the normal operating conditions of the CHM it is clear that for the former a cavity quality factor is needed which is several orders of magnitude larger. Partially, this is due to the magnitude of Δ_0 which involves different physics. In the CHM the influx of atoms into the storage bulb replaces directly the atoms flowing out. In the SCHM new atoms primarily replace atoms which have recombined. The increase of Q_c is also due to the larger transverse relaxation rate. In the CHM both the storage time of the atoms and the collisional relaxation time are of the order of one second with only a small contribution from dephasing at the surface. For our example temperature-density combination of 70 mK/10^9 cm^{-3}, in contrast, the resonant linewidth $\gamma_\perp$ is equal to about 50 s^{-1} with approximately equal contributions from dephasing in the volume and $\gamma_\perp^s$. To compensate for this rapid loss of coherence a much better cavity is needed.

3.5   Experimental considerations

In this section we discuss some experimental aspects connected with the realization of a SCHM. We first consider some cryogenic questions. Temperatures of the order of 50-100 mK are easily attainable with a ^{3}He-^{4}He dilution refrigerator, with cooling powers of a few hundred microwatts. Recombination of hydrogen can put a large heat load on the refrigerator. We calculate the heat load for the SCHM we have analyzed, with $\sigma = n_s V_b / A_b = 3 \cdot 10^6$ cm^{-2} where the area $A_b = 6 \cdot 10^4$ cm^2. The heat produced is

$$\dot{Q} = K_s \sigma^2 A_b \frac{D_0}{2} , \tag{3.12}$$

where $D_0 = 7 \cdot 10^{-19}$ J is the recombination energy released per pair of atoms. Using the experimental value of the recombination constant $K_s = 3 \cdot 10^{-5}$ K$^{-1/2}$ $\sqrt{T}$ cm^2 s^{-1} from Morrow *et al.* [8] we find 2 μW, which is easily absorbed by a dilution refrigerator. A connected problem posed by temperatures in the range 50-100 mK is that a gas of hydrogen loses thermal contact due to the Kapitza resistance between the helium film and the substrate. However, in the maser described here due to the low hydrogen surface densities, the heat production is substantially lower than has been experimentally studied in the past. Thus, the thermal gradients which develop may be smaller, resulting in some
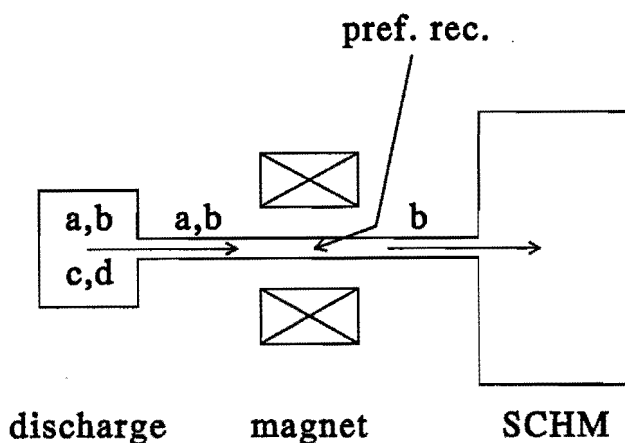
pref. rec.

```
          ┌───────┐        ┌───────┐
          │  ⊠    │        │       │
  ┌──────┬│───────│────────│   b   │
  │ a,b  ││  a,b  ⊠────→    ───────→│
  │──────││   →            │       │
  │ c,d  │└───────┘        │       │
  └──────┘        ┌───────┐│       │
                  │  ⊠    ││       │
                  └───────┘└───────┘
```

discharge   magnet   SCHM

Figure 3.10: Schematic picture of an experimental design to load pure b-state atoms in the SCHM.

flexibility in the range of accessible temperatures.

Finally, we consider the filling fluxes required for the SCHM. These are of the order of 10^{13} atoms per second. Such fluxes are easily achieved with existing discharge sources which can deliver 10^{14}-10^{16} atoms per second to a cell.

One of the interesting ideas to emerge from this study is the possibility of a maser working on the a-b transition. An experimental design which can produce a flux of almost pure b-state stoms is shown in Fig. 3.10. A low temperature discharge produces hydrogen atoms populating the four hyperfine states. A small (~ 1-2 tesla) magnet repels the c and d atoms and confines the a and b atoms in a volume at a low temperature (~ 300 mK). This density of atoms converts to pure b-state atoms by preferential recombination. The magnetic field and temperature of this volume can be adjusted so that b-state atoms can reach the maser by thermal escape with a flux sufficient for the a-b SCHM. A small superimposed field can prevent Majorana transitions among the hyperfine states.

3.6   Discussion and conclusions

The operation of the sub-Kelvin hydrogen maser is usually described by the Maxwell-Bloch equations. Short periods during which the atoms stick to the surface enter these equations through effective values for the atomic transition frequency and transverse relaxation rate. We have extended these Maxwell-Bloch equations to a description in which the surface is treated symmetrically with the volume, rather than as a perturbation, opening in particular the possibility to treat the pulsed operation of the maser in a regime where the sticking time is comparable to the pulse duration. Work along this line is under way [13]. We have shown that for current versions of the sub-Kelvin hydrogen maser, i.e., for short sticking times, the usual equations and effective parameters are recovered.

Starting from this new description, we have investigated the possibilities to construct a maser whose properties are mainly determined by atoms which reside at the surface, i.e., a surface maser. We have shown that for a maser which is based on the traditional scheme of a transition between the a and c levels of the hydrogen ground state a surface maser is realizable for realistic experimental parameters, for instance: $T = 70$ mK, $n_s + n_v = 10^9$ cm^{-3}, $A_b/V_b = 300$ cm^{-1}, $Q_c = 3 \cdot 10^6$. This result was obtained both by a simulation of the full set of Eqs. (3.5) and on the basis of the effective surface equations. The prospects for an a-b maser are even more favorable.

Apart from the intrinsic interest in the operation of the SCHM, such as the interesting role of recombination and the possibility to observe pulsed oscillation, two important motives for studying the influence of the surface on the maser operation and in particular the SCHM are the possibility to create a primary time standard and the precision measurement of properties connected with a two-dimensional gas of atomic hydrogen.

In this connection one could think of an extension of the measurement of the surface adsorption energy in Ref. [10] to a situation with lower surface densities, made possible by the greater sensitivity, with the associated advantage of a more reliable temperature determination. Another possibility worth considering would be to measure $\gamma_{\parallel}^s$ and $\gamma_{\perp}^s$ as a function of surface density and field orientation. In principle, this would enable an independent determination of the dipolar T_2 [10]. This could stimulate the development of a satisfactory theory of line-broadening including the coherent contribution of all dipolar fields. The main parts of $\gamma_{\parallel}^s$ and $\gamma_{\perp}^s$, due to recombination, would also be

a welcome addition to the knowledge desired for developing a satisfactory theory of surface recombination.

In order to obtain a primary time standard it is essential that the effective atomic frequency ω_{at} is independent of specific device parameters, such as those which determine the wall (volume) shift, but also spin-exchange and dipolar shifts, the influence of the substrate and the thickness of the helium film. From our analysis it follows that the volume shift can be suppressed in the SCHM. It is very unlikely, however, that the influence of the other processes can also be sufficiently reduced. For example, Morrow and Berlinsky [9] have calculated the spin-exchange frequency shift for hydrogen atoms adsorbed on a surface. Although in this calculation the motion of the atoms perpendicular to the surface is neglected it gives a good indication whether this effect seriously influences the operation of the SCHM. For our reference temperature-density combination this leads to a frequency shift $\Delta\omega_{at} \simeq 10\,\text{rad s}^{-1}$, given the fact that $(\rho_{cc} - \rho_{aa})$ is approximately 0.1 in our simulations. It is clear that already this effect is much too large to open possibilities for the SCHM as a primary time standard.

Under the conditions studied the resonance linewidth $\gamma_\perp$ ($\simeq 50\,\text{s}^{-1}$) is still much smaller than the typical cavity loss rate κ ($\simeq 1500\,\text{s}^{-1}$). Although the ratio between these two is less than in the CHM, fluctuations in the cavity frequency are still sufficiently suppressed to measure with great accuracy the above-mentioned surface processes.

Bibliography

[1] S. B. Crampton, W. D. Phillips, and D. Kleppner, Bull. Am. Phys. Soc. **23**, 86 (1978); R. F. C. Vessot, M. W. Levine, and E. M. Mattison, NASA Technical Memorandum No. 78104, 1978 (unpublished), p. 549; A. J. Berlinsky and W. N. Hardy, NASA Conference Publication No. 2220, 1982 (unpublished), p. 547.

[2] H. F. Hess, G. P. Kochanski, J. M. Doyle, T. J. Greytak, and D. Kleppner, Phys. Rev. A **34**, 1602 (1986); M. D. Hürlimann, W. N. Hardy, A. J. Berlinsky, and R. W. Cline, Phys. Rev. A **34**, 1605 (1986); R. L. Walsworth, I. F. Silvera, H. P. Godfried, C. C. Agosta, R. F. C. Vessot, and E. M. Mattison, Phys. Rev. A **34**, 2550 (1986).

[3] A. C. Maan, H. T. C. Stoof, B. J. Verhaar, and P. Mandel, Phys. Rev. Lett. **64**, 2630 (1990); **65**, 2319 (1990); P. Mandel, A. C. Maan, B. J. Verhaar, and H. T. C. Stoof, Phys. Rev. A **44**, 608 (1991).

[4] W. N. Hardy, M. D. Hürlimann, and R. W. Cline, Jpn. J. Appl. Phys. **26**, 2065 (1987); M. D. Hürlimann, Ph.D. thesis, University of British Columbia, Canada, 1989.

[5] P. W. Anderson and P. R. Weiss, Rev. Mod. Phys. **25**, 269 (1953); P. W. Anderson, J. Phys. Soc. Jpn. **9**, 316 (1954); A. Abragam, *The Principles of Nuclear Magnetism* (Clarendon Press, Oxford, 1961).

[6] M. Morrow and W. N. Hardy, Can. J. Phys. **61**, 956 (1983).

[7] B. J. Verhaar, J. M. V. A. Koelman, H. T. C. Stoof, O. J. Luiten, and S. B. Crampton, Phys. Rev. A **35**, 3825 (1987); J. M. V. A. Koelman, S. B. Crampton, H. T. C. Stoof, O. J. Luiten, and B. J. Verhaar, Phys. Rev. A **38**, 3535 (1988).

[8] M. Morrow, R. Jochemsen, A. J. Berlinsky, and W. N. Hardy, Phys. Rev. Lett. **46**, 195 (1981); **47**, 455 (1981); D. A. Bell, H. F. Hess, G. P. Kochanski, S. Buchman, L. Pollack, Y. M. Xiao, D. Kleppner, and T. J. Greytak, Phys. Rev. B **34**, 7670 (1986).

[9] M. Morrow and A. J. Berlinsky, Can. J. Phys. **61**, 1042 (1983).

[10] I. Shinkoda and W. N. Hardy, J. Low Temp. Phys. **85**, 99 (1991).

[11] L. Pollack, S. Buchman, and T. J. Greytak, Phys. Rev. B **45**, 2993 (1992).

[12] A. Nayfeh, *Perturbation Methods* (Wiley, New York, 1973).

[13] P. Mandel (private communication).

Chapter 4

Stability limit of the cryogenic hydrogen maser

Abstract

It is pointed out that the usual oscillation condition of the H maser is only a necessary condition for steady operation. Reducing the coupled field-matter dynamics to the complex Lorenz equations we derive a second requirement which together with the first forms a set of necessary and sufficient conditions for the steady operation to be stable. The instability of the steady state predicted by the equations should be easily accessible experimentally for the cryogenic H maser. It will be characterized by a pulsed output power which, depending on the detuning, is either periodic or chaotic.

Since its first realization by Goldenberg, Kleppner, and Ramsey [1] the hydrogen maser has been the most stable of all atomic frequency standards for short and intermediate measuring times. The relative stability of the hydrogen maser is observed to be better than one part in 10^{15}, which makes it a very useful instrument for long-baseline interferometry, tests of general relativity, precision interplanetary navigation (Voyager 2 mission), and various other applications both inside and outside physics.

A hydrogen maser operating at liquid-helium temperatures should have an even better frequency stability [2],[3]. Although early estimations predicted an improvement of more than 2 orders of magnitude [4], present indications show that it has an increased frequency stability of close to 1 order of magnitude [5]-[8].
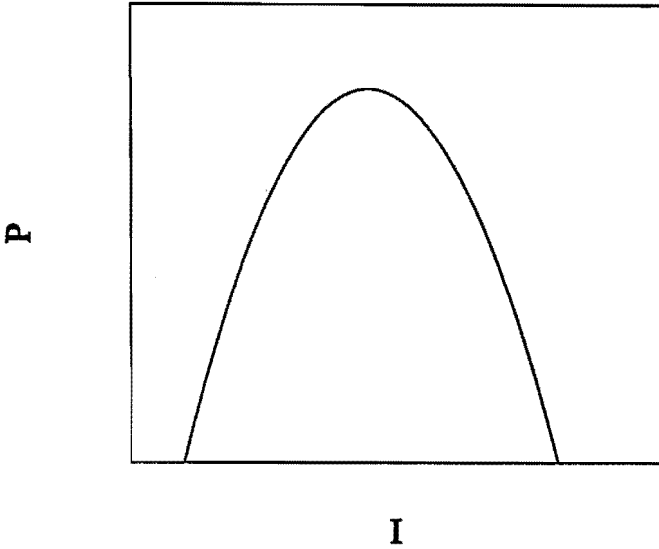
P

Figure 4.1: Power of H maser vs surplus flux of upper level.

The operation of the hydrogen maser has been described in Refs. [1] and [9]. A central result (see Fig. 4.1) is the so-called oscillation condition,

$$\frac{P}{P_c} = -2q^2 \left[\frac{I}{I_{th}}\right]^2 + (1 - Cq)\frac{I}{I_{th}} - 1 > 0, \tag{4.1}$$

in which P is the total power radiated by the atoms, I is the surplus flux of atoms entering the storage bulb in the upper level of the maser transition relative to the lower level, I_{th} is the threshold flux if we neglect density-dependent relaxation, P_c is the critical power, q is the maser quality factor, and $C = (T_2^0/T_1^0)^{1/2} + 2(T_1^0/T_2^0)^{1/2}$ with T_1^0 (T_2^0) the density-independent longitudinal (transverse) relaxation time [9].

It has not been recognized until now that the condition (4.1) is only necessary but by no means sufficient. More precisely, condition (4.1) expresses the existence of the steady-state solution for the number of photons in the cavity and therefore for the output microwave power. It remains to determine the domain in which this is also a stable solution.

The purpose of this Letter is to show that within the flux limits determined by condition

	$\gamma_\parallel$	$\gamma_\perp$	κ	g
Maser	1	1	10^5	10^{-2}
Laser	10^8	10^8	10^7-10^{10}	10^4

Table 4.1: Time constants (in sec^{-1}) for cryogenic H maser compared to typical laser.

(4.1) two regimes can exist, one in which the steady-state solution is stable and another in which spontaneous modulation of the amplitude and phase of the electromagnetic field takes place. This spontaneous modulation can be either periodic or chaotic, depending on the values adopted for the various parameters, and will affect in a similar way the output microwave power. We show that this time-dependent regime can be rather easily reached for the subkelvin hydrogen maser.

The maser dynamics can be described by essentially the same Maxwell-Bloch equations as a single-mode laser with homogeneous broadening. However, interesting differences exist between these two systems. A first aspect is that the two classes of systems display periodic and chaotic behavior in a very different range of parameters, because the maser decay rates are very different from the usual values found in the visible or ir domains (see Table 4.1). As a consequence, the analysis of the dynamical equations has to be specialized for this new domain of parameters. A second aspect which is worth stressing is that the derivation of the Maxwell-Bloch equations [see Eqs. (4.2)] for the H maser requires far less simplifying assumptions than in the case of the laser. For instance, the H maser is naturally homogeneously broadened. Furthermore, the cavity dimension is of the order of the maser wavelength so that effects related to the space dependence of the coupling constant are negligible.

Apart from the intrinsic interest associated with the availability of a system displaying deterministic chaos with a very low noise level, the observation of instability may have important applications for obtaining information on the maser which would be very difficult to obtain otherwise. It is *a priori* to be expected that the nonsteady regime will offer much more information than the frequency and the amplitude, obtainable from stationary operation. This is especially welcome in view of the overwhelming number of experimental parameters, such as hyperfine populations, which determine the maser

operation and are notoriously difficult to diagnose.

Reformulating the dynamics of the maser [9], the operation of the cryogenic H maser can conveniently be described by the Maxwell-Bloch equations

$$
\begin{aligned}
\dot{B} &= -i\omega_c B - \kappa B + gM \, , \\
\dot{M} &= -i\omega_{at} M - \gamma_\perp M + gB\Delta \, , \\
\dot{\Delta} &= -\gamma_\parallel (\Delta - \Delta_0) - 2g(BM^* + B^*M) \, ,
\end{aligned}
\tag{4.2}
$$

for the complex magnetic field B, the complex magnetization M, and the inversion Δ. Explicitly B is defined as the expectation value of the photon annihilation operator. In terms of the one-atom spin-density matrix we have, furthermore, $M = N\rho_{ca}$, $\Delta = N(\rho_{cc} - \rho_{aa})$, where N is the number of atoms. The cavity resonance frequency is denoted by ω_c, the atomic frequency by ω_{at}, the cavity damping rate by $\kappa = \omega_c/2Q_c = 1/T_c$, and the damping rates for M and Δ by $\gamma_\perp = 1/T_2$ and $\gamma_\parallel = 1/T_1$. The equilibrium value of Δ in the absence of atom-field interaction is denoted by Δ_0. Finally g, the one-photon Rabi frequency, is given by

$$
g^2 = \mu_0(\mu_e + \mu_p)^2 \eta \omega_c / 2\hbar V_c \, ,
\tag{4.3}
$$

with V_c being the cavity volume, μ_e (μ_p) the electron (proton) magnetic moment, and η the filling factor.

In this Letter we will only discuss the stability properties of the steady state, following the analysis made by Mandel and Zeghlache [10] for a detuned laser. We transform Eqs. (4.2) by introducing the new parameters

$$
\sigma = \kappa/\gamma_\perp \, , \quad b = \gamma_\parallel/\gamma_\perp \, , \quad R = g^2\Delta_0/\kappa\gamma_\perp \, ,
\tag{4.4}
$$

and new variables

$$
\begin{aligned}
B &= (\gamma_\perp/2g)(x_1 + ix_2)\exp(-i\omega_m t) \, , \\
M &= (\Delta_0/2R)(y_1 + iy_2)\exp(-i\omega_m t) \, , \\
\Delta &= \Delta_0(1 - z/R) \, ,
\end{aligned}
\tag{4.5}
$$

where ω_m is the yet unknown operating frequency of the maser. After rescaling the time according to $t = T_2\tau$, Eqs. (4.2) take the form

$$
\begin{aligned}
x_1' &= -\sigma(x_1 + \delta_c x_2 - y_1)\,, \\
x_2' &= -\sigma(x_2 - \delta_c x_1 - y_2)\,, \\
y_1' &= -y_1 + Rx_1 + \delta_{at} y_2 - x_1 z\,, \\
y_2' &= -y_2 + Rx_2 - \delta_{at} y_1 - x_2 z\,, \\
z' &= -bz + x_1 y_1 + x_2 y_2\,,
\end{aligned}
\tag{4.6}
$$

in which the prime stands for $d/d\tau$ and

$$
\delta_{at} = \frac{\omega_{at} - \omega_m}{\gamma_\perp}\,, \quad \delta_c = \frac{\omega_m - \omega_c}{\kappa}\,.
\tag{4.7}
$$

In the case of perfect tuning ($\omega_{at} = \omega_m = \omega_c$), Eqs. (4.6) have a class of solutions for which $x_2 = y_2 = 0$ for all times. The remaining variables $x = x_1$, $y = y_1$, and z obey the usual Lorenz equations [11].

To study the steady-state solutions of Eqs. (4.6), we set the derivatives in these equations equal to zero. Since ω_m is the operating frequency in the steady state, x_2 can be chosen to be zero. This leads to the dispersion equation or cavity-pulling relation $\delta_{at} = \delta_c \equiv \delta$ and to three fixed points: $x_1 = y_1 = y_2 = z = 0$ and $x_1 = y_1 = \pm(bz)^{1/2}$, $y_2 = \mp\delta(bz)^{1/2}$, $z = R - 1 - \delta^2$, respectively. The last two solutions are physically identical, since they differ in phase only. For $R \le 1 + \delta^2$ only the trivial zero-field solution exists and is stable. A necessary condition for the finite-field solution to exist is $R > 1 + \delta^2$, which generalizes Eq. (4.1) for a detuned cavity.

The inequality $R > 1 + \delta^2$ gives a lower bound for the domain of existence and stability of the finite-amplitude solution. However, the linear stability analysis of this solution indicates that a second threshold may occur at higher photon numbers, when R reaches a critical value R_H which depends in a rather complicated way on the parameters of the problem. Using the relative magnitudes of the parameter values given in Table 4.1 and retaining the dominant contributions in $\epsilon = 1/\sigma$ with b and δ being functions of the order of 1, we find that there is always an upper bound for the stability of the steady state. It is reached when the photon number equals the critical value $|B_H|^2 = (R_H - 1 - \delta^2)/4T_1 T_2 g^2$. Restricting ourselves to the case of small detuning ($\frac{1}{3} - \delta^2 \gg \epsilon$), the second requirement for stable steady oscillation is

$$
\frac{T_1}{T_t}\frac{P - P_H}{P_H} = \left(-2q + \frac{1}{\kappa T_t}\frac{1 - 3\delta^2}{(1 + \delta^2)^2}\right)\frac{I}{I_{th}} - \frac{T_2^0}{T_t} < 0\,,
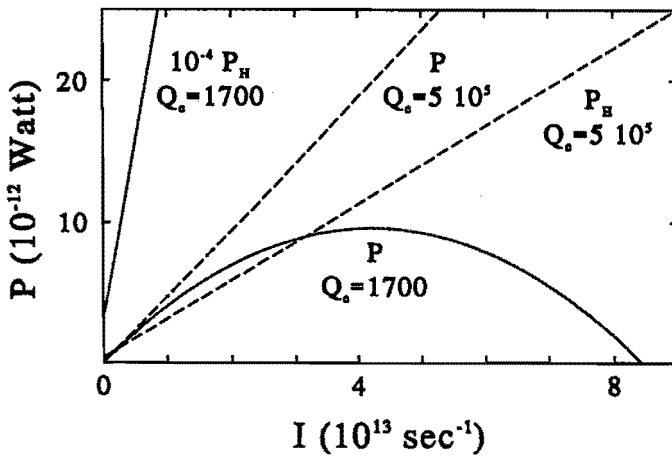\tag{4.8}
$$

Figure 4.2: Power P vs surplus flux, compared to threshold power P_H for onset of nonsteady oscillation. Solid lines: actual parameter values for the University of British Columbia maser. Dashed lines: increased Q_c value.

in which $T_t = (T_1^0 T_2^0)^{1/2}$.

In Fig. 4.2 we display graphically the two conditions of stability (4.1) and (4.8) for the steady state. We present the radiated power P as well as the quantity P_H. For definiteness we take $\delta = 0$, and for $T_1^0 = T_2^0$ and the product qQ_c we take the University of British Columbia cryogenic-maser [7] values 0.6 sec and 27, respectively. Clearly, from Fig. 4.2 we see that the actual Q_c value of order 1700 does not admit nonsteady oscillation. It has been kept low deliberately to reduce fluctuations of the maser frequency due to cavity pulling, but may easily be increased to reach the unstable domain $Q_c > \omega_c/2g\sqrt{\Delta_0}$, which is equivalent to the condition $R > R_H$ when $\delta = 0$. For instance, Fig. 4.2 shows that the new oscillation regime can be reached by increasing Q_c to values of order 5×10^5.

Calculations for the Harvard-Smithsonian maser [12] with $qQ_c = 17$ show that in this case an increase of Q_c from the present magnitude 7×10^4 by a factor of order 20 would be sufficient. From a similar analysis it follows that unstable oscillation is very difficult to achieve for room-temperature H masers. This is mainly due to the much lower maximum densities allowed by the oscillation condition (4.1) due to the faster collisional
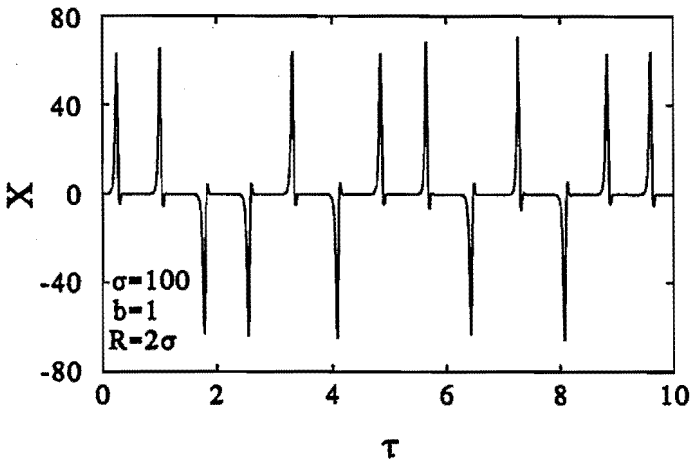
Figure 4.3: Field amplitude as a function of time for zero detuning, both scaled as described in text.

relaxation.

Hence, the cryogenic H maser promises to be an experimental realization of the Lorenz equations in the domain $R, \sigma \gg 1$ and $b \approx 1$. This domain, partly investigated by Fowler and McGuinness [13], is characterized by pulses for x and y, i.e., for the field and magnetization amplitudes. An example of this behavior is displayed in Fig. 4.3. A detailed analysis of Eqs. (4.2) in the relevant domain of parameter space will be published in a separate paper.

Bibliography

[1] H. M. Goldenberg, D. Kleppner, and N. F. Ramsey, Phys. Rev. Lett. **5**, 361 (1960).

[2] S. B. Crampton, W. D. Phillips, and D. Kleppner, Bull. Am. Phys. Soc. **23**, 86 (1978).

[3] R. F. C. Vessot, M. W. Levine, and E. M. Mattison, NASA Technical Memorandum No. 78104, 1978 (unpublished), p. 549.

[4] A. J. Berlinsky and W. N. Hardy, in *Proceedings of the Thirteenth Annual Precise Time and Time Interval Applications and Planning Meeting*, NASA Conference Publication No. 2220 (Goddard Space Flight Center, Greenbelt, MD, 1982), p. 547.

[5] B. J. Verhaar, J. M. V. A. Koelman, H. T. C. Stoof, O. J. Luiten, and S. B. Crampton, Phys. Rev. A **35**, 3825 (1987).

[6] J. M. V. A. Koelman, S. B. Crampton, H. T. C. Stoof, O. J. Luiten, and B. J. Verhaar, Phys. Rev. A **38**, 3535 (1988).

[7] M. D. Hürlimann, W. N. Hardy, A. J. Berlinsky, and R. W. Cline, Phys. Rev. A **34**, 1605 (1986); W. N. Hardy, M. D. Hürlimann, and R. W. Cline, Jpn. J. Appl. Phys. **26**, 2065 (1987).

[8] A. C. Maan, H. T. C. Stoof, and B. J. Verhaar, Phys. Rev. A **41**, 2614 (1990).

[9] D. Kleppner, H. C. Berg, S. B. Crampton, N. F. Ramsey, R. F. C. Vessot, H. E. Peters, and J. Vanier, Phys. Rev. **138**, A972 (1965).

[10] P. Mandel and H. Zeghlache, Opt. Commun. **47**, 146 (1983); H. Zeghlache and P. Mandel, J. Opt. Soc. Am. B **2**, 18 (1985).

[11] E. N. Lorenz, J. Atmos. Sci. **20**, 130 (1963); C. Sparrow, *The Lorenz Equations: Bifurcations, Chaos, and Strange Attractors* (Springer-Verlag, New York, 1982).

[12] R. L. Walsworth, I. F. Silvera, H. P. Godfried, C. C. Agosta, R. F. C. Vessot, and E. M. Mattison, Phys. Rev. A **34**, 2550 (1986); (private communication).

[13] A. C. Fowler and M. J. McGuinness, Physica (Amsterdam) **5D**, 149 (1982).

Chapter 5

Dynamics of the cryogenic hydrogen maser

Abstract

We examine the dynamical behavior of the cryogenic hydrogen maser. Studying the coupled field-matter equations, which have been reduced to the complex Lorenz equations, we obtain two operating domains, one in which steady-state oscillation takes place and a time-dependent domain that is characterized by a pulsed output power. For the latter we obtain bifurcation diagrams, both with and without detuning, that display both periodic and chaotic attractors. Finally, we study the influence of thermal noise on this time-dependent domain and show that for reasonable experimental conditions the pulse triggering will be stochastic, but the pulse buildup and decay can be deterministic.

5.1 Introduction

From the moment it was first proposed and constructed 30 years ago [1] interest in the hydrogen maser has been concentrated almost without exception on its steady oscillation mode. This is understandable in view of its practical use as the most stable existing frequency standard for averaging times of seconds to days: Achievable relative frequency instabilities are 10^{-15} for the room-temperature H maser and 10^{-16} for its sub-Kelvin version [2],[3], in both cases for 1-h averaging time. A recent review of the history, principles, and applications of the H maser can be found in Ref. [4]. Although the

condition for the steady oscillation to be stable had been derived for masers in general [5]-[8], it was recognized very early already that the circumstances prevailing in the conventional room-temperature H maser are far removed from an unstable regime. In fact, it was pointed out that the relative magnitudes of the relaxation rates allow for an adiabatic elimination of the magnetization, leading to the conclusion that the field amplitude would tend either to zero or to steady oscillation.

Only recently [9] it was noticed by the present authors that the unstable regime is much closer for sub-Kelvin H masers. It can be reached, starting from the usual operating conditions, by a readily achievable increase of the cavity quality factor Q_c. In addition, we dealt briefly with the kind of time-dependent behavior to be expected in the new regime and pointed to the interest that would be associated with its observation. First, the time-dependent regime will offer much more information than the frequency and amplitude parameters which are given by the stationary operation. Given the number of experimental parameters which determine the maser dynamics and which are often difficult to diagnose, this extra information is especially welcome. A second point of interest is that the sub-Kelvin hydrogen maser is a realization of the (complex) Lorenz equations in a parameter regime $[R, \sigma \gg 1, b = O(1)]$ which has hardly been investigated. Although Fowler and McGuinness [10] have partially investigated the real Lorenz equations in this parameter regime, the behavior of the complex Lorenz equations is largely unknown in that domain of parameters.

In this paper we treat these aspects in a more detailed way. In Sec. 5.2 we recapitulate the derivation of the dynamical equations — on the one hand, to make our discussion self-contained and, on the other hand, to give an unambiguous definition of variables and constants. The latter is desirable since more than one convention is in use. Moreover, we have to deal with a magnetic transition, contrary to the more usual situation, in which an electrical transition is involved. In Sec. 5.3 we study the linear stability of the steady solution and determine numerically typical bifurcation diagrams. In particular, we show that, even on resonance, periodic solutions are the rule and chaotic solutions have only a set of restricted domains. Finally, in Sec. 5.4 we analyze numerically the influence of noise on the deterministic evolution studied so far. We determine the spread in pulse frequency and peak intensity due to noise. We also determine the conditions in which the time evolution of a pulse will be deterministic, given the fact that its triggering will

always be stochastic in the domain of parameters considered.

5.2 The Maxwell-Bloch equations

We start the derivation of the Maxwell-Bloch equations for the cryogenic H maser by expanding [11] the electromagnetic (EM) field in the cavity in modes n, with frequency ω_n:

$$\mathbf{B}(\mathbf{r},t) = \sum_n \frac{1}{c\sqrt{\epsilon_0}} p_n \mathbf{b}_n(\mathbf{r}) , \quad \mathbf{E}(\mathbf{r},t) = \sum_n \frac{\omega_n}{\sqrt{\epsilon_0}} q_n \mathbf{e}_n(\mathbf{r}) , \qquad (5.1)$$

with $\{\mathbf{b}_n(\mathbf{r})\}$ and $\{\mathbf{e}_n(\mathbf{r})\}$ being orthonormal vector fields in the cavity of the hydrogen maser and c the velocity of light. Using Maxwell's equations, it is easily seen that the expansion coefficients p_n and q_n can be interpreted as the canonical variables of a harmonic oscillator. Quantizing the EM field in analogy to the harmonic oscillator and introducing creation and annihilation operators $a_n^\dagger$ and a_n, Eqs. (5.1) can be rewritten as

$$\mathbf{B}(\mathbf{r},t) = -\sum_n \frac{i}{c} \left[\frac{\hbar\omega_n}{2\epsilon_0} \right]^{1/2} (a_n - a_n^\dagger) \mathbf{b}_n(\mathbf{r}) , \qquad (5.2)$$

$$\mathbf{E}(\mathbf{r},t) = \sum_n \left[\frac{\hbar\omega_n}{2\epsilon_0} \right]^{1/2} (a_n + a_n^\dagger) \mathbf{e}_n(\mathbf{r}) .$$

From now on, we will confine ourselves to a monomode EM field corresponding to the TE_{011} mode of the cavity and will leave out the subscript n.

The Hamiltonian of the total system of atoms and field is

$$H = H_{\text{atom}} + H_{\text{field}} + H_{\text{interact}} , \qquad (5.3)$$

with

$$H_{\text{atom}} = \tfrac{1}{2}\hbar\omega_{at} \sum_i \sigma_{3i} ,$$

$$H_{\text{field}} = \hbar\omega_c a^\dagger a , \qquad (5.4)$$

$$H_{\text{interact}} = i\hbar g \sum_i (a^\dagger \sigma_i^- - a\sigma_i^+) .$$

In Eqs. (5.4), σ_3 and $\sigma^\pm$ are the familiar Pauli spin matrices for the atomic two-level system, ω_{at} (ω_c) is the atomic transition (cavity) frequency, and g is the Rabi frequency divided by the square root of the number of photons in the cavity

$$g = \left[\frac{\mu_0(\mu_e + \mu_p)^2 \omega_c \eta}{2\hbar V_c} \right]^{1/2} , \qquad (5.5)$$

where η is the filling factor and V_c is the volume of the cavity. The summation over i is a summation over the atoms in the storage bulb.

The Hamiltonian H can now be used to obtain the Heisenberg equations of motion

$$
\begin{aligned}
\frac{da}{dt} &= \frac{i}{\hbar}[H,a] &&= -i\omega_c a + gJ^- , \\
\frac{dJ^-}{dt} &= \frac{i}{\hbar}[H,J^-] &&= -i\omega_{at} J^- + gaJ_3 , \\
\frac{dJ_3}{dt} &= \frac{i}{\hbar}[H,J_3] &&= -2g(aJ^+ + a^\dagger J^-) ,
\end{aligned}
\tag{5.6}
$$

where we have introduced the notation

$$
J^\pm = \sum_i \sigma_i^\pm , \quad J_3 = \sum_i \sigma_{3i} .
\tag{5.7}
$$

Taking the expectation value on both sides of Eqs. (5.6) and neglecting quantum fluctuations in the EM field then leads us to

$$
\begin{aligned}
\frac{dB}{dt} &= -i\omega_c B + gM , \\
\frac{dM}{dt} &= -i\omega_{at} M + gB\Delta , \\
\frac{d\Delta}{dt} &= -2g(BM^* + B^* M) ,
\end{aligned}
\tag{5.8}
$$

with the field, magnetization, and population inversion defined by

$$
B = \langle a \rangle , \quad M = \langle J^- \rangle , \quad \Delta = \langle J_3 \rangle .
\tag{5.9}
$$

Note that the field B is normalized so as to equal the square root of the number of photons, whereas M and Δ are normalized so as to be equal to $N\rho_{ca}$ and $N(\rho_{cc} - \rho_{aa})$, respectively, in terms of the number of atoms N and the one-atom density matrix ρ.

Equations (5.8) are the field-matter equations for the hydrogen maser in the absence of relaxation. Including the phenomenological relaxation terms, we find

$$
\begin{aligned}
\frac{dB}{dt} &= -(i\omega_c + \kappa)B + gM , \\
\frac{dM}{dt} &= -(i\omega_{at} + \gamma_\perp)M + gB\Delta , \\
\frac{d\Delta}{dt} &= -\gamma_\parallel(\Delta - \Delta_0) - 2g(BM^* + B^* M) .
\end{aligned}
\tag{5.10}
$$

The cavity loss rate is denoted by $\kappa = 1/T_c$ and the relaxation rates for the magnetization and population inversion by $\gamma_\perp = 1/T_2$ and $\gamma_\parallel = 1/T_1$, the so-called transverse and

longitudinal relaxation rates. The latter are primarily determined by the finite residency time of the atoms in the storage bulb and by collisional relaxation. The value towards which Δ relaxes in the absence of field-matter interaction is denoted by Δ_0.

Eqs. (5.10) are the Maxwell-Bloch equations. They describe the time-dependent behavior of both the room-temperature and sub-Kelvin hydrogen masers. In the following sections we will discuss the correspondence between these equations and the Lorenz equations and investigate the time-dependent behavior of the solutions.

5.3 Dynamics of the cryogenic H maser

To analyze the Maxwell-Bloch equations, we first introduce the following scaling:

$$
\begin{aligned}
B &= (\gamma_\perp/2g)X\exp(-i\omega_m t)\,, \\
M &= (\Delta_0/2R)Y\exp(-i\omega_m t)\,, \\
\Delta &= \Delta_0(1 - Z/R)\,, \qquad\qquad (5.11)\\
\tau &= \gamma_\perp t\,, \\
R &= g^2\Delta_0/(\kappa\gamma_\perp)\,, \\
\sigma &= \kappa/\gamma_\perp\,, \quad b = \gamma_\parallel/\gamma_\perp\,,
\end{aligned}
$$

where ω_m is chosen to be the maser operating frequency in steady state. In terms of this scaling, the Maxwell-Bloch equations (5.10) are transformed into the complex Lorenz equations [12]

$$
\begin{aligned}
\frac{dX}{d\tau} &= \sigma[-(1 - i\delta_c)X + Y]\,, \\
\frac{dY}{d\tau} &= -(1 + i\delta_{at})Y + RX - XZ\,, \qquad\qquad (5.12)\\
\frac{dZ}{d\tau} &= -bZ + \tfrac{1}{2}(XY^* + X^*Y)\,,
\end{aligned}
$$

where the detunings are defined by

$$
\delta_c = (\omega_m - \omega_c)/\kappa\,, \quad \delta_{at} = (\omega_{at} - \omega_m)/\gamma_\perp\,. \qquad\qquad (5.13)
$$

Let us consider the time scales involved in our problem. Typical values (in sec^{-1}) for the time constants of the cryogenic H maser are

$$
\gamma_\parallel \simeq \gamma_\perp = 1\,, \quad \kappa = 10^5\,, \quad g = 10^{-2}\,. \qquad\qquad (5.14)
$$

Note the unusual orders of magnitude, in comparison with typical laser values. The value of g follows directly from Eq. (5.5). The maser γ values are of the order of the inverse residency time in the storage bulb. Spontaneous emission contributions are completely negligible. One of the advantages of the sub-Kelvin H maser relative to its room-temperature version is the fact that atomic densities and thus Δ_0 can be much higher for the same collisional relaxation rates. This makes it possible to achieve steady oscillation with modest cavity quality factors, which is of importance in reducing the frequency instability due to cavity pulling. The higher atomic density and lower temperature also provide for a reduced influence of thermal noise on steady oscillation by increasing the signal-to-noise ratio.

Given the large difference between the field and atomic decay rates of the cryogenic maser, it would seem natural to adiabatically eliminate the field variable which may be thought to relax five orders of magnitude faster than the atomic variables. However, the consideration of the unperturbed time scales is not sufficient to justify the asymptotic expansion known as adiabatic elimination of the fast variables. This point was discussed by Lugiato *et al.* [13], who stressed that the classification in slow and fast variables must be based on the relaxation times of the full problem including the effect of field-matter interaction (see also Oppo and Politi [14] for an alternative point of view). An analysis of these effective time scales will be presented after we have discussed the stability properties of the steady solutions of Eqs. (5.12). For simplicity, we restrict ourselves throughout this paper to the special case $b = 1$, in which we can use the explicit analytic results obtained previously [15] for the complex equations (5.12). The case $b \neq 1$ has been treated recently by Ning and Haken [16] and the results are considerably more complicated. With $b = 1$, Eqs. (5.12) have a trivial steady state,

$$X = Y = Z = 0, \tag{5.15}$$

corresponding to the absence of stimulated photons, and a finite steady state,

$$\mathrm{Re}(X) = \mathrm{Re}(Y) = \pm\sqrt{Z}, \quad Z = R - 1 - \delta^2, \tag{5.16}$$
$$\mathrm{Im}(X) = 0, \quad \mathrm{Im}(Y) = \mp\delta\sqrt{Z}, \quad \delta_{\mathrm{at}} = \delta_c \equiv \delta.$$

The trivial solution (5.15) is stable below the first threshold of oscillation defined by $R_1 = 1 + \delta^2$. At this threshold the nontrivial steady solution emerges as a stable solution.

In the bad cavity situation ($\sigma > 2$) which is prevalent in the cryogenic maser, the steady solution (5.16) loses its stability at the "maser second threshold" R_H. The critical control parameter R_H or the corresponding critical photon number $|X_H|^2 = R_H - 1 - \delta^2$ (in units of the saturation photon number N_s) for the second threshold is the real positive solution of

$$a_2|X_H|^4 + a_1|X_H|^2 + a_0 = 0,$$

$$a_2 = (1 + 3\sigma)(\sigma - 2),\qquad\qquad\qquad\qquad (5.17)$$

$$a_1 = (\sigma + 1)(\sigma + 2)(2\sigma^2 - 5\sigma - 5) - \delta^2(\sigma - 1)^2(6\sigma^2 + 7\sigma + 4),$$

$$a_0 = -2(\sigma + 1)[(\sigma + 1)^2 + \delta^2(\sigma - 1)^2][(\sigma + 2)^2 + \delta^2(\sigma - 1)^2].$$

In the limit $\sigma \to \infty$, whose consideration is suggested by the parameters (5.14), two domains have to be distinguished: a small detuning region, where

$$1 - 3\delta^2 > 0 \text{ and } |X_H|^2 = \sigma\frac{(1 + \delta^2)^2}{1 - 3\delta^2} + O(1),\qquad (5.18)$$

and a large detuning region, where

$$1 - 3\delta^2 < 0 \text{ and } |X_H|^2 = \tfrac{2}{3}\sigma^2(3\delta^2 - 1) + O(\sigma).\qquad (5.19)$$

As proved in Ref. [15], the Hopf bifurcation which takes place at $R = R_H$ is subcritical in the small detuning domain, the only domain we shall analyze for the cryogenic maser parameters. In this case a linear stability analysis does not give information on the nature of the long-time solution which is reached beyond the second threshold.

With these results, we are now in a position to explain why the adiabatic elimination of the field variable is not possible. As shown by Fowler and McGuinness [10], the solutions of Eqs. (5.12) for $R > R_H$ with $\sigma \gg 1$ and on resonance (i.e., $\delta_{at} = \delta_c = 0$) are pulse trains which can be either periodic or chaotic. This remains true for δ_{at} and δ_c sufficiently small. For the sake of this discussion, we introduce the scaling

$$X = \sigma x, \quad Y = \sigma y, \quad Z = \sigma z, \quad \tilde{t} = \sigma\tau = \kappa t, \quad R = \sigma r, \quad (5.20)$$

$$\epsilon = 1/\sigma \ll 1, \quad \delta_c = O(1), \quad \delta_{at} = O(1), \quad r = O(1). \quad (5.21)$$

In these variables, Eqs. (5.12) become

$$x' = -(1 - i\delta_c)x + y,$$

$$y' = -\epsilon(1 + i\delta_{at})y + rx - xz,\qquad\qquad (5.22)$$
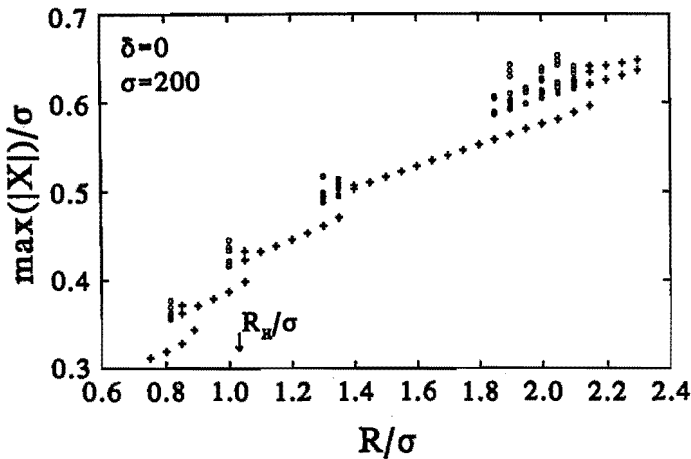
$$z' = -\epsilon z + \tfrac{1}{2}(xy^* + x^*y),$$

Figure 5.1: Bifurcation diagram of the complex Lorenz equations on resonance: plot of the maximum maser magnetic-field amplitude $|X|$ (divided by σ) vs the reduced pump parameter R/σ. Crosses indicate periodic solutions while circles correspond to chaotic solutions. The fixed point loses its stability at R_H/σ.

where the prime stands for the derivation with respect to $\tilde{t}$. These equations have two types of solutions. Between pulses, x and y become $\exp[-O(1/\epsilon)]$ and $z = O(1)$. This solution depends on the slow-time variable $\tau = \epsilon\tilde{t}$ given by (5.11) and the variable z can be adiabatically eliminated. The pulses themselves, however, are described by solutions for which all three variables x, y, and z are $O(1)$ functions that depend on the fast time $\tilde{t}$. Hence, during the pulses no variable can be adiabatically eliminated. As a result, the adiabatic elimination of the field X in Eqs. (5.12) is not valid to describe the nonsteady solutions.

The number and the nature of the attractors which Eqs. (5.12) can display besides the fixed points have been investigated by direct numerical integration of the differential equations. Although we know from the work of Fowler and McGuinness that chaotic and periodic solutions are expected to exist and to coexist, no general picture of the
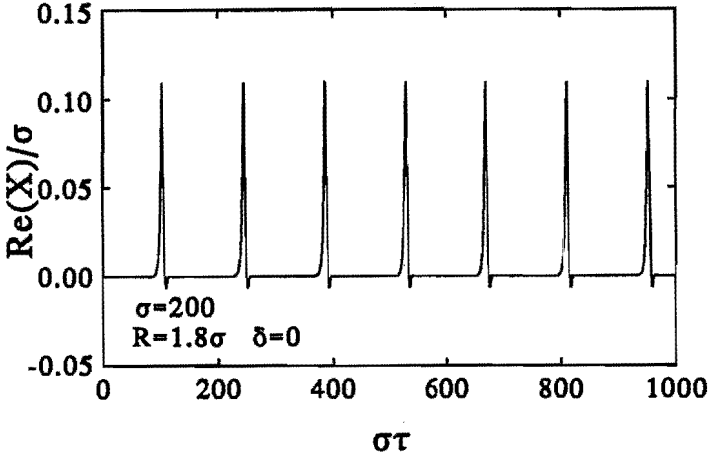
Figure 5.2: Example of a periodic solution above the maser second threshold: the real part of the maser magnetic field (in units of σ) vs $\sigma\tau = \kappa t = t/T_c$.

bifurcation diagram has been provided in the special limit

$$\sigma \gg 1, \quad R = O(1). \tag{5.23}$$

A bifurcation diagram is displayed in Fig. 5.1 for $\sigma = 200$ and on resonance ($\delta = 0$). For each value of R, Eqs. (5.22) are integrated and the maximum of the field amplitude is recorded. When the solution is found to be periodic, the maxima are represented in the diagram by crosses. For legibility, only large maxima, such that $\max(|X|)/\sigma = O(1)$, are drawn. Five branches of solutions are visible in Fig. 5.1. The topological difference between these branches is the number of smaller maxima in each period. In the lowest branch, there is one smaller maximum per period. Each of the next branches has one more small maximum than the previous branch. If we classify the maxima in each period of a periodic solution by order of increasing size, each maximum is larger than the previous one by about two orders of magnitude. It is therefore difficult to show more than two of them in a figure. A typical periodic solution is shown in Fig. 5.2. To increase the resolution, we have plotted the real part of X rather than the modulus of X. The abcissa coordinate is $\sigma\tau \equiv \kappa t$. This solution has five extrema per period but only
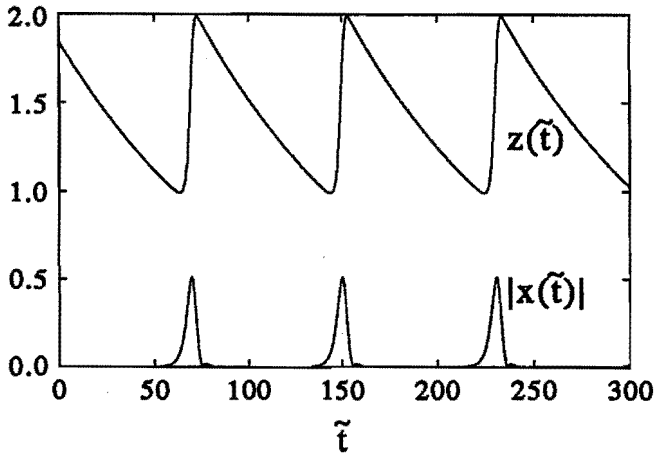
Figure 5.3: Time evolution of $z(\tilde{t})$ and $|x(\tilde{t})|$ showing the coupling between the variations of the two variables. This figure is obtained by solving Eqs. (5.22) on resonance ($\delta = 0$) with the parameters $r = 1.5$ and $\epsilon = 0.01$.

the first two are resolved graphically. Some solutions are chaotic in time. Their $O(1)$ maxima, which are recorded over the same time duration for the entire figure (Fig. 5.1) are represented by circles. An example of a chaotic solution is given in our previous report on this subject [9].

When the maser is in the pulsing regime (periodic or chaotic), a complex interplay between the atoms and the field takes place. Between pulses, the atomic population inversion Δ builds up (hence, z decreases) due to the fact that atoms enter the storage bulb in the upper state while the number of photons in the cavity is negligible. When a critical population inversion is reached, a burst of photons is emitted, which corresponds to a sudden atomic deexcitation and the consequent release of stimulated photons in the maser cavity leading to the pulse. This is shown in Fig. 5.3.

Quite surprisingly, the domain of periodic solutions is much larger than the domain of chaotic solutions. Furthermore, the first three branches overlap with the domain of stable steady state. The coexistence of periodic, chaotic, and steady solutions was recently reported by Ning and Haken [17] for $\sigma = 2$ and $b = 0.01$ in a study of anomalous

switching. The left-hand sides of the four upper branches show a similar structure. As R is decreased, a period-doubling sequence is observed and a chaotic solution is reached. In many instances, higher-period solutions were observed but not reported in the figure, to retain some clarity. For example, many instances of period-8 solutions were recorded over very narrow domains.

The bifurcation diagram of Fig. 5.1 is very sensitive to detuning. Figures 5.4 and 5.5 display how the bifurcation diagram is affected by increasing δ. Already for $\delta = 0.01$, the chaotic domains have disappeared (or they are so small that they escaped our numerical capabilities) but the branches of periodic solutions are still very distinct. However, as δ is increased to 0.1, only two branches of periodic solutions remain. They still differ by the number of extrema. The simplification of the bifurcation diagram with increasing detuning has already been reported [18] in the case of finite σ.

Returning to the resonant case, we have analyzed the influence of σ. Using the procedure described earlier, we have also obtained the bifurcation diagrams for σ equal to 100 and to 50. They are shown in Figs. 5.6 and 5.7, respectively. As σ decreases, the number of branches of solutions decreases as well. Furthermore, a comparison of the three diagrams obtained under resonant condition suggests that the pulse peak scales like σ:

$$\max(X) \propto \sigma. \tag{5.24}$$

One aspect which is not apparent in these bifurcation diagrams is the extension of each solution's basin of attraction. For instance, in the case $\sigma = 100$ depicted in Fig. 5.6, if we start on the steady state and increase R by sufficiently small steps, the solution will jump onto the chaotic part of the second branch rather than onto the periodic part of the first branch. Hence, the bifurcation diagrams do not yet tell the complete story.

Another useful piece of information is the variation of the frequency of the periodic solutions versus R, i.e., the inverse of the time duration between two consecutive $O(1)$ pulses. For our reference bifurcation diagram given in Fig. 5.1, the frequencies are displayed in Fig. 5.8. Domains of period doubling and chaos are not reported in this figure. The frequency varies significantly versus σ. This is clearly realized by comparing Fig. 5.8 with Fig. 5.9 where the frequency of the periodic solutions is displayed on resonance for $\sigma = 50$. Let us consider the period measured on time traces such as that
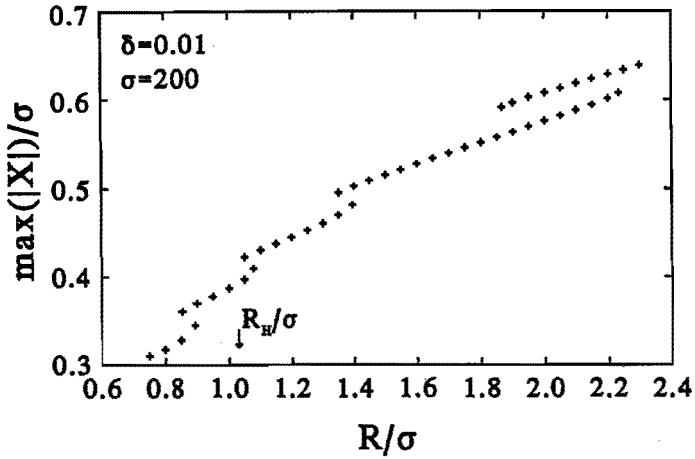
Figure 5.4: Same as in Fig. 5.1 but with a very small detuning $\delta = 0.01$.
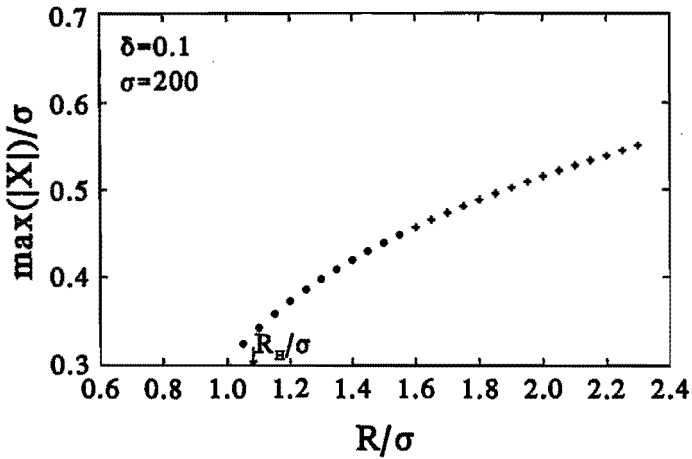
Figure 5.5: Same as in Fig. 5.4 but for a larger detuning $\delta = 0.1$. The • and the + signs refer to periodic solutions with different numbers of (small) maxima per period.
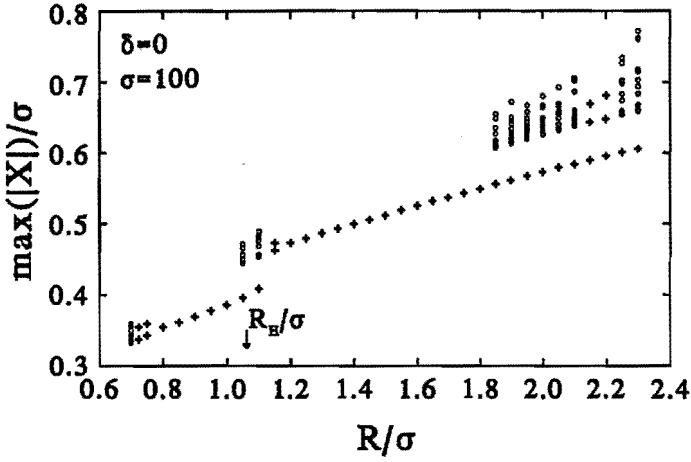
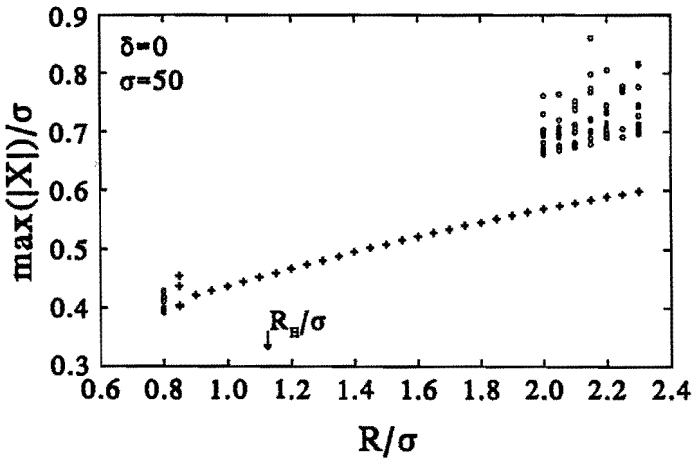Figure 5.6: Same as in Fig. 5.1 but for $\sigma = 100$.

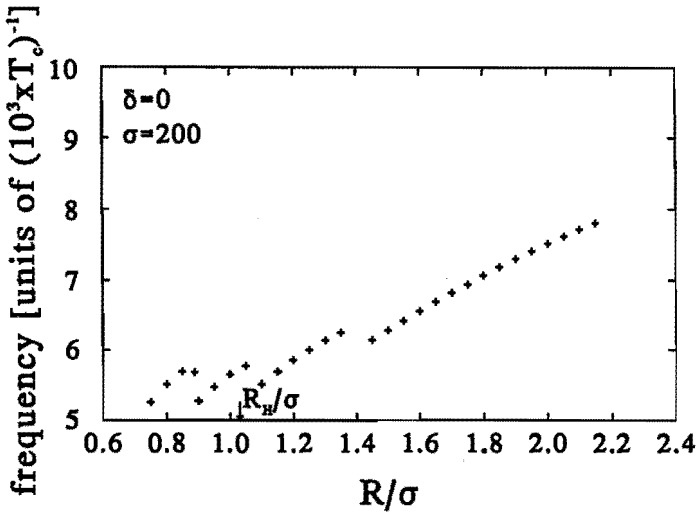Figure 5.7: Same as in Fig. 5.1 but for $\sigma = 50$.

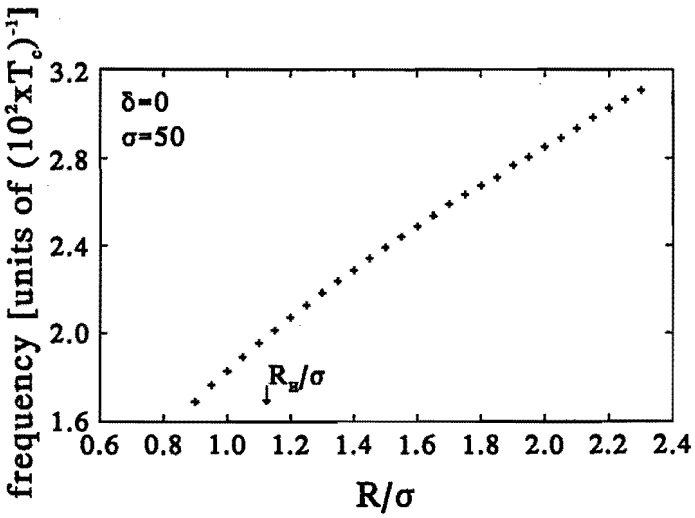Figure 5.8: *Frequency of the periodic solutions displayed in Fig. 5.1.*

Figure 5.9: *Frequency of the periodic solutions displayed in Fig. 5.7.*

shown in Fig. 5.2. On resonance and for $R = 1.2\sigma$, for instance, we have

$$X(\tilde{t}) \;=\; X(\tilde{t} + \tilde{p}) \;\equiv\; X[\kappa(t + p)]$$

and the following numerical values are obtained:

$$
\begin{aligned}
\sigma &= 50, & \kappa p &= 48.22, \\
\sigma &= 100, & \kappa p &= 93.63, \\
\sigma &= 200, & \kappa p &= 170.91.
\end{aligned}
\tag{5.25}
$$

Hence, κp is an $O(\sigma)$ function and the physical frequency is of the order of the atomic polarization decay rate $\gamma_{\perp}$. This is indeed coherent with the fact that we are dealing with a bad cavity. Despite this result, we have drawn our frequency plots in units of T_c^{-1} because they were obtained by solving Eqs. (5.22) for which T_c^{-1} is the natural unit.

5.4   Influence of thermal noise

In the previous sections, we have studied the deterministic evolution of the maser equations. However, two physical mechanisms may induce a stochastic contribution to the time evolution of the magnetic field: spontaneous emission and thermal noise. As mentioned previously, spontaneous emission is negligible for the cryogenic maser, but thermal noise contributes to the average photon number the amount

$$\langle n \rangle_{\text{th}} \;=\; 1/[\exp(h\nu/kT) - 1].$$

For the cryogenic maser at $\nu = 1.42$ GHz (corresponding to a wavelength of 21.1 cm), the thermal photon number $\langle n \rangle_{\text{th}}$ equals 14.2 at 1 K, 6.85 at 0.5 K, and 1.02 at 0.1 K. Although these photon numbers are fairly small, they are in fact large compared with the photon numbers obtained between pulses in the deterministic periodic and chaotic domains. Therefore, we have to investigate to what extent they may affect our analysis.

   A convenient way to model the influence of thermal noise is to add a stochastic source term $\xi(t)$ to the equation for the magnetic field B in (5.10). The corresponding modification to Eqs. (5.22) on resonance is

$$
\begin{aligned}
x' &= -x + y + 10^{-7}[\xi_1(\tilde{t}) + i\xi_2(\tilde{t})], \\
y' &= -\epsilon y + rx - xz, \\
z' &= -\epsilon z + \tfrac{1}{2}(xy^* + x^*y),
\end{aligned}
\tag{5.26}
$$
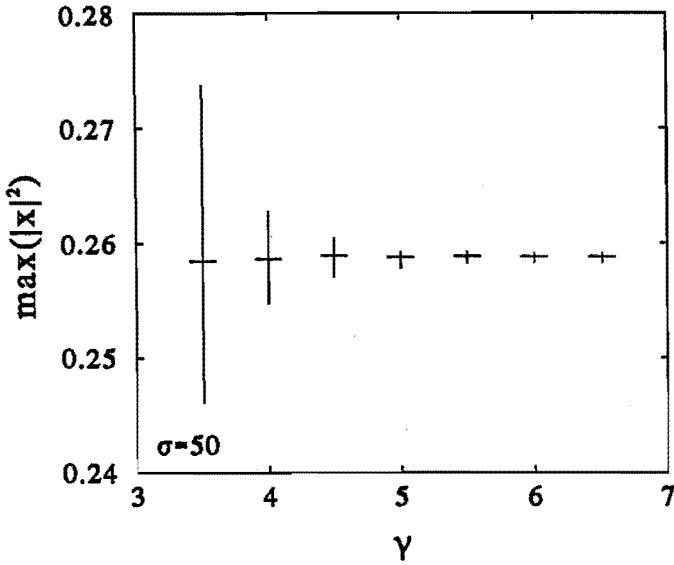
Figure 5.10: Distribution of the maxima vs the noise amplitude in the pulsed regime in the presence of noise for r = 1.5, σ = 50, and on resonance. The vertical lines give the spread of the distribution and the horizontal bars are the mean values for a sample taken during 2000 time units.

where $10^{-\gamma} = (2g/\kappa)\sqrt{(n)_{th}}$. We have solved these stochastic equations numerically using for $\xi_1(\tilde{t})$ and $\xi_2(\tilde{t})$ a pseudo-random-number Gaussian distribution, with zero mean and unit variance. Although no detuning was included, we kept the complex form of the equations and a complex noise source to account for phase and amplitude fluctuations of the magnetic field. In Fig. 5.10 we plot the distribution of peaks of the periodic solution for $r = 1.5$ and $\sigma = 50$ versus the parameter γ. The horizontal bars are the average values. For the same sample, we plot in Fig. 5.11 the frequency distributions. We observe that in these two figures, the averages practically do not vary with γ. For small γ (i.e., large noise amplitudes) there is a significant spread around the mean. For $\gamma > 4.5$, this spread becomes constant. We have verified that this spread is also present when the noise is turned off; it corresponds therefore to the numerical precision of our calculation.
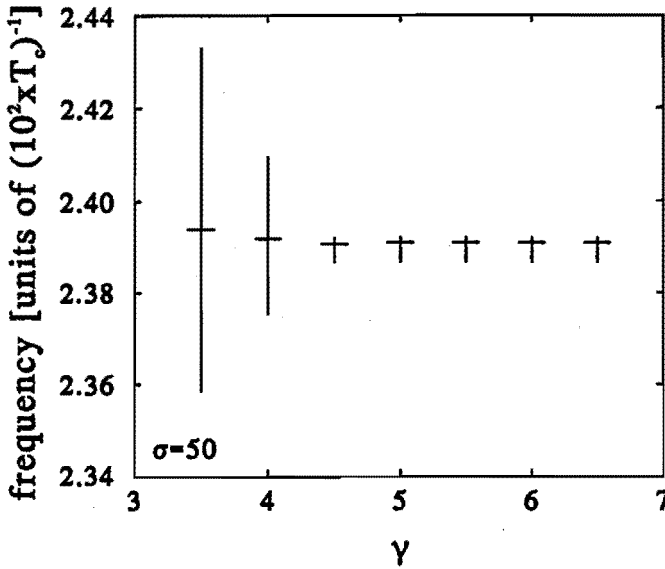
Figure 5.11: *Distribution of the peak frequencies for the samples used in Fig. 5.10. The vertical lines give the spread of the distribution and the horizontal bars are the mean values.*

When σ is increased, these results are significantly altered. For $\sigma = 100$, we see in Fig. 5.12 that as γ increases, two domains occur. For $\gamma < 5$, the mean value increases with γ but the spread of the distributions does not vary in the same ratio as the added noise. In the second domain, $\gamma \geq 5$, the mean values remain practically constant and the variance decreases. For $\sigma = 200$, only the first domain (increasing mean value with γ) is observed in the whole range studied, up to $\gamma = 6.5$. To interpret these results, it should be borne in mind that the domain $\sigma \gg 1$ which we investigate is characterized by pulsed rather than harmonic solutions in the nonsteady regime. In particular, in the time domain comprised between two consecutive pulses, it was shown [10] that x and y are exponentially small, being typically $\exp[-O(1/\epsilon)]$ functions. This is much smaller than either added noise or numerical roundoff errors. Therefore, one expects that the triggering of the pulse, which takes place when x and y are larger than $\exp[-O(1/\epsilon)]$ but still smaller than $O(1)$, will not be deterministic in numerical simulations. However, in the absence of added noise,
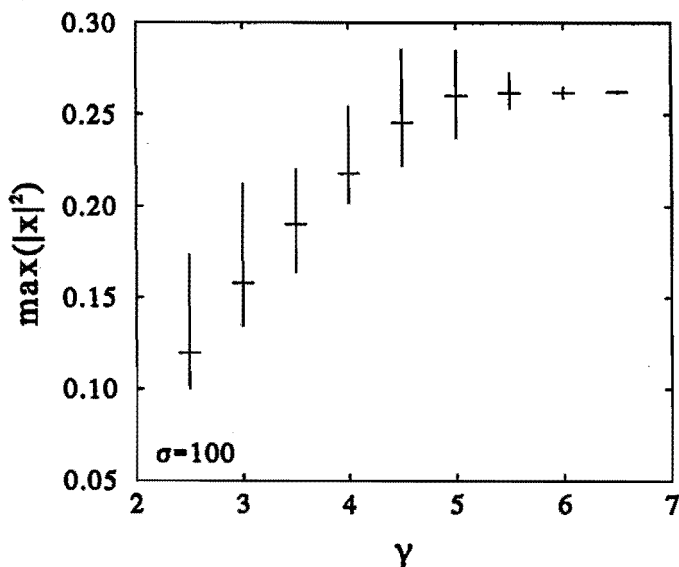
Figure 5.12: Same as in Fig. 5.10 but for $\sigma = 100$.

the variance of the distributions is so small that it does not appear in the Figs. 5.1 and 5.4-5.9. As the value of $\dot{x}$ and y between pulses becomes progressively smaller with increasing σ, thermal noise will have a larger influence for higher values of σ. This is apparent in Figs. 5.10-5.12, where convergence of the maxima versus γ takes place at progressively higher γ values. When these results are extrapolated to the σ values and the noise levels found in a realistic cryogenic hydrogen maser, it is expected that the pulsed behavior will be triggered by the stochastic noise, i.e., the hydrogen maser is in the first domain of Fig. 5.12 where the maxima have not yet converged as a function of γ.

The influence of thermal noise will be largest between two pulses. The remaining question is whether the pulse shape itself is determined by stochastic processes or that the time development of a pulse is a deterministic evolution. If the latter is the case, study of the pulse would still yield useful information on both the parameters determining the behavior of the hydrogen maser and the complex Lorenz equations. If, however, the evolution of a pulse would be a stochastic process as the evolution between the pulses,
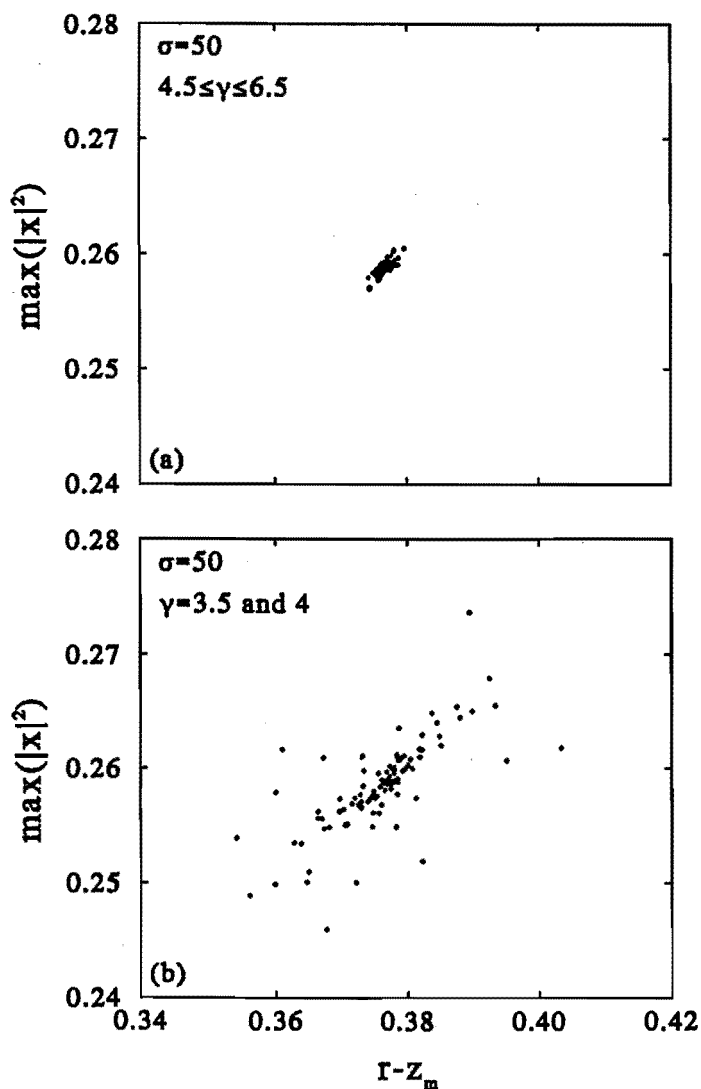
Figure 5.13: Maximum of $|x|^2$ vs $r - z_m$ for each pulse of the samples used in Fig. 5.10. For the sake of legibility, we have plotted separately but on the same scale the two domains $\gamma < 4.5$ (high dispersion of points) and $\gamma \geq 4.5$ (small dispersion of points) since they overlap.
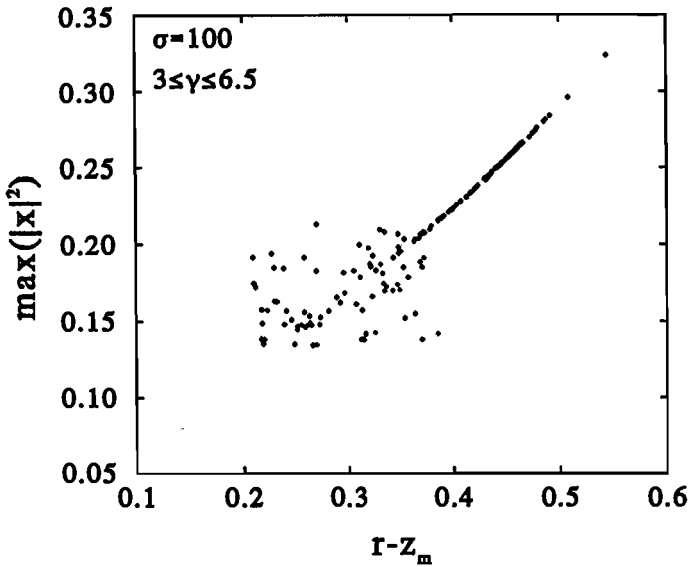
Figure 5.14: Maximum of $|x|^2$ vs $r - z_m$ for each pulse of the samples used in Fig. 5.12. The cloud of points results from the samples with $\gamma = 3$ and 3.5; the line is made up of the points of the samples with $\gamma \geq 4$.

observation of the time-dependent domain would yield information on the influence of the noise on the system but not on the Lorenz equations themselves. To analyze whether the pulse is deterministic or not, we have plotted in Figs. 5.13-5.15 the maximum of $|x|^2$ versus $r - z$ at the beginning of the pulse for $\sigma = 50$, 100, and 200, and for various values of γ. The choice of $r - z$ instead of z is a matter of convenience only. The value of z at the beginning of the pulse [10] is called z_m and is determined by the condition $|x|^2 + |y|^2 = \epsilon^2$. The reason for this is that the pulse itself can be described by the Lorenz equations neglecting all terms of order ϵ with x, y, and z being $O(1)$. As a result, ϵ can be chosen as the zero level for the pulse. It can be seen in Figs. 5.13-5.15 that for each σ there are two domains separated by a critical value γ_c. Below γ_c, there is no correlation between z at the beginning of the pulse and $\max(|x|^2)$: We observe a cloud of points indicating a stochastic process. Above γ_c, there is a clear correlation between the two variables and all points fall nicely on a single curve when the pulse
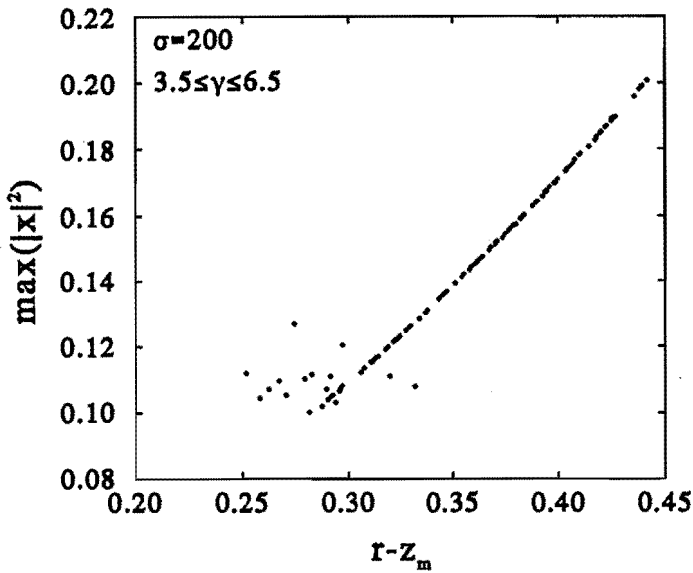
Figure 5.15: Maximum of $|x|^2$ vs $r - z_m$ for $r = 1.5$, $\sigma = 200$, and on resonance, for each pulse of a sample taken during 2000 time units for each γ. The cloud of points results from the samples with $\gamma = 3$ and 3.5; the line is made up of the points of the samples with $\gamma \geq 4$.

triggering is stochastic or are concentrated in a very small domain (whose width is due to the numerical noise) when the triggering is deterministic. The surprising result is that in all three cases displayed in Figs. 5.13-5.15, we have found that $\gamma_c \simeq 4$. More precisely, for $\sigma = 50$, we have $4 < \gamma_c < 4.5$, while for $\sigma = 100$ and 200, we have $3.5 < \gamma_c < 4$. Hence, this critical parameter is only weakly dependent on σ, at least in the range considered here. Extrapolating the constant value of γ_c to the high-σ regime of a realistic hydrogen maser, we expect the corresponding value of γ, i.e., about 6, to be larger than γ_c, so that the pulse evolution will be deterministic.

For the discussion which we have given, the actual value of the thermal noise is of crucial importance. This, however, depends on a couple of control parameters: κ, T, and ν. Whereas changing κ would merely change the influence of any noise on the maser operation, changing the latter two parameters would also change the ratio of thermal to

quantum noise. Although quantum fluctuations are negligible with respect to the thermal noise for $T = 0.5$ K and $B = 0$, they become progressively more important for smaller T and larger B (i.e., larger ν). Experimental realization of this new regime would thus be very interesting from the point of view of the study of the Lorenz equations with both thermal and quantum noise.

A source of noise which is unavoidable in the computer calculations is the numerical noise due to roundoff errors and the inherent limited precision in the integration code. With the code used to solve Eqs. (5.26), we have verified explicitly that in the absence of noise ($\gamma = \infty$), the solutions are periodic (with a precision of three significant digits) after a sufficiently long time. However, when the numerical precision was changed, $\max(|x|^2)$ appeared as a sensitive function of the numerical noise, while the period was remarkably independent of that noise. Although numerical noise has probably introduced a bias in our calculations, a strictly noise-free experiment is also impossible. Hence, the possible bias introduced in our numerical results should also be found in the experimental results.

5.5   Conclusions

The cryogenic hydrogen maser is a device which is known for its extreme frequency stability. We have shown that apart from this stable steady oscillation, a second operation mode exists that is readily achievable in the cryogenic hydrogen maser by increasing the quality factor of the maser cavity. By analyzing the dynamical maser equations, the Maxwell-Bloch equations, we have identified this operation mode with a pulsed output consisting of very sharp pulses separated by relatively long periods of almost zero output power. By systematically scanning through parameter space, bifurcation diagrams have been obtained that have enabled us to make statements about the complex Lorenz equations in a domain of parameter space $[R, \sigma \gg 1, b = O(1)]$ which had hardly been investigated.

Furthermore, we have analyzed the influence of thermal noise on the operation of the cryogenic maser. Whereas the number of stimulated photons is large compared to the number of thermal photons in the steady mode of operation allowing for a deterministic semiclassical description of the maser operation, it is small in between the pulses in the time-dependent domain. We have modeled the thermal noise by including a stochastic

Gaussian noise term in the Maxwell-Bloch equations and have concluded that the time-dependent regime of the cryogenic hydrogen maser will still be characterized by pulsed behavior. The sequence of pulses, however, will not be deterministic but stochastic, both in the maxima of the pulses and the periods in between them, as the pulses will be triggered by the thermal noise. The evolution of a single pulse, on the other hand, can still be deterministic.

In terms of the Lorenz equations, our numerical work gives a good picture of the behavior to be expected in this part of the parameter space. The occurrence of only a few small domains of chaotic behavior compared to relatively large domains of periodic behavior is especially remarkable. Furthermore, the coexistence of a stable steady state, a periodic solution, and a chaotic solution is apparent. As a last point, the stabilizing effect of the detuning should be noted. The question remains, however, whether the cryogenic hydrogen maser is useful to study the Lorenz equations as such, due to the influence of thermal noise. If, on the other hand, one is interested just in this influence, the hydrogen maser will be an excellent tool, thereby giving the possibility to observe a gradual transition from thermal to quantum noise in a single experimental setup.

The second context in which our work is of interest is from the viewpoint of the hydrogen maser. As mentioned before, the operation of the hydrogen maser is determined by the interplay of a large number of parameters which are often difficult to diagnose. In this case the influence of thermal noise means that the sequence of pulses will not give the information which can be expected from the operation without noise. As, however, the evolution of a single pulse can remain deterministic, the time-dependent domain may still prove to be an interesting domain from this point of view as well.

Bibliography

[1] H. M. Goldenberg, D. Kleppner, and N. F. Ramsey, Phys. Rev. Lett. **5**, 361 (1960).

[2] M. D. Hürlimann, W. N. Hardy, A. J. Berlinsky, and R. W. Cline, Phys. Rev. A **34**, 1605 (1986); W. N. Hardy, M. D. Hürlimann, and R. W. Cline, Jpn. J. Appl. Phys. **26**, 2065 (1987).

[3] R. L. Walsworth, I. F. Silvera, H. P. Godfried, C. C. Agosta, R. F. C. Vessot, and E. M. Mattison, Phys. Rev. A **34**, 2550 (1986).

[4] N. F. Ramsey, Rev. Mod. Phys. **62**, 541 (1990).

[5] A. G. Gurtovnik, Izv. Vyssh. Uchebn. Zaved. Radiofiz. **1**, 83 (1958).

[6] A. Z. Grasyuk and A. N. Orayevskiy, Radiotekh. Elektron. **9**, 524 (1964) [Radio Eng. Electron. Phys. **9**, 424 (1964)].

[7] C. Audoin, Ph.D. thesis, Université de Paris-Sud, France, 1967.

[8] J. H. Shirley, Am. J. Phys. **36**, 949 (1968).

[9] A. C. Maan, H. T. C. Stoof, B. J. Verhaar, and P. Mandel, Phys. Rev. Lett. **64**, 2630 (1990); **65**, 2319 (1990).

[10] A. C. Fowler and M. J. McGuinness, Physica D (Amsterdam) **5**, 149 (1982).

[11] J. C. Slater, Rev. Mod. Phys. **18**, 441 (1946).

[12] J. D. Gibbon and M. J. McGuinness, Physica D (Amsterdam) **5**, 108 (1982). The complex equations derived by these authors are obtained more precisely by chosing $\omega_m = \omega_c$. Hence the nontrivial solution of Eqs. (5.12) keeps a harmonic time dependence which is spurious since the intensity is constant.

[13] L. A. Lugiato, P. Mandel, and L. M. Narducci, Phys. Rev. A **29**, 1438 (1984).

[14] G.-L. Oppo and A. Politi, in *Instabilities and Chaos in Quantum Optics II,* edited by N. B. Abraham, F. T. Arecchi, and L. A. Lugiato (Plenum, London, 1988), p. 363.

[15] P. Mandel and H. Zeghlache, Opt. Commun. **47**, 146 (1983).

[16] C.-Z. Ning and H. Haken, Phys. Rev. A **41**, 3826 (1990).

[17] C.-Z. Ning and H. Haken, Phys. Rev. A **41**, 6577 (1990).

[18] H. Zeghlache and P. Mandel, J. Opt. Soc. Am. B **2**, 18 (1985).

Chapter 6

A new method to calculate three-body scattering
below the break-up threshold

Abstract

We propose a new method to solve the Faddeev equations for three-nucleon scattering below
the threshold for break-up. Instead of a discretization of both relative positions or momenta
we expand the Faddeev component in a set of two-nucleon basis states. These basis states
incorporate already the effect of the two-nucleon forces. This method is applied to neutron-
deuteron scattering using local s-wave Malfliet-Tjon potentials. The calculations show
rapid convergence and good agreement with previous calculations for quartet scattering.
Convergence is less for doublet scattering due to a node occurring in the configuration space
Faddeev component at short distances in the two-nucleon subsystem.

6.1 Introduction

Three-nucleon scattering is an important test laboratory for nuclear dynamics. Dynamical
models for nuclear interactions can be probed in a highly nontrivial manner by comparing
their predictions to a rich bulk of experimental data. With the advent of supercomputers
it became possible to solve the three-nucleon Faddeev equations directly for any type
of nucleon-nucleon (NN) interaction [1]. This went parallel with an increased precision

and sophistication of experiments [2]. So far agreement between theory and experiment is in general rather good [3], using realistic *NN* forces with all their complexities, but there are also a few exceptions. One of them is the low energy analyzing power A_y where a striking discrepancy sticks out [4] and still poses a puzzle. This discrepancy is even present below the nucleon-deuteron break-up threshold [5]. New experiments are planned measuring more complicated spin observables below break-up [6]. It is therefore of great practical interest to supplement the very few existing techniques which solve the Faddeev equations precisely [1],[7]-[9] for any type of realistic *NN* forces by new and possibly more efficient methods. It is the aim of this paper to propose a simple but nevertheless precise approach which has already been successfully used for three-nucleon bound state calculations in the nonrelativistic [10] and relativistic context [11].

With the exception of Ref. [9] the existing precise techniques in momentum or configuration space treat both types of relative coordinates explicitly. In contrast, here we express the dependence on the two-nucleon subsystem coordinate through a judiciously chosen set of basis states. These basis states incorporate already the effect of two-nucleon forces in the two-nucleon subsystem and therefore it is expected that only few are needed to provide a well converged description. This reduces the dimension of the total problem dramatically and allows to perform such a calculation even on small workstations. Since the basis states are square integrable the method is first of all only suited for scattering below the threshold for real break-up. Since it is an exact method it describes of course fully the virtual break-up.

The proposed method is not only of interest for three-nucleon scattering but is also relevant in an atomic physics context, i.e., three-body recombination of atomic hydrogen which has been the limiting process in a class of experiments trying to reach Bose-Einstein condensation [12]. The calculation of the recombination rate involves the evaluation of a matrix element of the interatomic magnetic dipole interaction between an initial state and a final state [13]-[19]. The initial state has been calculated rigorously by solving the Faddeev equations [14],[16]. The final state can, in principle, be calculated in the same way. However, due to the large number of channels which have to be included in the calculation this is not possible with present supercomputers. The method which we develop in this paper can be used to solve the Faddeev equations also for the final state.

This paper is organized as follows. The formalism is described in Sec. 6.2. An application to neutron-deuteron (n-d) scattering using local s-wave NN forces is given in Sec. 6.3. In Sec. 6.4 we present some conclusions.

6.2 Theory

A system of three particles, e.g., three nucleons or three hydrogen atoms, can be described by state vectors $|\Psi^{\pm}\rangle$ which are eigenstates of the Hamiltonian

$$H = H_0 + V , \tag{6.1}$$

where V represents all two-body interactions. We neglect a possible three-body force. Using the spectator-index notation [20] V can be written as

$$V = \sum_{\beta} V_{\beta} \equiv V_{\alpha} + V^{\alpha} , \tag{6.2}$$

and a channel Hamiltonian can be defined as

$$H_{\alpha} = H_0 + V_{\alpha} . \tag{6.3}$$

From now on we take $\alpha = 1$. The kinetic energy in the center of mass system together with the internal energies are represented by H_0.

We consider a state vector $|\Psi^+\rangle$ describing the scattering process initiated by a particle incident on a bound two-particle target system. In the application to atomic hydrogen we have to find a state of the type $|\Psi^-\rangle$, since we want to describe the final state after the operation of the dipole interaction. Such a solution can, however, be obtained from a $|\Psi^+\rangle$ state by time-reversal. The latter can be written as

$$|\Psi^+\rangle = (1 + P)|\psi_1\rangle , \tag{6.4}$$

where $P = P_{12}P_{23} + P_{13}P_{23}$ is the sum of two cyclic permutation operators and $|\psi_1\rangle$ is a Faddeev component. This Faddeev component satisfies the Faddeev equation

$$|\psi_1\rangle = |\phi_1\rangle + G_0^+ t_1 P |\psi_1\rangle , \tag{6.5}$$

or equivalently

$$(H_1 - E^+)|\psi_1\rangle = -V_1 P |\psi_1\rangle , \tag{6.6}$$

where $|\phi_1\rangle$ describes the initial state of the scattering process, i.e., $|\phi_1\rangle$ is an eigenstate of the channel Hamiltonian H_1. The resolvent operator $1/(E^+ - H_0)$ is denoted by G_0^+, t_1 is the two-body transition operator for pair 1 and $E^+ = E + i\epsilon$. Equation (6.6) is often solved in the momentum basis consisting of the relative momentum p of the two particles in pair 1 and the momentum q of the third particle relative to pair 1, discretizing these momenta and performing a matrix inversion. As already indicated in the introduction it would be of interest to dispose of an additional technique which in the case of three-nucleon scattering would be more efficient, allowing it to run also on smaller computers, and in the case of hydrogen would make it possible to solve the final state exactly including virtual break-up which has been neglected up to now in the calculations but has turned out to give a large contribution to the recombination process [18],[19]. In the following we will restrict ourselves to three-nucleon scattering.

In the present approach the dependence of the Faddeev component on the two-nucleon subsystem coordinate is described by basis states. These basis states first of all comprise the complete set of bound states of the two-nucleon system. The remaining basis states describe the continuum, i.e., the virtual break-up. Including scattering states of pair 1 seems to be difficult, however, since it involves a non-denumerable set of non-localized wave functions. A possible way out was already suggested in Refs. [18],[19]. Since the three-nucleon break-up channel is closed, the two-nucleon continuum has to build up only configurations in a restricted part of three-nucleon configuration space. Therefore, the possibility arises to add a (expectedly small) set of judiciously chosen states. This discrete representation of the continuum, previously successfully applied in a somewhat different way to three-nucleon bound state calculations [10],[11], is treated in the following.

We have to deal with two different kinds of two-nucleon subsystems: those which contain bound states and those which do not contain bound states. In both cases the continuum is generated by including the lower states of a potential consisting of a harmonic oscillator potential added to the two-nucleon interaction potential. If bound states exist the projections on the bound subspace are eliminated by Schmidt orthogonalization and in both cases the rigorous two-nucleon Hamiltonian is diagonalized in the added subspace. This procedure ensures that all the characteristics of the two-nucleon force are already present in the basis states.

Denoting the set of momentum wave functions thus obtained by $\phi_n^{lts}(p)$, with l the relative orbital angular momentum quantum number of the two nucleons, t their combined isospin, s their combined spin and n the radial quantum number, it is now possible to give an explicit expression for the Faddeev component $|\psi_1\rangle$. It is given by

$$
|\psi_1\rangle = \sum_{nlts\lambda} \int dp\,p^2 \int dq\,q^2 \phi_n^{lts}(p) b_n^{lts\lambda}(q) \cdot
$$
$$
|pq(l\lambda)LM_L(t\tfrac{1}{2})TM_T(s\tfrac{1}{2})SM_S\rangle_1 , \qquad (6.7)
$$

where $b_n^{lts\lambda}(q)$ represents the yet unknown motion of the third nucleon with respect to the nucleons in pair 1, with relative orbital angular momentum quantum number λ. The summation over n contains both the bound states and the continuum states. Furthermore, l and λ are coupled to form L and M_L whereas t (s) and $\tfrac{1}{2}$ couple to T (S) and M_T (M_S). The fermionic character of the nucleons requires $l + t + s$ to be odd. If the summation in Eq. (6.7) would be carried out over an infinite number of basis states the expansion would be exact. The calculation of the scattering process has now been reduced to calculating $b_n^{lts\lambda}(q)$.

By operating on the Faddeev equation (6.6) from the left with ${}_1\langle pq(l\lambda)LM_L(t\tfrac{1}{2})TM_T|$ ${}_1\langle(s\tfrac{1}{2})SM_S|$ and after some manipulations the following equation for $b_n^{lts\lambda}(q)$ is obtained

$$
b_n^{lts\lambda}(q) = \delta_{nn_0}\delta_{ll_0}\delta_{tt_0}\delta_{ss_0}\delta_{\lambda\lambda_0}\frac{\delta(q-q_0)}{qq_0} + \frac{1}{E^+ - e_n^{lts} - 3q^2/4m} \cdot
$$
$$
\sum_{n'l't's'\lambda'} \int dq'\,q'^2 V_{nlts\lambda,n'l't's'\lambda'}(qq') b_{n'}^{l't's'\lambda'}(q') , \qquad (6.8)
$$

with

$$
V_{nlts\lambda,n'l't's'\lambda'}(qq') = \int dp\,p^2 \phi_n^{lts}(p) \int dp'\,p'^2 \phi_{n'}^{l't's'}(p') \cdot
$$
$$
{}_1\langle pq(l\lambda)LM_L(t\tfrac{1}{2})TM_T(s\tfrac{1}{2})SM_S|V_1 \cdot
$$
$$
P|p'q'(l'\lambda')LM_L(t'\tfrac{1}{2})TM_T(s'\tfrac{1}{2})SM_S\rangle_1 . \qquad (6.9)
$$

The subscript 0 in Eq. (6.8) denotes the initial state consisting of a bound state and a free nucleon. This term represents the inhomogeneous solution. The nucleon mass is denoted by m and e_n^{lts} is the energy value for the wave function $\phi_n^{lts}(p)$ in the subspace of the bound states and added continuum states. For the evaluation of the matrix element in Eq. (6.9) we refer to Ref. [20]. Equation (6.8) is formally identical to a two-body

Lippmann-Schwinger equation and can be solved in the usual way by the introduction of the half-shell T-matrix:

$$T_n^{lts\lambda}(q) = \sum_{n'l't's'\lambda'} \int dq' q'^2 V_{nlts\lambda,n'l't's'\lambda'}(qq') b_{n'}^{l't's'\lambda'}(q') . \qquad (6.10)$$

We thus, finally, obtain

$$T_n^{lts\lambda}(q) = V_{nlts\lambda,n_0l_0t_0s_0\lambda_0}(qq_0) + \sum_{n'l't's'\lambda'} \int dq' q'^2 V_{nlts\lambda,n'l't's'\lambda'}(qq') \cdot$$

$$\frac{1}{E^+ - e_{n'}^{l't's'} - 3q'^2/4m} T_{n'}^{l't's'\lambda'}(q') . \qquad (6.11)$$

This equation is solved numerically by matrix inversion.

6.3   Numerical method and results

The theory of the previous section has been applied to n-d scattering using s-wave Malfliet-Tjon potentials. The initial isospin state is given $|(t\frac{1}{2})TM_T\rangle_1 = |(0\frac{1}{2})\frac{1}{2}M_T\rangle_1$. Two different scattering processes are possible, i.e., doublet and quartet scattering. In the latter we start from a totally symmetric spin state $|(s\frac{1}{2})SM_S\rangle_1 = |(1\frac{1}{2})\frac{3}{2}M_S\rangle_1$. Furthermore, confinement to s-wave scattering means $l = 0$ and $\lambda = 0$. The requirement of $l + t + s$ to be odd implies that the above channel is the only channel involved in the calculations. The two-nucleon interaction potential for $t = 0$ is taken to be [21],[22]

$$V(r) = V_R \frac{e^{-\mu_R r}}{r} - V_A \frac{e^{-\mu_A r}}{r} , \qquad (6.12)$$

with the numerical values given in Table 6.1 as the MT III (spin-triplet) potential. This potential has one bound state with an energy of -2.23 MeV, corresponding to the deuteron. In the case of doublet scattering we start from the spin state $|(s\frac{1}{2})SM_S\rangle_1 = |(1\frac{1}{2})\frac{1}{2}M_S\rangle_1$. Since the two-nucleon subsystem has $t = 0$, the two-nucleon interaction in this channel is again given by the MT III potential. However, a coupling exists with the channel having $|(s\frac{1}{2})SM_S\rangle_1 = |(0\frac{1}{2})\frac{1}{2}M_S\rangle_1$ and $|(t\frac{1}{2})TM_T\rangle_1 = |(1\frac{1}{2})\frac{1}{2}M_T\rangle_1$. The analytical form of the interaction in the two-nucleon subsystem in this channel is given by Eq. (6.12) but with different numerical values for the constants, corresponding to $t = 1$. This potential is the MT I (spin-singlet) potential for which the parameters are given in Table 6.1.

	MT I	MT III
V_A (MeV fm)	513.968	626.885
μ_A (fm^{-1})	1.550	1.550
V_R (MeV fm)	1438.720	1438.720
μ_R (fm^{-1})	3.110	3.110

Table 6.1: Potential parameters for the Malfliet-Tjon models [22].

In order to obtain the wave functions $\phi_n^{lts}(p)$ in momentum space the Schrödinger equation has been solved in configuration space using a modified Numerov integration method. The continuum functions have been generated by adding a harmonic oscillator potential to the "real" *NN* potentials, as described in the previous section. With the functions thus obtained the Schmidt orthogonalization has been performed, also in configuration space. Care should be taken that the lowest state of the potential generating the continuum is sufficiently different from the bound state of the real potential. If this is not the case the Schmidt orthogonalization will result in an amplification of numerical noise. The two-nucleon Hamiltonians have, subsequently, been diagonalized. The second derivative with respect to the distance between the nucleons in the kinetic energy part of the Hamiltonians has been discretized by using a five-points discretization.

This total set of basis wave functions has been transformed to momentum space. The advantage of calculating the basis wave functions in configuration space and a subsequent transformation to momentum space as compared to a calculation done directly in momentum space is that the latter requires a matrix inversion since the two-nucleon interaction potentials adopted are not diagonal in momentum space. This makes the calculations very time consuming if a sufficiently good accuracy is to be achieved. The expression $\int dp\,p^2 \phi_n^{lts}(p) V^{lts}(pp')$, with $V^{lts}(pp')$ the two-nucleon interaction in momentum space, which naturally arises in the evaluation of Eq. (6.9), is obtained in a similar way by transforming the product $\phi_n^{lts}(r)V(r)$ to momentum space. It is then possible to evaluate the matrix element in Eq. (6.9) and to perform the matrix inversion which will solve Eq. (6.11). We discretized the q variable in Eq. (6.11) and then solved Eq. (6.11) for progressively more n values, i.e., we increased the number of continuum

functions until convergence took place.

In comparing the results with previous calculations the following should be noted. The value of $T_n^{lts\lambda}(q)$ on the energy shell corresponds to the transition matrix element for n-d scattering. This transition matrix is connected to the scattering matrix via

$$S_n^{lts\lambda}(q) = \delta_{nn_0}\delta_{ll_0}\delta_{tt_0}\delta_{ss_0}\delta_{\lambda\lambda_0} + \frac{4\pi i m}{3}\sqrt{qq_0}T_n^{lts\lambda}(q), \qquad (6.13)$$

which is a unitary matrix. Since both the doublet and the quartet scattering processes are elastic the single S-matrix element involved can be written as

$$S_{n_0}^{l_0t_0s_0\lambda_0}(q_0) \equiv e^{2i\delta}. \qquad (6.14)$$

The phase shift δ is the quantity which we compare with previous calculations together with the scattering length a which is related to the phase shift via $\delta \sim -q_0a$ for $q_0 \to 0$.

First of all we have calculated the quartet scattering. The continuum has in this case been created by choosing the spring constant k of the harmonic oscillator potential $\frac{1}{2}kr^2$ equal to 0.5 MeV fm^{-2} and including 20 continuum states. In Table 6.2 the value of the phase shift for quartet scattering δ_4 is given as a function of the number of basis states used in the calculations for a laboratory energy of 2.45 MeV. In Table 6.3 δ_4 is given for a laboratory energy of 3.27 MeV. Both these energies are below the deuteron break-up threshold. In Table 6.4 the scattering length a_4 is given, obtained at an energy of 10^{-6} MeV. These values should be compared with $\delta_4(2.45\text{ MeV}) = 113.3°$, $\delta_4(3.27$ MeV$) = 106.4°$ and $a_4 = 6.442$ fm given by Payne *et al.* [22],[23]. The agreement between these values and our calculations is excellent. Furthermore, convergence takes place after only a few added continuum functions, which is a very satisfactory result and shows that the present method is indeed very efficient.

The situation is completely different in the case of doublet scattering. In this case the doublet scattering length a_2 has been calculated and compared with the value $a_2 = 0.70$ fm by Payne *et al.* [22]. Although the calculations show results which are close to this value ($\pm$ 10 %) convergence does not take place for a satisfying number of added continuum states.

The marked difference between quartet and doublet scattering can be understood by studying the configuration space calculations of Ref. [22]. Due to the Pauli principle only two of the three nucleons can come close together in the quartet case. This means

n	δ_4 (deg)	n	δ_4 (deg)	n	δ_4 (deg)
1	126.6	8	113.2	15	113.2
2	124.9	9	113.2	16	113.2
3	117.5	10	113.2	17	113.2
4	114.1	11	113.2	18	113.2
5	113.5	12	113.2	19	113.2
6	113.3	13	113.2	20	113.2
7	113.3	14	113.2	21	113.2

Table 6.2: *The quartet phase shift δ_4 as a function of the number of basis states n included in the calculation for a laboratory energy of 2.45 MeV.*

n	δ_4 (deg)	n	δ_4 (deg)	n	δ_4 (deg)
1	123.2	8	106.6	15	106.6
2	122.9	9	106.6	16	106.6
3	115.1	10	106.6	17	106.6
4	108.2	11	106.6	18	106.6
5	107.0	12	106.6	19	106.6
6	106.7	13	106.6	20	106.6
7	106.6	14	106.6	21	106.6

Table 6.3: *The quartet phase shift δ_4 as a function of the number of basis states n included in the calculation for a laboratory energy of 3.27 MeV.*

n	a_4 (fm)	n	a_4 (fm)	n	a_4 (fm)
1	5.831	8	6.421	15	6.419
2	6.297	9	6.418	16	6.419
3	6.351	10	6.420	17	6.419
4	6.421	11	6.419	18	6.419
5	6.408	12	6.419	19	6.419
6	6.424	13	6.419	20	6.419
7	6.416	14	6.419	21	6.419

Table 6.4: The quartet scattering length a_4 as a function of the number of basis states n included in the calculation.

that the deuteron structure in the two-nucleon subsystem is hardly disturbed and only a few smooth continuum functions are needed to describe the Faddeev component. In the doublet case, however, the perturbation of the deuteron structure is much more pronounced, even leading to a node in the Faddeev component at very short distances in the two-nucleon subsystem.

The continuum for doublet scattering has been obtained in the same way as for quartet scattering, i.e., the lower states of a harmonic oscillator potential added to the two-nucleon interaction potential have been calculated. Whereas in the latter case only a few states are necessary to get a converged description, for doublet scattering not only continuum functions are needed that describe the long wavelength deviations from the deuteron structure, but also short wavelength functions that describe the node in the Faddeev component. If both these types of functions are created by one single harmonic oscillator potential many continuum states have to be included in order to describe the system which makes the method less efficient as is evident from the above calculations. It should be noted, however, that this problem is not inherent to the present approach. The only requirements for the continuum states are that they are square integrable and orthogonal to each other and the bound state. There are no limitations, however, to the way in which the continuum states are obtained. In particular, it is possible to

create a combination of two sets of functions, one with a harmonic oscillator potential having a small spring constant for the long-wavelength behavior and one with a harmonic oscillator potential having a large spring constant to describe the node in the Faddeev component. The remainder of the calculations would be the same as described in Sec. 6.2. It is expected that by this method also the calculations for doublet scattering will converge after only a few added extra basis states. At the moment, however, these calculations have not yet been performed.

6.4 Conclusions

We have proposed a new method to calculate three-body scattering below the break-up threshold. This method calculates the state vector by solving the Faddeev equations. Instead of the conventional method which solves the Faddeev equations by using two different relative position or momentum variables this method replaces the role of the eigenstates of one of the two variables by an expectedly smaller set of basis states, which are better adapted to the actual problem and in particular more suitable for describing virtual break-up. Essential in this approach is the way in which the continuum is treated. Due to this new approach the problem should be solvable with smaller computers.

The new method has been tested by means of n-d scattering with s-wave Malfliet-Tjon potentials. We find very good agreement between our calculations of the phase shift and the scattering length for this process and the values given in the literature in the case of quartet scattering. Furthermore, our calculations show a rapid convergence as a function of the number of channels which have to be included in the calculations in this case. The results for doublet scattering are less positive, not showing convergence after many added continuum states.

We have identified the problems in the case of doublet scattering with a node occurring in the configuration space Faddeev component at short distances which cannot be calculated with a few basis states which are lying just above the break-up threshold. Instead, short wavelength functions have to be incorporated in the approach, automatically resulting in the inclusion of many more basis wave functions if the continuum is created by adding a harmonic oscillator potential to the NN interaction potential. A possible solution would be to create a combination of two sets of functions, one for the long- and

one for the short wavelength behavior. Expectations are that in this way also the results for doublet scattering will show a rapid convergence as a function of the number of basis states which are used in the calculations.

Bibliography

[1] H. Witala, W. Glöckle, and T. Cornelius, Few-Body Systems **3**, 123 (1988).

[2] I. Slaus and A. Marušić, Nucl. Phys. A **543**, 213c (1992); R. Machleidt, W. Glöckle, I. Slaus, W. Tornow, and H. Witala (to be published).

[3] W. Glöckle, H. Witala, and T. Cornelius, Nucl. Phys. A **508**, 115c (1990); W. Glöckle, H. Witala, and T. Cornelius, in *Proceedings of the 25th Zakopane School on Physics, Vol. 2: Selected Topics in Nuclear Structure*, edited by J. Styczen and Z. Stachŭra (World Scientific, Singapore, 1990), p. 300 and references therein.

[4] H. Witala and W. Glöckle, Nucl. Phys. A **528**, 48 (1991).

[5] J. E. McAninch, W. Haeberli, H. Witala, W. Glöckle, and J. Golak (to be published).

[6] A. Ross (private communication).

[7] C. R. Chen, G. L. Payne, J. L. Friar, and B. F. Gibson, Phys. Rev. C **44**, 50 (1991).

[8] T. Takemiya, Prog. Theor. Phys. **74**, 301 (1985).

[9] Y. Koike, Phys. Rev. C **42**, 2286 (1990).

[10] W. Glöckle and R. Offermann, Phys. Rev. C **16**, 2039 (1977).

[11] H. C. Jean, Ph.D. thesis, University of Iowa, USA, 1992.

[12] I. F. Silvera, J. Low Temp. Phys. **89**, 287 (1992).

[13] Y. Kagan, I. A. Vartanyants, and G. V. Shlyapnikov, Zh. Eksp. Teor. Fiz. **81**, 1113 (1981) [Sov. Phys. JETP **54**, 590 (1981)].

[14] L. P. H. de Goey, T. H. M. v. d. Berg, N. Mulders, H. T. C. Stoof, B. J. Verhaar, and W. Glöckle, Phys. Rev. B **34**, 6183 (1986).

[15] L. P. H. de Goey, H. T. C. Stoof, B. J. Verhaar, and W. Glöckle, Phys. Rev. B **38**, 646 (1988).

[16] L. P. H. de Goey, Ph.D. thesis, Eindhoven University of Technology, The Netherlands, 1988.

[17] H. T. C. Stoof, L. P. H. de Goey, B. J. Verhaar, and W. Glöckle, Phys. Rev. B **38**, 11221 (1988).

[18] H. T. C. Stoof, B. J. Verhaar, L. P. H. de Goey, and W. Glöckle, Phys. Rev. B **40**, 9176 (1989).

[19] H. T. C. Stoof, Ph.D. thesis, Eindhoven University of Technology, The Netherlands, 1989.

[20] W. Glöckle, *The Quantum Mechanical Few-Body Problem* (Springer-Verlag, Berlin, 1983).

[21] R. A. Malfliet and J. A. Tjon, Nucl. Phys. A **127**, 161 (1969).

[22] G. L. Payne, J. L. Friar, and B. F. Gibson, Phys. Rev. C **26**, 1385 (1982).

[23] G. L. Payne, W. H. Klink, W. N. Polyzou, J. L. Friar, and B. F. Gibson, Phys. Rev. C **30**, 1132 (1984).

Summary

The room temperature hydrogen maser is the most stable time and frequency standard currently available for measurement intervals between 1 and 10^4 seconds. The relative frequency stability of state-of-the-art room temperature hydrogen masers is typically better than one part in 10^{15} for averaging times of 10^4 seconds. Some years ago a sub-Kelvin version has been developed. This cryogenic hydrogen maser was expected to have an increased frequency stability by three orders of magnitude. These expectations were supported by both quantum mechanical and semiclassical calculations on the influence of collisions on the atomic lineshift and -broadening. Calculations done in our group at Eindhoven University of Technology, however, in which the hyperfine structure was included in a proper way, showed that the maximum increase of the frequency stability is restricted to one order of magnitude.

The availability of an extremely stable frequency standard is desirable for various fields of research, such as very-long baseline interferometry, tests of general relativity and interplanetary navigation. For this reason it is of interest to search for possibilities to increase the stability of the hydrogen maser despite the above-mentioned influence of collisions. In Chapter 2 such a possibility is considered. In particular, the effect of a permanent magnetic field on the collisions between two hydrogen atoms and the subsequent influence on the stability of the cryogenic hydrogen maser are treated. It is shown that the introduction of a magnetic field does not produce the hoped for increase in frequency stability.

The hydrogen maser is not only used for very precise time keeping, but due to the very narrow linewidth of the maser output it is also suited to obtain information on the hydrogen gas. In Chapter 3 a variation on the cryogenic hydrogen maser is proposed, i.e., the surface cryogenic hydrogen maser. This proposed maser operates at lower temperatures and has an increased area to volume ratio of the storage bulb compared to the cryogenic hydrogen maser. The operating conditions for such a maser are evaluated and it is pointed out that the output characteristics are determined by the two-dimensional gas of hydrogen atoms at the surface of the storage bulb. This maser could be used to obtain new and more accurate information on the properties of hydrogen gas adsorbed at a superfluid ^{4}He surface.

The two subjects mentioned above, i.e., the use as a frequency standard and the description of the properties of a gas of atomic hydrogen, have for a long time been the only applications of the hydrogen maser. In recent years, however, interest has also been devoted to the use of the hydrogen maser outside these areas. In Chapters 4 and 5 the operation of the cryogenic hydrogen maser is described in a regime of operation which is characterized by a pulsed output power. By studying the hydrogen maser it is possible to obtain information on the behavior of solutions of the Lorenz equations, of which the hydrogen maser is a faithful realization and which are a basic set of equations in the field of nonlinear dynamics, in a parameter regime which has hardly been investigated.

During the last decade various experiments with atomic hydrogen have been performed other than the hydrogen maser. Many experiments have been set up in order to achieve Bose-Einstein condensation. Up to now, however, these attempts have failed due to the large decay rates of the hydrogen gas. It has turned out that three-body recombination of the hydrogen atoms plays the most important role in this decay. In Chapter 6 a new method is proposed to calculate the recombination rate. As an example this method is applied to a basic scattering problem in nuclear physics, i.e., the scattering of a neutron from a deuteron.

Samenvatting

De kamertemperatuur waterstof maser is de meest stabiele tijd en frequentie standaard voor meettijden tussen 1 en 10^4 seconden. De relatieve frequentie stabiliteit van de huidige kamertemperatuur waterstof masers is in zijn algemeenheid beter dan één op 10^{15} voor middelingstijden van 10^4 seconden. Enkele jaren geleden is een sub-Kelvin versie ontwikkeld. Van deze cryogene waterstof maser werd verwacht dat hij een frequentie stabiliteit zou hebben die drie orden van grootte beter was. Deze verwachtingen werden ondersteund door zowel quantummechanische als semi-klassieke berekeningen aan de invloed van botsingen op de atomaire lijnverschuiving en -verbreding. Berekeningen gedaan in onze groep aan de Technische Universiteit Eindhoven echter, waarin de hyperfijn struktuur op een correcte wijze was meegenomen, toonden aan dat de maximale verbetering van de frequentie stabiliteit beperkt blijft tot één orde van grootte.

Het voorhanden zijn van een extreem stabiele frequentie standaard is wenselijk voor

verschillende vakgebieden, zoals very-long baseline interferometry, het testen van de algemene relativiteitstheorie en interplanetaire navigatie. Daarom is het van belang om te zoeken naar mogelijkheden om de stabiliteit van de waterstof maser te verbeteren ondanks de bovengenoemde invloed van botsingen. In Hoofdstuk 2 wordt een dergelijke mogelijkheid onderzocht. In het bijzonder wordt het effect van een permanent statisch magneetveld op de botsingen tussen twee waterstof atomen behandeld en de daaruit volgende invloed op de stabiliteit van de cryogene waterstof maser. Er wordt aangetoond dat de invoering van een magneetveld geen aanleiding geeft tot de intuïtief verwachte toename in de frequentie stabiliteit.

De waterstof maser wordt niet alleen gebruikt als erg stabiele klok, maar vanwege de kleine bandbreedte van het uitgangssignaal van de maser is hij ook geschikt om informatie te verkrijgen over het waterstof gas. In Hoofdstuk 3 wordt een variatie op de cryogene waterstof maser voorgesteld, namelijk de oppervlakte cryogene waterstof maser. De maser in dit voorstel werkt bij lagere temperaturen en heeft een grotere oppervlak/volume verhouding dan de cryogene waterstof maser. Het werkingsgebied voor een dergelijke maser wordt onderzocht en er wordt op gewezen dat het uitgangssignaal bepaald wordt door het twee-dimensionale gas van waterstof atomen aan het oppervlak van de opslagbol. Deze maser kan gebruikt worden om nieuwe en meer nauwkeurige informatie te verkrijgen over de eigenschappen van waterstof gas dat geadsorbeerd is aan een met superfluïde ^{4}He bedekt oppervlak.

De twee bovengenoemde onderwerpen, namelijk het gebruik als frequentie standaard en het beschrijven van de eigenschappen van een gas van atomair waterstof, zijn gedurende lange tijd de enige toepassingen van de waterstof maser geweest. Recentelijk hebben wij echter ook aandacht besteed aan het gebruik van de waterstof maser buiten deze gebieden. In de Hoofdstukken 4 en 5 wordt de werking van de waterstof maser beschreven in een regime dat gekenmerkt wordt door een pulserend uitgangsvermogen. Door het bestuderen van de waterstof maser is het mogelijk informatie te verkrijgen over het gedrag van oplossingen van de Lorenz vergelijkingen, waarvan de waterstof maser een getrouwe weergave is en die een elementair stelsel vergelijkingen zijn in de nietlineaire dynamica, in een parameter regime dat nog nauwelijks onderzocht is.

Gedurende de laatste tien jaar zijn er naast de waterstof maser nog verscheidene andere experimenten gedaan met atomair waterstof. Een groot aantal experimenten is

uitgevoerd om Bose-Einstein condensatie te bereiken. Tot nu toe zijn deze pogingen echter mislukt vanwege het snelle verval van het waterstof gas. Het is gebleken dat drie-deeltjes recombinatie van de waterstof atomen de belangrijkste rol speelt in dit verval. In Hoofdstuk 6 wordt een nieuwe methode voorgesteld om de recombinatie constante te berekenen. Als voorbeeld wordt de methode toegepast op een elementair probleem in de kernfysika, namelijk de verstrooiing van een neutron aan een deuteron.

Curriculum Vitae

Geboren	:	6 maart 1967 te Schiedam
Augustus 1979 - Mei 1985	:	Gymnasium β aan het Augustinianum te Eindhoven
September 1985 - Juni 1989	:	Studie technische natuurkunde aan de Technische Universiteit Eindhoven
		Afstudeerrichting: theoretische natuurkunde
		Afstudeerbegeleiding: prof. dr. B. J. Verhaar en dr. ir. H. T. C. Stoof
		Afstudeermanuscript: *De werking van de cryogene waterstof maser bij sterk B-veld*
		Toegekend judicium: cum laude
Juli 1989 - Juni 1993	:	Promotieonderzoek aan de Technische Universiteit Eindhoven
		Begeleiding: prof. dr. B. J. Verhaar

118

Stellingen
behorende bij het proefschrift van
A. C. Maan

Eindhoven, 15 juni 1993

Door de wijze waarop het triplet-continuüm wordt behandeld in de berekening van drie-deeltjes recombinatie in atomair waterstof m.b.v. "resonating-group theory" wordt het sterk repulsieve karakter van de triplet-potentiaal voor een belangrijk deel buiten beschouwing gelaten.

H. T. C. Stoof, B. J. Verhaar, L. P. H. de Goey en W. Glöckle, Phys. Rev. B **40**, 9176 (1989).
H. T. C. Stoof (privé mededeling).

In de afleiding van de triplet-potentiaal tussen twee waterstof atomen door Jamieson *et al.* op basis van resultaten van Frye *et al.* wordt geen rekening gehouden met de beperkingen die Frye *et al.* zelf reeds aan hun berekeningen toekennen.

M. J. Jamieson, A. Dalgarno en J. N. Yukich, Phys. Rev. A **46**, 6956 (1992).
D. Frye, G. C. Lie en E. Clementi, J. Chem. Phys. **91**, 2366 (1989).
E. Tiesinga (privé mededeling).

In het experimenteel relevante regime van lage intensiteiten is een één-manifold quantummechanische berekening van een optische botsing waarschijnlijk voldoende om het deeltjesverlies uit een (magneto-optische) trap te beschrijven.

H. M. J. M. Boesten, B. J. Verhaar en E. Tiesinga, Phys. Rev. A (ingezonden ter publicatie).

Door een incorrecte behandeling van het regime van grote impulsoverdrachten is de werkzame doorsnede voor het omklappen van een spin onder absorptie of emissie van een magnon vele malen kleiner dan door Bashkin voorspeld.

E. P. Bashkin, Pis'ma Zh. Eksp. Teor. Fiz. **49**, 320 (1989) [JETP Lett. **49**, 363 (1989)].

5

Voor een laser gebaseerd op een overgang tussen het bovenniveau en een lineaire superpositie van de twee onderniveaus in een drie-niveau systeem, waarbij de atomen in de onderniveaus ingevangen zijn in een andere, niet-wisselwerkende superpositie, is het gebruik van de term "laserwerking zonder toestandsinversie" misleidend.

O. Kocharovskaya en P. Mandel, Phys. Rev. A 42, 523 (1990).

6

Bij het evalueren van supercomputers is vanuit gebruikersoogpunt niet de werkelijke rekentijd van belang maar de totale tijd die verstreken is vanaf het versturen van de job tot het verkrijgen van de output.

7

De matige kwaliteit van veel voordrachten tijdens conferenties maakt het belang van voldoende aandacht voor het presenteren van resultaten tijdens de stage- en afstudeerperiode duidelijk.

8

Het verdient aanbeveling faxapparatuur zodanig te construeren dat het nummer ingetoetst kan worden voordat het papier moet worden ingevoerd.